RESIDUAL STRESS IN CERAMIC AND SEMICONDUCTING MATERIALS

By

SEAN MCCOY LANGAN

A dissertation submitted to the

Graduate School-New Brunswick

Rutgers, The State University of New Jersey

In partial fulfillment of the requirements

For the degree of

Doctor of Philosophy

Graduate Program in Materials Science and Engineering

Written under the direction of

Adrian B. Mann

And approved by

_____

_____

_____

_____

New Brunswick, New Jersey

October, 2017

ABSTRACT OF THE DISSERTATION

Residual Stress in Ceramic and Semiconducting Materials

By SEAN MCCOY LANGAN

Dissertation Advisor:

Dr. Adrian B. Mann

Machining of ceramic, semiconductor, and single crystal materials is almost always necessary, but is the most damaging, as well as the most expensive , step of material production. In order for there to be continued progress towards more advanced materials, more advanced machining techniques are necessary.

In this study, one such technique that is a derivative of Single Point Diamond Turning (SPDT), Micro Laser-Assisted Machining, or Micro-LAM, is examined. Three main thrusts were looking at silicon machined with a load-controlled machine, silicon machined with an ultra-high precision machine, and sapphire. Micro-Raman spectroscopy was used to evaluate these materials for residual stress, relative phase purity, and relative crystallinity, all of which can be affected negatively by machining processes.

It was found that Micro-LAM produces excellent results. When the laser power was optimized, it allowed for materials with low residual stress, high relative phase purity and relative crystallinity, as well as excellent surface finishes. Furthermore, Micro-LAM

was found to be superior to traditional SPDT due to the addition of laser assistance.

These results are discussed, as well as the impact of changing the machining parameters

on the resulting material.

Acknowledgements

An advanced degree in engineering cannot be achieved without the help of many, many people, and I would like to take this opportunity to thank them. First, I would like to thank Dr. Mann and Dr. Birnie for being my advisors during my time in grad school, and for their support and guidance. They taught me far, far more than I could say about how to be a scientist and an engineer, and any future success I have (however unlikely that may be!) is from me standing on their shoulders. Further thanks goes to my two other committee members, Dr. Haber and Dr. Ravindra, for their guidance and support.

I am extraordinarily grateful for the support of Dr. Deepak Ravindra, Micro-LAM, Inc., and the NSF funded Ceramic, Composite, and Optical Materials Center. Without them, I could not have had these last few years to study and complete this project. My eternal thanks.

I would also like to thank my fellow graduate students. My groupmates throughout the years, Emma, Josh, Brian, Vishnu, and Ross. Shawn gets a special shout out here for being my partner in crime. We had some good times keeping the Raman working and finagling things around the department. The looks on Dr. Mann's face when we would both come to talk to him at the same time and he knew that something had gone wrong were always priceless! Seriously though, you were the best groupmate a guy could ask for! Bob, who taught me everything about everything, thank you so much, I hope to be half the engineer you are someday. Also, Vlad, thank you for teaching me all about the Raman.

The support staff in the department is invaluable. Claudia, Nahed, and Sheela are all absolutely top notch. A special shout-out goes to Michelle, who I would not have finished this without. Her advice, and ability to bail me out when I made a mistake, were completely invaluable. Thank you so much for everything Michelle!

To my friends back home in Chicago, in Boston, and here in New Jersey, I love you all dearly, and I am unbelievably blessed that there are far, far too many of you to name here. You all were rocks in times of hardships and you made the joy much sweeter. You made getting work done very, very difficult and I'm completely okay with that. Next rounds on me guys. Love yah.

To Kelly and Sean, I absolutely couldn't have finished this without you. Thank you so much. Also Kelly, Sean loves me more than you. You know it's true!

To my extended family, the Campbells, the Langans, the Ginns, The Butts, the Steinhausers, and so many others. It's a great problem to have, having too many family members to mention. Thank you and I love you all.

To my fiancé Annette, for your constant love and support. You are my rock and I love you Netters.

To my parents, for their constant support and unyielding love. You, along with Annette, believed in me when I did not believe in myself. How do you thank your parents for all they have done for you? Are words even sufficient? You will never know how much you mean to me, and I'm the luckiest kid in the world. I love you.

Lastly, to God. Thanks for all you have done for me.

Preface

This dissertation is partially based on the following papers

1. Evaluation and Optimization of Micro-Laser Assisted Machining of Silicon. Sean M.
Langan, Deepak Ravindra, and Adrian B. Mann; submitted to Materials and
Manufacturing Processes 2017. Manuscript LMPP-2017-0592

2. Minimizing Surface Damage in Silicon with Micro-Laser Assisted Machining. Sean
M. Langan, Deepak Ravindra, and Adrian B. Mann; submitted to Machining Science and
Technology 2017. Manuscript LMST-2017-0153

3. Mitigation of Damage During Surface Finishing of Sapphire Using Laser-Assisted
Machining. Sean M. Langan, Deepak Ravindra, and Adrian B. Mann; submitted to
Precision Engineering 2017. Manuscript PRE_2017_310.

4. Relating Residual Stresses to Machining and Finishing in Silicon Carbide. Benjamin
P. Groth, Sean M. Langan*, Richard A. Haber, and Adrian B. Mann; Ceramics
International 42 (2016) 799-807.

> *The author of this dissertation performed surface roughness tests for this paper
> and edited the final manuscript.

The relevant chapters of this thesis contain these papers as submitted, with some
minor changes.

Also, Chapter 5 is an adaptation of work presented at a Gordon Research
Conference on Thin Film and Small Scale Mechanical Behavior from 2014.

Table of Contents

List of Tables

List of Figures

x

1. Introduction

Ceramics have become one of the most important classes of materials used in engineering today. Ceramics have a wide variety of uses that range from high temperature refractories and abrasive materials [1] to piezoelectric materials and laser components [2].

Fabricating solid parts that can meet tight engineering tolerance and surface finish requirements is a difficult task. "Raw" parts almost never meet the engineering requirements, and must almost always be subjected to a machining process. In this context machining is the removal of material, usually through a grinding or lapping process. While these processes allow a material to fall within tolerance or achieve a desired surface finish, they are also the primary source of damage to a ceramic material during production [3]. This damage, often referred to as residual stress, can lead to inferior material performance as well as possible early failure. As such, the residual stress left in materials from machining must be better understood. This understanding could potentially lead to machining techniques that impart less stress on a material. One of these techniques is Micro-Laser Assisted Machining, or Micro-LAM. Micro-LAM uses diamond turning with a laser shining through the diamond to thermally soften the material. The combination of these two processes can lead to ductile regime machining, which could be beneficial to materials.

In this study, we examined the stress left on materials from traditional machining techniques as well as the Micro-LAM technique with Micro-Raman spectroscopy. Raman spectroscopy because it can provide phase and residual stress information on a scale smaller than many other techniques while being user-friendly and readily available.

By examining how the results of machining techniques, we are developing a greater understanding of how stress is imparted on materials, as well as how to optimize machining techniques to make for better, more reliable ceramics and semiconductors.

2. Background

2.1. Machining Ceramics

After they are formed, ceramics rarely have the shape or surface finish necessary for their eventual use, and most do not fall within the necessary tolerance. Machining is the process of removing material so that the ceramic can fall within the parameters. The difficulty is that these processes are the primary source of damage to the ceramic material during its production 3 and can account for up to 90% of final product cost [4]. It is important to understand the various machining techniques in use so they can be improved upon.

a. Grinding

Grinding is often one of the first steps to occur after a material is fabricated or after it is sawn [5]. In grinding, the abrasive material, such as diamond or cubic boron nitride or silicon carbide, is not free flowing but is attached to a "paper or platen" [5]. The binding for the abrasives is designed to release grains once they have been blunted, while being able to resist the wear from the ceramic piece [6]. There are two kinds of bonding systems, a single grain layer that only has one layer of abrasive grains attached to the wheel through an electroplated nickel bond, and a multi-grain layer that has multiple layers of grains attached to the wheel through a metal, resin, or vitreous bond [5]. During the grinding process, the platen moves across the sample at 200-1000rpm, and it is a relatively fast process since the abrasive grains are large, usually greater than 40μm [7].

b. Lapping

Lapping is a process used to achieve flat surfaces, and can be thought of as an intermediate between grinding and polishing. Like grinding and polishing, it uses an abrasive grit to remove material. It produces a flat surface and can be used to get a material within desired tolerances [8]. The process can take place either with the abrasive fixed or the abrasive free in a slurry contacting the piece being machined [7]. Lapping is performed with smaller grits than grinding, 5-20 µm, and at lower speeds [7]. The end result of the lapping process is generally an "isotropic surface structure" and a non-reflective surface [8].

c. Polishing

Polishing shares many characteristics with grinding and lapping, but it generally ends with a lower surface roughness than the other techniques could provide [8]. Polishing involves successively smaller grit sizes, each of which scratches the surface of the sample. Each smaller grit removes the scratches left by the larger grit before it, replacing them with smaller scratches. The polishing grits can go down as small as ¼ µm, and these abrasives are almost always free in a slurry [4]. Unlike grinding and lapping, polishing is not used to reduce the size of the material in any significant way, but is only used to improve the surface finish of the material [9].

d. Laser Machining

Laser machining uses a laser to remove material, or in the case of laser assisted machining, assist in the removal of material. The laser either decomposes the sample surface, or melts the sample surface [10]. It has been found that a continuous laser is best for a cutting manner of machining [11]. Laser machining has several advantageous qualities, in that it is non-contact. This eliminates usual problems such as tool wear and undesirable interactions between the machining tool and the sample being machined [11].

Laser assisted machining is when traditional machining processes are assisted by a laser. This technique does not seek to decompose or melt the material, only to heat the part of the material being machined, allowing for reduced cutting forces as well as better surface finish [11].

e. Ultrasonic Machining

In ultrasonic machining, electricity is changed into vibrations through a transducer, causing the machining tool to vibrate during machining while an abrasive slurry is applied [12]. This slurry is then vibrated, hitting the sample and causing "material removal due to microchipping" [12].   The technique can even be used to drill multiple holes simultaneously [12] as can be seen in Figure 1, which is useful for cutting back on machining time.
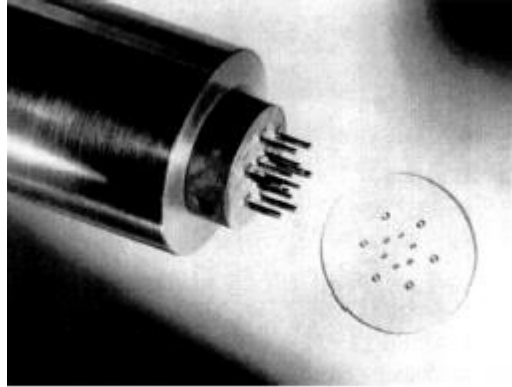
Figure 2.1: The tool and finished part from an ultrasonic machining setup capable of drilling multiple holes simultaneously. Figure from [12].

2.2. Ductile Mode Machining

a. The Science Behind Ductile Mode Machining

Recently, ductile mode machining has arisen as a possible alternative to conventional machining techniques. Unlike conventional machining, which causes microcracks in a material through brittle fracture as seen in Figure 8, ductile mode machining works by creating a ductile phase on the surface of the brittle material, machines more easily.
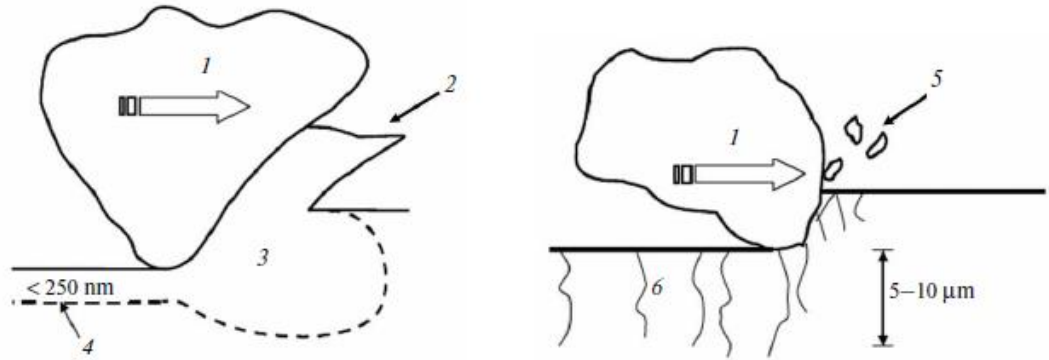
Figure 2.2 from [6]: Ductile mode machining (left) and brittle mode machining (right). According to [6], "(1) abrasive grain, (2) ductile removal of chips, (3) metal phase, (4) transformed amorphous layer, (5) brittle chips, (6) microcracks."

Much of the mathematics behind this process are laid out by Bifano, *et al.* [13] and can be understood energetically. The energy to deform a volume material plastically (E_p) can be defined as:

$$(2.1) \; E_p = \sigma_y V_p$$

Where σ_y is the yield stress and V_p is the volume of the material being plastically deformed. Similarly, the energy to fracture an area of a material (E_f) is:

$$(2.2) \; E_f = G A_f$$

Where G is the Griffith crack propagation parameter and A_f is the area being fractured. It is explained that since A_f and V_p are both proportional to machining depth, d, specifically that $A_f \sim d^3$ and $V_p \sim d^2$ then we can express the ratio of the energies as proportional to the machining depth

$$(2.3) \ \frac{Plastic \ Flow \ Energy}{Fracture \ Energy} = \frac{E_p}{E_f} \propto d$$

Thus, if the cut is shallow enough, plastic flow may be more energetically favorable than fracture. The depth at which plastic flow becomes energetically unfavorable is known as the critical depth, or d_c, which is:

$$(2.4) \ d_c = \frac{ER}{H^2}$$

Where R is the fracture energy of the material, H is the hardness and E is the elastic modulus. Since:

$$(2.5) \ R \sim \frac{K_c^2}{H}$$

Where K_c is the fracture toughness, then:

$$(2.6) \ d_c \propto \left(\frac{E}{H}\right)\left(\frac{K_c}{H}\right)^2$$

As most of these are known quantities for common materials, the critical depth for machining with plastic flow can be found. However, it was found experimentally in Bifano's work that a correction factor of 0.15 gave best results, making it:

$$(2.7) \ d_c = 0.15\left(\frac{E}{H}\right)\left(\frac{K_c}{H}\right)^2$$

However, since brittle materials are by definition brittle they do not normally behave in a ductile way. It has been shown that under high compressive and shear stresses brittle materials can undergo a high-pressure phase transformation to a metallic phase allowing ductile behavior [14]. Aside from depth of cut and applied pressure, the ductile to brittle transition is also governed by feed rate and tool geometry (including the

cutting edge radius, and the rake angle). This ductile mode would allow for machining without many of the disadvantages associated with conventional machining.

Ductile mode machining uses these two phenomena in a way that allows for less destructive machining of the material. By combining high stresses to allow the material to be machined in the ductile regime, and high precision to assure that the machining occurs at less than the critical depth where ductile flow becomes energetically unfavorable, the material can be machined in the ductile mode.

b. Micro-LAM Process

The Micro-LAM process is based on the same principles of ductile mode machining with several significant differences. Like ductile mode machining, it relies on a brittle to ductile transition to machine the part without the damage associated with tradition machining (microcracking, chipping, etc.) [6].
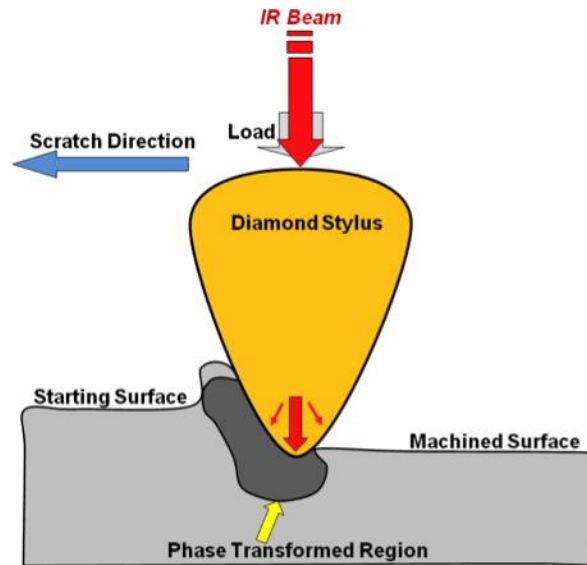
Figure 2.3: Diagram of the Micro-LAM process (from [15]). A diamond stylus machines the material by creating a ductile phase through high pressure, while a laser shines through the stylus onto the material to thermally soften it.

The Micro-LAM process (which stands for Micro Laser Assisted Machining) is similar to Single Point Diamond Turning (SPDT) but the diamond tip is embedded in an epoxy, seen in Figure 10 that is connected to a laser via a 10 μm fiber optic cable [15]. The laser is then shined through the cable to the epoxy and then diamond tip. This laser heats the material being machined, making the brittle to ductile transition occur more easily by increased thermal softening and less brittle behavior [16]. This heating of course is material specific since different materials absorb different wavelengths different amounts.
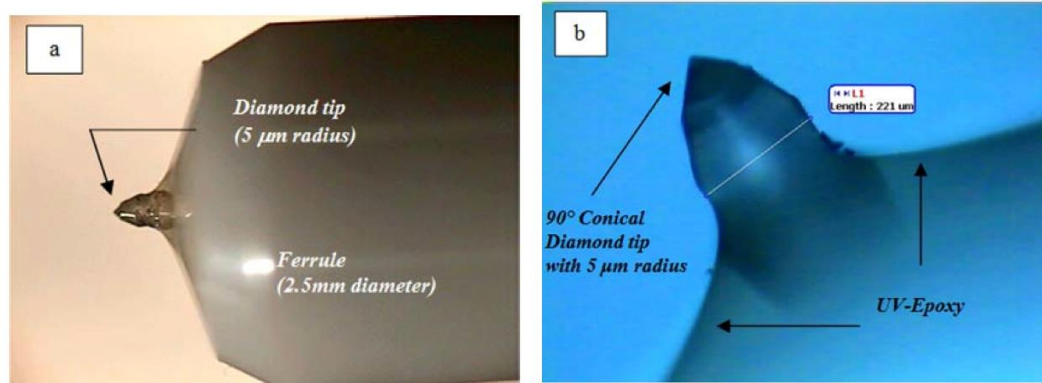
Figure 2.4: a) Wide view of the ferrule and attached diamond machining tool. b) Close-up of the diamond machining tool. [15]

Like traditional diamond ductile mode machining, Micro-LAM seeks to eliminate the traditional problems associated with machining (brittle fracture, microcracks, and large residual stresses). The Micro-LAM process, by adding laser heating as well, seeks to further reduce these undesirable features. The results so far [17] indicate that the laser heating leads to a reduction in hardness of approximately 50%.

There has been much progress made on the Micro-LAM technique in recent years. Particularly extensive work has been done on silicon with the Micro-LAM technique. Silicon is an important material that is extensively used in many fields. In almost all scenarios, it requires time consuming machining while exposing it to harsh conditions, making it a good candidate for the Micro-LAM process.

Many applications of silicon require a highly polished surface to be made from a rough, original surface. In [18] unpolished silicon wafers were subjected to the micro-lam process. The R_a was reduced from .85µm to .23µm in one pass of the Micro-LAM

tool, a significant improvement. Furthermore, the R_z is also significantly improved with a final value of 2.23 µm from 13.4 µm. These results were further improved with a second pass. There was however some tool wear during this process, as seen in Figure 11. This tool wear could be machined out of the diamond stylus, but it is a factor to consider in the implementation of this technique.
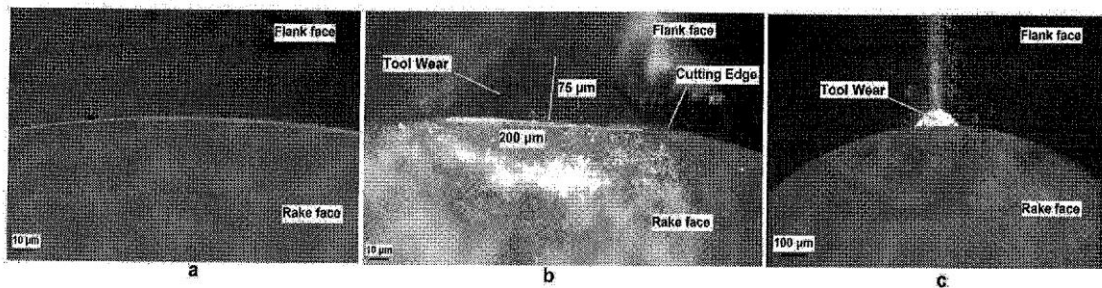
Figure 2.5 from [18] Tool bit a) before machining b) after machining c) after machining at lower magnification.

Another study [19] was able to achieve a R_a of 5 nm, which allowed for the surface to be more reflective than a conventionally polished silicon wafer. Polished silicon wafers are used in numerous engineering applications, and it has been proposed that ductile regime machining like Micro-LAM is a faster machining method [18]. In this same study, it was found that with increased cutting rate, the depth of cut is lowered, and it was found that increasing the feed/rev size also decreased cutting depths (here, 10, 20, and 30 µm feeds were used).

Other work has been done on the fundamental processes that are at play during the Micro-LAM process. As seen in Chapter 6, silicon undergoes complex phase changes while under pressure and it is important to understand these phase changes

during the Micro-LAM process.   It was found that if the conditions for Micro-LAM are not optimized, other silicon phases are created during the machining process, as seen in Figure 12.
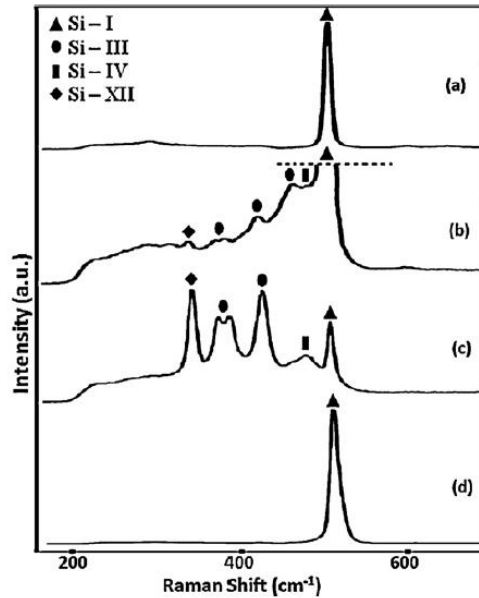
Figure 2.6: Raman spectra of a) unmachined silicon sample b) machining without laser c) machining with laser set at 10W and d) laser set at 45W. Figure from [20]

It was found [20] that if the silicon is machined by single point diamond turning without a laser, or when the laser is set to the wrong parameters, multiple phases are created during the high pressure phase transformation. Here, the phases that are created are Si-III, Si-IV and Si-XII, in addition to the original Si-I phase. The authors postulate that the laser anneals the additional phases back to Si-I.   As had been found before, cuts with the laser have a better depth of cut than cuts without the laser. It was also found that cuts with the optimized laser power give a better depth of cut than the unoptimized laser

power. Clearly, optimizing the power of the laser is an important part of the Micro-LAM

process, as it affects both the depth of cut as well as the formation of additional phases.

Another extensively used ceramic, silicon carbide, has been studied as well.

Tests were performed on single crystal 4H SiC [17] featuring single point diamond

turning both with and without the laser, and all other conditions the same. It was found

that the scratch with the laser had a depth almost twice that of the scratch without a laser.

The authors estimate that the laser heated material has a hardness of 13GPa, half the

original hardness of 26GPa. Another study on 4H SiC [15] also showed a greater depth

of cut when a laser was present when both scratches had the same cutting force. This

study scratched the samples while simultaneously ramping up the cutting force from 2 to

70mN. It found that with the scratch with the laser experiences brittle fracture later in the

cut, and therefore at a higher force, as can be seen in Figure 13.
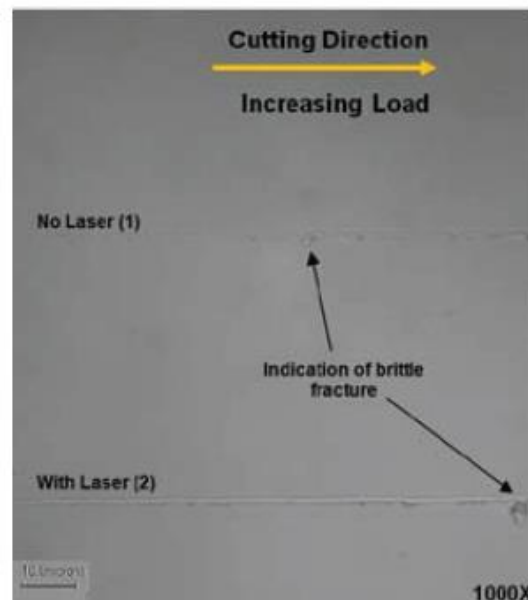
Figure 2.7: Scratches performed on 4H SiC with and without laser, and the corresponding

points of brittle fracture. Image from [15]

Another extensive study was performed on 3C SiC that had been fabricated by CVD [21]. The material was machined in 6 passes, during which the R_a was taken from 1.23μm to 88 nm, which is substantial, and can be seen in Figure 14.
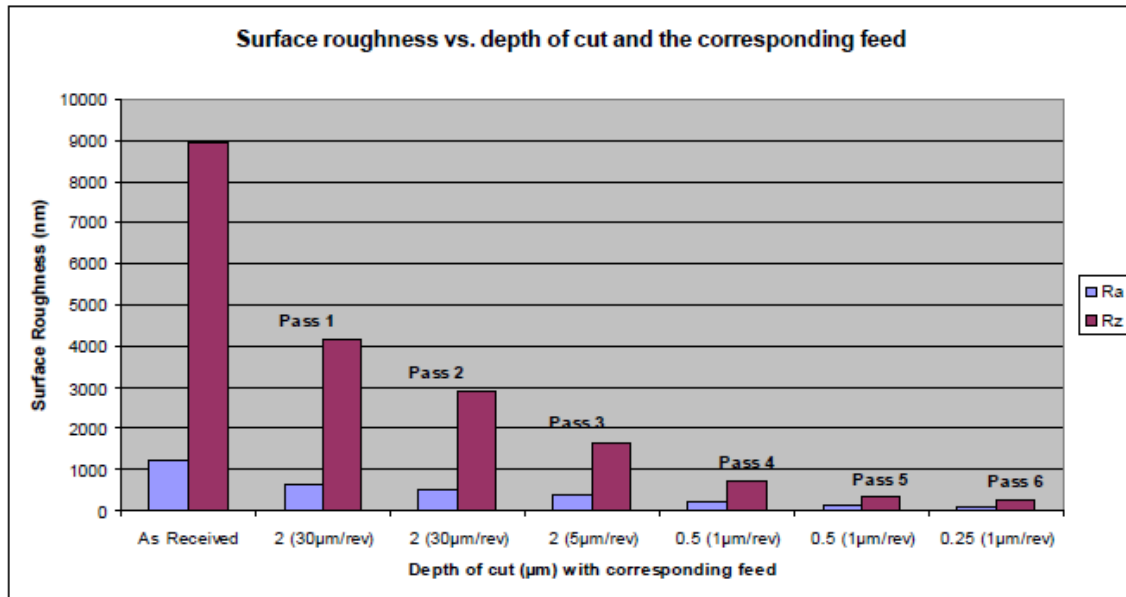
Figure 2.8: Surface roughness (both R_a and R_z) for the as received material, as well as after each pass. Image from [21].

This material was then characterized by Raman spectroscopy and scanning acoustic microscopy. The Raman spectroscopy revealed that post machining there was a layer of amorphous material on the surface of the material, a leftover of the brittle to ductile transition. The scanning acoustic microscopy revealed that there were none of the classic pitfalls of brittle machining, such as cracking or other damage.

The machining process was also recently performed on soda lime glass. Glass is notoriously hard to machine, but incredibly useful and ubiquitous. If the Micro-LAM

process could be improve glasses machinability it would be very useful to the glass industry, and hopefully allow more complicated shapes to be made. Multiple scratches were performed on soda lime glass, both with and without laser heating, and it was found that the laser heating proved beneficial [22]. The laser heating provided greater depths of cut (once at very high laser power the material melts and flows back into the scratch, causing a lesser depth of cut), and for 50mN and 100 mN loads allows for the cut to be completely ductile. These are all desirable characteristics, showing it as a promising technique for machining glass.

Micro-LAM has also been performed on quartz in [23] yielding good results. Like soda lime glass, quartz is very brittle and difficult to machine using traditional techniques. With the Micro-LAM the R_a and R_z (measurements of surface roughness) were significantly lowered, as can be seen in Figure 15.
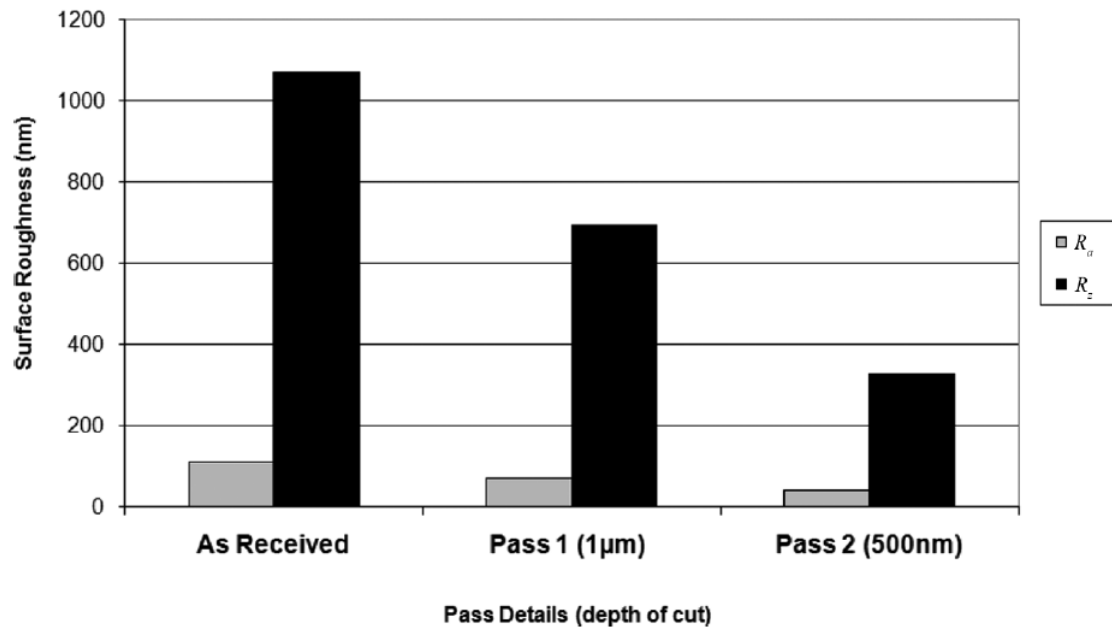
Figure 2.9: The surface roughness of quartz after the Micro-LAM process (from [23])

This machining showed no brittle behavior but instead behaved in a fully ductile manner. Limited feed marks were found on the material, and the surface roughness was found to be appropriate for the quartz to be used for laser applications [23]. The Micro-LAM process remains a promising method for machining quartz, an important material but one that is difficult to machine.

2.3. Stress

All of the machining steps mentioned previously are important in the production of ceramic and semiconductor materials. However, they are all harsh processes that can be the number one source of damage during material production [3] introducing large amounts of stress and strain. Stress and strain are important materials concepts. Stress is "the intensity of force at a point" or:

(2.8) $\sigma = \partial F / \partial A$ when $\partial A \rightarrow 0$

While over a larger area it is simply defined as

(2.9) $\sigma = F/A$

Where F is force and A is area [24]. Engineering strain is defined as

(2.10) $\varepsilon_E = \Delta L / L_o$

Which is essentially the change in length of an object divided by its original length [24]. The "true" strain of a material is defined as

(2.11) $\varepsilon_T = \int \frac{dL}{L} = \ln\left(\frac{L}{L_o}\right)$ [24]

These quantities of stress and strain are related to another. When a material is stressed, it experiences strain, and vice versa. The Young's Modulus, *E,* of a material relates the stress and strain [25].

(2.12) $\varepsilon_{xx} = \frac{\sigma_{xx}}{E}$

As mentioned in the introduction, machining is the primary source of damage to ceramics during production. There are considered to be three kinds of residual stress generated during machining [26]. First order stresses occur over several grains and are macroscopic. Second order stresses are within a single crystallite, and are often formed by differences in thermal and mechanical behavior between grains. Third order residual stresses are atomic scale, for example dislocations, or atomic substitution.

Microplastic deformation often forms dislocations or twinning in materials, as well as lattice defects [26]. Macroscopic deformation can create stress on the microscopic and macroscopic scale. It is described that during grinding the hydrostatic compressive stress creates both scales of stress, and it is higher transverse to the movement of the grinding [26]. Residual stresses from machining of ceramic materials are complex, and need to be closely studied to be understood.

2.4. Raman

Characterizing materials is a vital aspect of materials engineering. While it is important to make a material, if one cannot prove that they have done so, or discern its

properties, it is worthless. Raman spectroscopy is one method of characterization, and it

is vitally important in looking at machining effects in materials.

a. The Science of Raman

The basis of R scattering lies in atomic vibrations, making them important to

understand. The traditional understanding is based on two masses (atoms) connected by

a spring. If the spring is stretched a distance of Δr, the restoring force is equal to [27]:

$$(2.13) \quad f = -k\Delta r$$

where k is the force constant of the bond. Once these masses are released it

oscillates and is described as harmonic motion [27], or as a harmonic oscillator. The

potential energy (V) of this harmonic oscillator with the atoms being moved a distance of

X away from equilibrium can be described as [27]:

$$(2.14) \quad V = \frac{1}{2}kX^2$$

However, real molecules do not undergo harmonic oscillation, because at large X the

restoring force is less than the model.   Furthermore real molecules do not have

continuous energy levels, but discrete energy levels [27]. As such, the energy states are

[27]:

$$(2.15) \quad E_n = hv(n + \tfrac{1}{2})$$

Where h is Planck's constant, v is the fundamental vibration frequency, and n is the

energy level [0,1,2, etc.]. For many applications, the harmonic oscillator model is

sufficient [27].
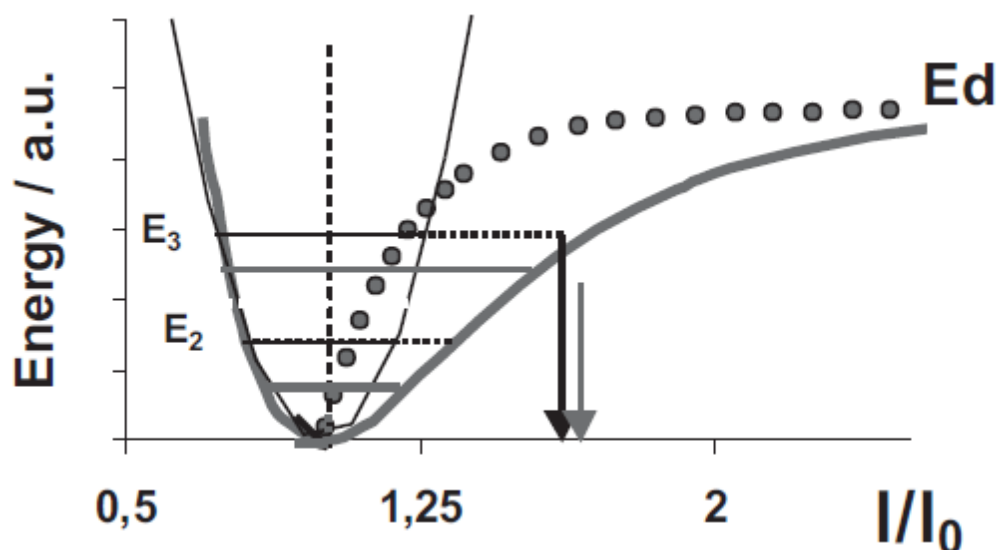
Figure 2.10: Energy vs displacement for a bond from [28]. The thin parabola is the harmonic oscillator, and the thick line is the anharmonic osciallator. The horizontal lines represent the discrete energy levels associated with the molecule.

The Raman phenomenon was discovered in 1928 by Chandrasekhra Venkata Raman using sunlight as the light source [29]. When most light hits a material, it can be scattered with the same frequency as it had when it hit the material, which is called Rayleigh scattering [27], and is shown in Figure 3. It is known as an elastic collision, and during this process the electrons in the sample vibrate in the same frequency as the radiation, and then the material radiates energy in all directions [27].

Sometimes however, the collisions are inelastic. During these the phonon hits the sample, exciting it into a higher vibrational state. The sample then relaxes into a higher or a lower energy state than it was originally in, called Stoke and Anti-Stoke scattering

respectively. This Raman scattering (as it is now commonly known) can be measured as a

shift in the exciting light source, which is typically a laser in modern applications.

Excited states

Virtual
energy states

$h(\omega)$ $h(\omega)$ $h(\omega)$ $h(\omega-\omega_k)$ $h(\omega)$ $h(\omega+\omega_k)$

Vibrational
energy states

Ground states $h\omega_k$ $-h\omega_k$

**Rayleigh
scattering**

**Stoke
Raman
scattering**

**Anti-Stoke
Raman
scattering**
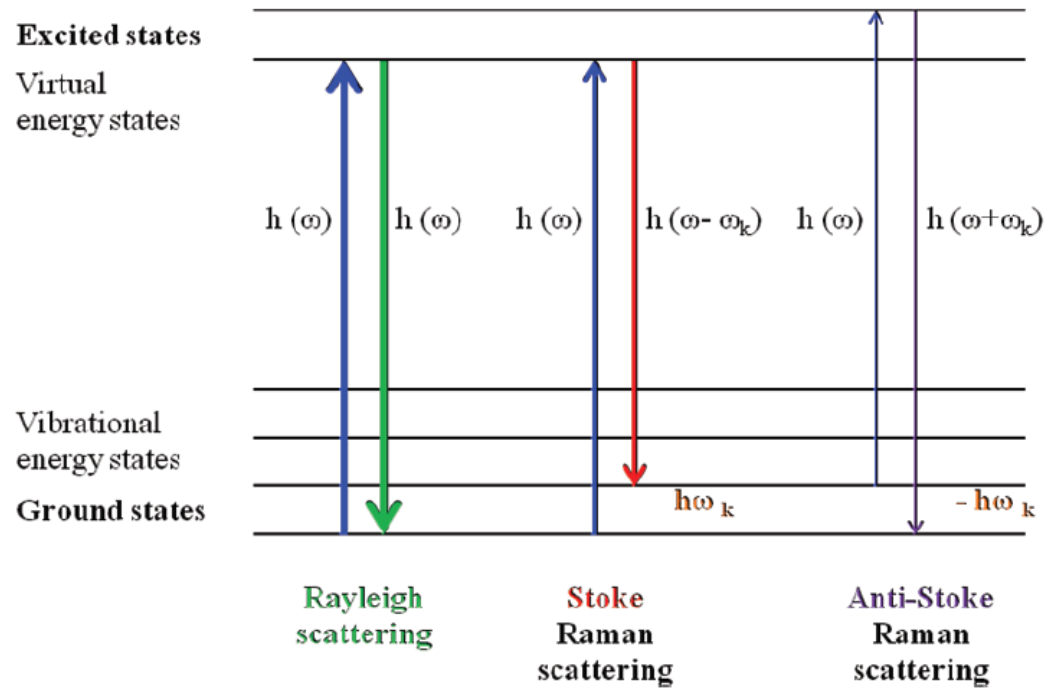
Figure 2.11 Raman and Rayleigh scattering illustrated. From [30]

In order for a molecule to be Raman active it must be capable of having its

polarizability change when it is hit with a laser [29]. At a fundamental level, permanent

dipole moment of a molecule, μ, with a positive and a negative charge is:

$$(2.16) \quad \mu = er$$

Where e's are the charges of the particles in question and r is the distance that separates

them [31]. When this is exposed to an electric field, a dipole can be induced in the

molecule, due to the attraction of the nuclei and electrons to various parts of the electric field [31]. This induced dipole, μ_{ind} can be described as:

$$(2.17) \quad \mu_{ind} = \alpha\varepsilon$$

Where ε is the electric field and α is the polarizability of the molecule. [31].

The oscillation of the electric field associated with light can be described by the equation:

$$(2.18) \quad \varepsilon = \varepsilon_o \cos 2\pi v t$$

Where v is the frequency of the light, ε_o is the field's maximum value, and t is time [31]. From this, the induced dipole in molecule being hit with the life can be found as

$$(2.19) \quad \mu_{ind} = \alpha\varepsilon_o \cos 2\pi v t \quad [31]$$

Since the polarizability of the molecule will depend on the bond length (because bonds can compress and lengthen) the polarizability term needs to be modified to

$$(2.20) \quad \alpha = \alpha_o + (\Delta\alpha)\cos 2\pi v_o t$$

Here, $\Delta\alpha$ is the change in polarizability, α_o is the "equilibrium polarizability" and v_o is the equilibrium vibrational frequency [31]. This is then put into equation (12) and simplified to give:

$$(2.21) \quad \mu_{ind} = \alpha_o\varepsilon_o \cos 2\pi v t + (1/2)\Delta\alpha\varepsilon_o[\cos 2\pi(v+v_o)t + \cos 2\pi(v-v_o)t]$$

In this equation, it is seen that Stokes, $v+v_o,$ anti-Stokes, $v-v_o$, and Rayleigh $v_o,$ can be present when the electronic dipole of a molecule interacts with light [31].

b. Raman Spectrometer Explanation

While many types of Raman spectrometers exist, the basic design principles are consistent throughout. The basic design is shown in Figure 4. The excitation source for modern Raman spectroscopy is a laser, which an improvement on the lamps that were used in earlier systems [29].
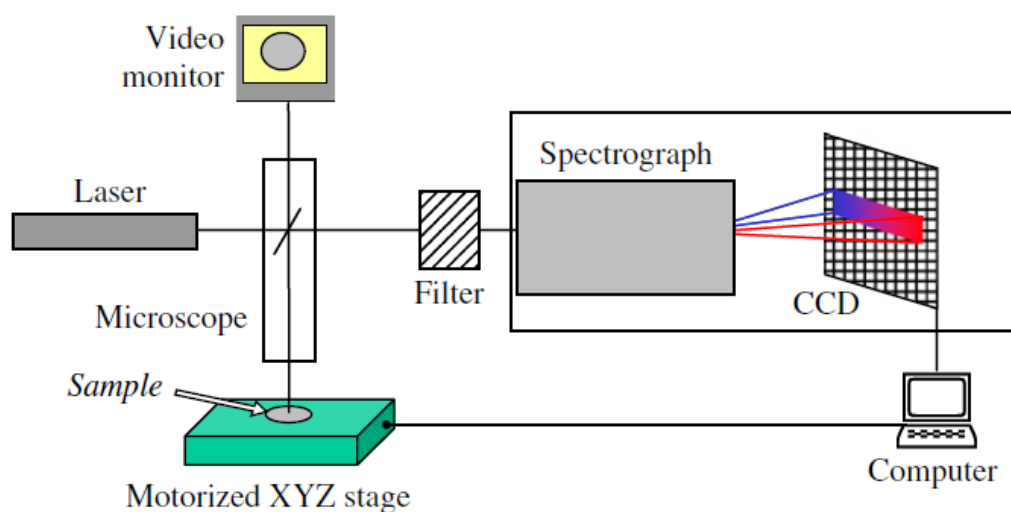
Figure 2.12: The basic setup of a Raman spectrometer (from [32])

This light is then shined on the sample, often by the use of a mirror but sometimes by fiber optics. The light then reflects from the sample to a filter. The filter is mainly in place to eliminate the Rayleigh scattering because it is 10^6 times more intense than the Raman lines that actually give sample information [29].   Then, a CCD is used to record the light and it is mathematically converted to the spectrum that is seen on the computer.

The motorized stage seen in Figure 4 is also noteworthy because it allows for precise sample mapping. Since micro-raman has a spot size on the order of microns, chemical and physical properties of the material can be mapped in a manner that is not possible with numerous other techniques.

c. Raman for Stress Measurement

Measuring residual stress in materials has been a significant challenge to the engineering community for a number of years. Since residual stress can have a significant effect on material properties, it is important to measure it after production and machining processes if one is to fully understand the material and predict how it will behave. Many of the traditional tests destroy the material in the process, further complicating the matter. In order to maximize production efficiency, techniques need to be created that allow for non-destructive material testing of residual stresses, such as Raman spectroscopy.

Raman spectroscopy fundamentally measures the vibrations in the bonds between atoms. Changes in that molecular environment should affect the Raman spectra. For example, if a molecular bond is lengthened or compressed, that theoretically should change the Raman spectra. Since stress and strain occur when a bond is stretched or compressed, this should theoretically change the Raman spectra. This has been shown to happen in a variety of materials [28], as a stressed material has a shift in the Raman frequencies from an unstressed material.

This change derives from the harmonic/anharmonic oscillator approximation for a molecular bond. The potential energy [28] can be described with the change in bond length, $\Delta l = (l - l_o)$, as:

$$(2.22) \quad V = \left(\frac{1}{2}\right) k(l - l_o)^2$$

This however is the case for a harmonic potential. The anharmonic potential is described as:

$$(2.23) \quad V(l) = (l-l_o)^2 + k'(l-l_o)$$

This anharmonicity leads to the wavenumber shift when the material is strained, which can be expressed as:

$$(2.24) \quad \Delta v = S^\varepsilon \times \Delta \varepsilon$$

Where $\Delta \varepsilon$ is the strain (described in [28] as the tensile strain) and Δv is the shift in the wavenumber [28]. This equation can be rewritten into a more useful form as:

$$(2.25) \quad \Delta v = S^\varepsilon \times \Delta \varepsilon = S^\varepsilon \times \frac{\Delta \sigma}{100 \times E} = S^\sigma \times \Delta \sigma$$

For hydrostatic pressures, S^ε is not used to show how the wavenumber changes with stress, but the Grüneisen coefficient (Υ^G) instead [28], which is defined as:

$$(2.26) \quad \gamma = -\frac{\partial \log v}{\partial \log V}$$

Where V is the volume [28]. Only taking changing pressure into account, the relationship between γ_i and S_i is:

$$(2.27) \quad S_i^\sigma = \frac{v_i^0 \times \gamma_i}{B}$$

with B as the bulk modulus [28].

Raman has several distinct advantages as a method for measuring residual stress. It is a nondestructive technique, requiring little-to-no sample preparation. Parts could be taken straight from the assembly line and tested before being sold. Also, because micro-Raman can be performed with an extremely small spot size, Raman allows a part to be mapped, which can find areas of high and low stress. Finding the "local" stresses can be advantageous, and cannot be done with XRD, which gives the stress over large areas of the sample. Theoretically, Raman could be incorporated into a production line to weed out faulty materials. Raman cannot be performed on metals however, and also requires fine calibration, both of which are disadvantages of the technique. Those disadvantages aside, it is a valuable technique that will continue to expand and improve.

d. Difficulties with Raman Measurements for Residual Stress

In piezospectroscopy, great care must be taken to remove uncertainties in order to make the results as quantitative as possible. One of the many difficulties is removing as much uncertainty as possible, much of which is related to the material specific equations connecting the peak shift to the stress present. Often, these equations lose much of their quantitative value. A study by Sergo, *et al.* [33], found that the additives in a material can greatly affect how peaks shift with stress. Sergo, *et al.*, looked at three different materials, a high purity powder that was hot isostatically pressed, the same powder with 5% Y_2O_3 and 1% Sc_2O_3, and a commercial powder that was only 88% silicon nitride and also contained Mg, Ce, Sr, Al, Fe and Y. As can be seen in Table 2.1, there is a significant discrepancy between the peak shifts of the various samples.

	Pure	Pure w/ Additives	Commercial
862 Peak (cm^{-1}/GPa)	3.9 ± 0.2	6.3 ± 0.2	4.5 ± 0.2
925 Peak (cm^{-1}/GPa)	3.4 ± 0.3	4.8 ± 0.5	4.2 ± 0.16
936 Peak (cm^{-1}/GPa)	3.6 ± 0.2	3.6 ± 0.4	4.2 ± 0.16

Table 2.1: Peak shifts for the various silicon nitride formulations. Figure adapted from [33]. Note: The peaks listed are approximate and are for the pure sample, as the different formulations have slightly different peaks, most likely caused by their slightly differing makeups.

It is clear that the peak shift in silicon nitride changes based on what additives and impurities are present. This complicates matters when looking at residual stress in polycrystalline materials, since they often have a wide variety of additives as sintering aids. When using peak shift residual stress equations from the literature for polycrystalline samples, it can be hard to say if the results will be more quantitative or qualitative in nature.

The problem extends to single crystal materials as well. For sapphire, two separate papers calculating the response to uniaxial stress found two separate results, as seen in Table 2.2.

Frequency (cm^{-1})	Shin *et al.* Peak Shift (cm^{-1}/GPa) [34]	Watson *et al.* Peak Shift (cm^{-1}/GPa) [35]
380	2.3 ± 0.2	1.37 ± 0.06
417	1.7 ± 0.1	2.11 ± 0.06
432	1.8 ± 0.1	2.95 ± 0.08
451	1.0 ± 0.2	1.66 ± 0.10
578	2.7 ± 0.3	2.77 ± 0.12
646	5.0 ± 0.4	n/a
751	2.5 ± 0.3	4.80 ± 0.20

Table 2.2: Peak shift at different frequencies under uniaxial tests from two sources. Adapted from [36].

It would be logical to assume that tests on single crystals, especially when the tests are the same (uniaxial, biaxial, etc.) would be the same, but that is clearly not the case.

While Raman spectroscopy for residual stress measurements has many excellent qualities and provides solid qualitative data, finding quantitative data can be more difficult. Extra care has to be taken with the measurements to assure that as many variables as possible are removed to assure the data is as accurate as possible.

2.5. Materials

This work focuses on ceramic and semiconductor materials. Through working closely with industrial partners, the following materials were identified as good candidates to measure the effect of machining on residual stress.

a. Silicon

Silicon is a widely used material in the electronics and optics industry, and has been extensively studied. Silicon features a diamond structure, as seen in Figure 16 [37].
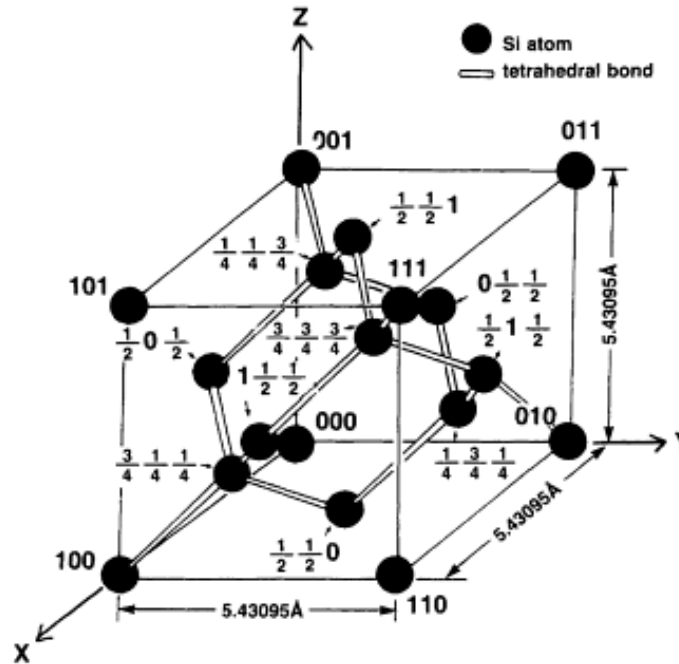
Figure 2.13: The crystal structure of Silicon from [37].

Silicon also undergoes a complex phase change under pressure, which is important in the current study because of the high pressures encountered during machining, as can be seen in Figure 17. Depending on the rate of unloading, the phases will go through a different pathway. It was also found that at smaller cut depths more amorphous silicon is present while at deeper cuts more Si-XII, Si-III and Si-IV was found. It was postulated that the smaller cuts had less stress associated with them, which leads to faster unloading, and hence the amorphous silicon.
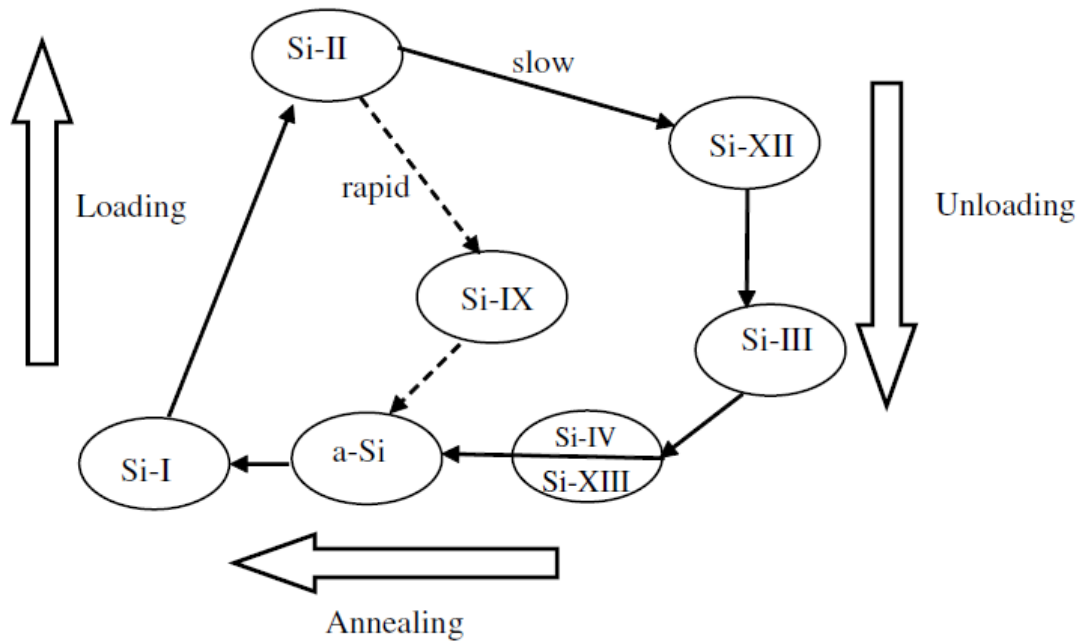
Figure 2.14: Diagram of how silicon transforms phases upon loading and unloading.

Figure from [38]

Silicon is extensively used in the electronics and computer industries. Silicon solar panels are currently the one of the most used solar technologies in the world, and they also have the highest efficiency [39]. Also, most "semiconductor and microelectronic devices" are built on silicon wafers [40].

Previous work has been done on silicon to relate stress to a peak shift in the Raman spectra. In this work the equation from Weinstein and Piermarini [41] is used. It is modified in the style of [42] to remove the quadratic term and change the unstressed peak shift. It becomes

(2.33) $\omega = \omega_o + 0.52P$

Here, ω is the peak position, ω_o is the unstressed peak position, and P is the stress.

b. Sapphire

Sapphire is the clear, single crystal form of the ceramic alumina. Alumina is one of the most widely and diversely used ceramic materials, and as such it has been extensively studied. Alumina has numerous polytypes including $\alpha,\eta,\delta,\chi,\theta,\rho,\gamma,\kappa$[42], β, and β'' [44]. α-Alumina, a very common form, has a corundum crystal structure, with alternatively stacking A and B planes as seen in Figure 18 [42].
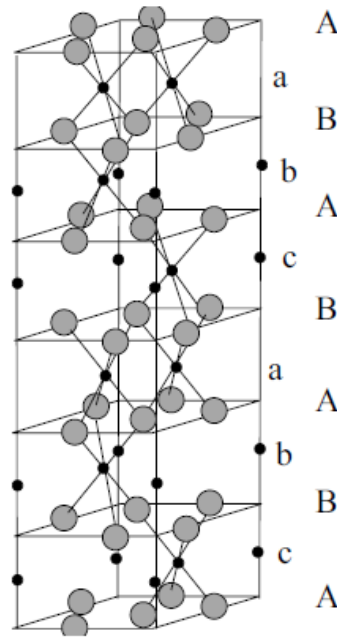
Figure 2.15: Crystal structure of α-alumina. The small circles are aluminum, while the large circles are oxygen. Figure from [42]

Alumina has a variety of uses including "firebricks, abrasives, and integrated circuit (IC) packages" and its production exceeds 45 million tons [42]. β, and β''alumina are "high temperature solid electrolytes", and has applications in "energy storage, alkali-metal thermal-to-electronic conversion (AMTEC) cells, and gas sensors" [44].

Single crystal α-alumina is generally known as sapphire, and is becoming an important material. Sapphire has high strength and hardness and good wear resistance [45] which combined with its clarity make it an optimal material for windows and domes [46] as well as lenses [47] and LEDs. Sapphires exceptional physical properties mean it can perform in environments that some traditional transparent materials cannot [47].

As previously mentioned, extensive work has been done on aluminas residual stress. In this work, the relations developed by *Gallas, et al.* [48] are used. They describe the shift of the peak at 417 cm^{-1} as:

(2.34) $v = 0.0022x + v_o$

Here, v is the peak position, v_o is the unstressed peak position, and x is the stress in MPa. It has also been found that some vibrations can only be seen with the Raman if the laser is polarized a particular way [36]. Some peaks, and therefore vibrations, are only present when the laser is polarized so it is parallel to the basal plane, while others are only present when the laser is perpendicular to it, as can be seen in Figure 2.16.
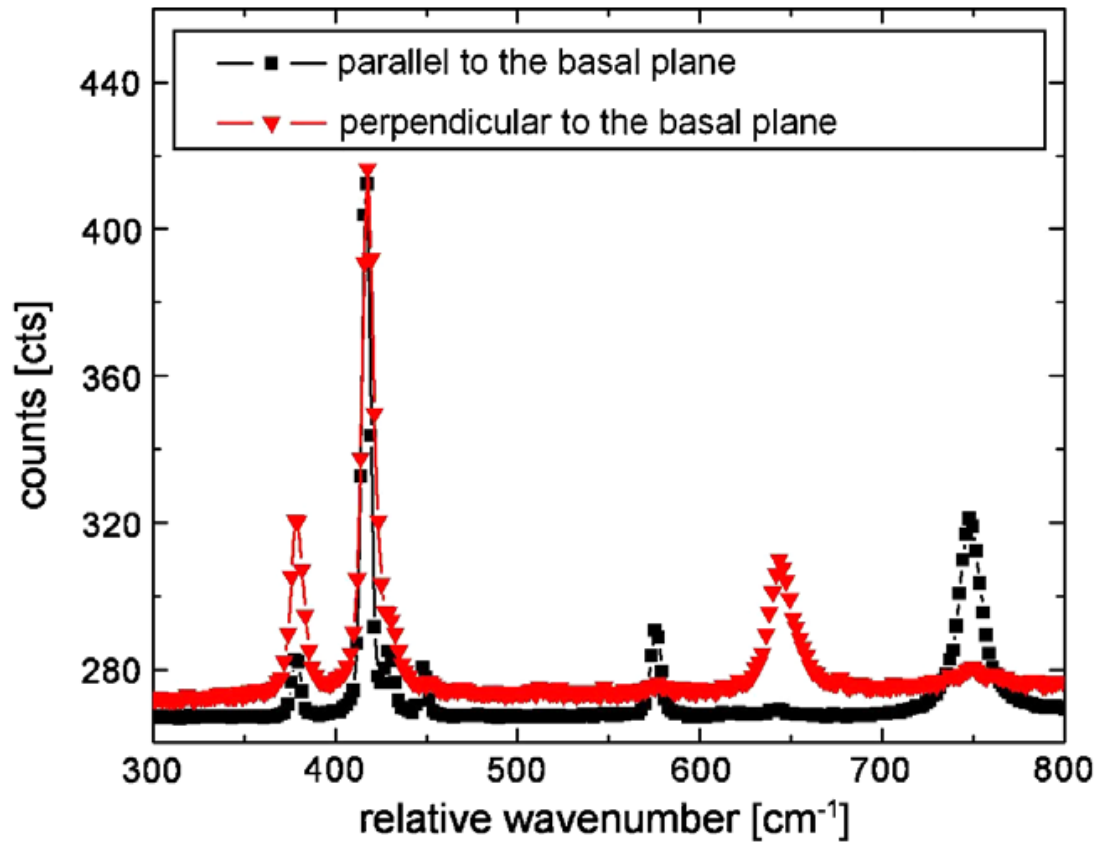
Figure 2.16: Raman spectrum of Sapphire, showing the effects of polarizing the laser

parallel and perpendicular to the basal plane. Figure from [36].

3. Experimental

3.1. Micro-LAM Process

The Micro-LAM procedure combines diamond turning with a laser to produce a unique machining technique. The samples were run either on a modified universal micro tribometer, which is load controlled, or an ultraprecision CNC lathe, which is depth controlled.

The load controlled setup can be seen in Figure 3.1. The sample is machined by a diamond tool tip, which is connected to a laser by a 10µm fiber optic cable. The laser itself can be substituted out to accommodate the needs of the particular material being machined. The turning tool is made up of 2 separate parts, a ferrule and a diamond tip with a 5µm radius, connected with an epoxy that the IR laser can pass through.
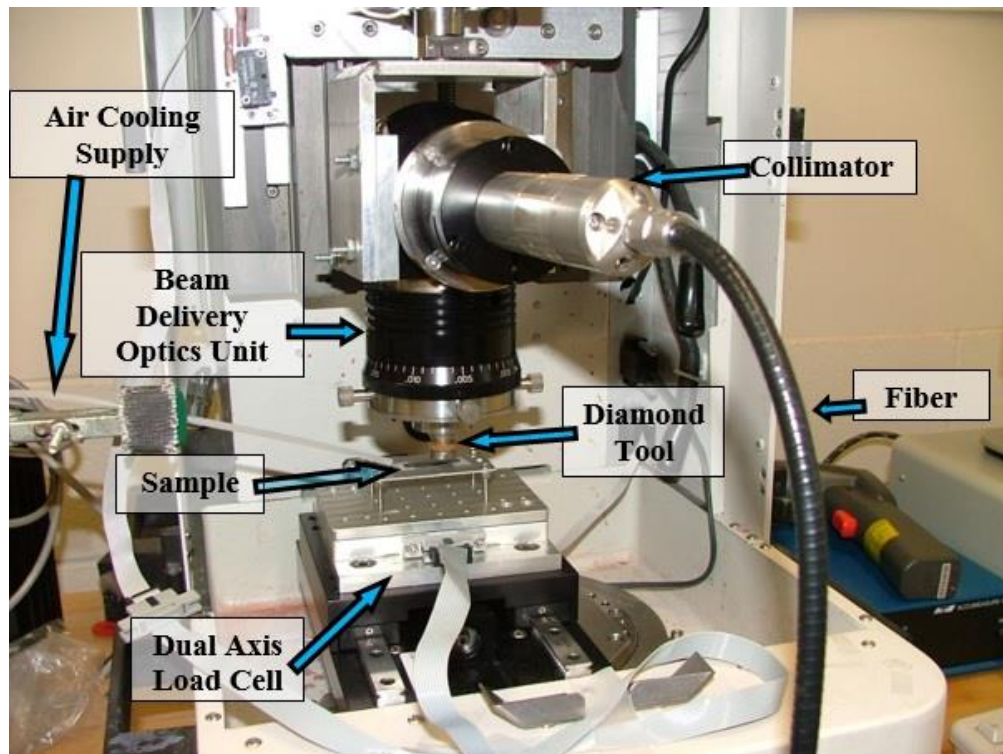
Figure 3.1: Micro-LAM load controlled machining setup.

The depth controlled setup is shown in Figure 3.2. For depth controlled machining, a Precitech N250 ultraprecision CNC lathe is used. This lathe has a 16 picometer resolution, allowing for positional accuracies of 2-4 nm in both the x and y directions during cutting. This machine features air bearings that eliminate metal on metal contact that is seen in other lathes, allowing for more precise control during machining. Meanwhile, the Optimus (Micro-LAM, inc.) system takes all the various parts for connecting the laser to the diamond tip shown in Figure 3.1 and streamlines them into one piece of equipment.
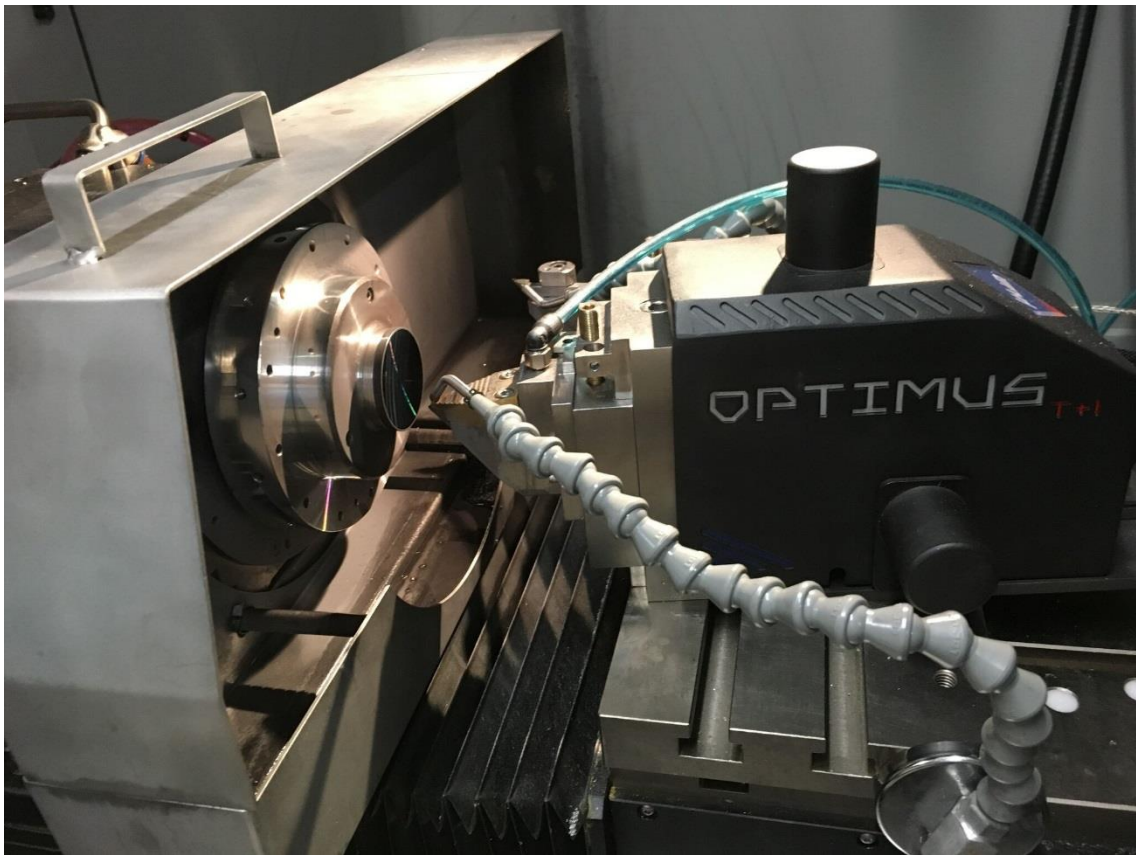
Figure 3.2: Ultraprecision CNC lathe for depth controlled machining.

Since machining using a brittle to ductile transition requires the machining to be above a critical depth, the critical depth needs to be known for the machining to occur

properly. For load controlled machining, a load is entered that allows the diamond tool

bit to remain above this critical depth. The depth controlled setup is preferable;it is less

likely to go below the critical depth due to hitting imperfections in the material, and

requires fewer calculations. It is also stiffer during machining than a load controlled

setup, allowing for better machining.

Samples were machined on these machines with a variety of machining

parameters, including variable laser power, feed rate, and machining load. These samples

were then transported to Rutgers for characterization.

3.2. Raman Spectroscopy

All samples in this study were examined and characterized with micro-Raman

spectroscopy. Raman's accessibility, relatively quick scan times, non-destructive nature,

small spot size, as well as the data that can be gleaned from it, made it the perfect tool.

All spectra in this sample were acquired using a Raman inVia spectrometer using

the Wire 3.4 software associated with the system. First, single crystal control samples

were used to find the baseline peak location for the sample. From there, the scan

parameters for the sample were set, including a wide variety of factors. The particular

laser (in this study either 514 or 633 nm) , as well as the laser's intensity, were chosen.

The laser was set either to "regular" or "high" confocality. When the laser is at the

"high" confocal setting, a virtual pinhole is created using a decreased slit width as well as

a decreased CCD area. This allows for a shallower sampling depth of the material, at the

expense of spectral intensity. Samples, both confocal and regular, with a low intensity required extra acquisitions to achieve necessary intensity.

Samples in this study were examined either with a line scan or a map. With a line scan, a single line of Raman spectrum were taken 2 μm apart. Maps are area scans, with 2 μm scan spacing.

3.3. Spectrum Processing

After the spectra were taken, they were processed with the same Wire 3.4 program used to take them. First, the spectra were baselined, and then any artifacts such as plasma lines were removed. From there the peaks were fit with a series of curves, from which the peak position, width, and intensity could be found.

These numbers were taken and processed in Microsoft Excel. From the change in peak position from the control sample, the stress of the material could be calculated from equations relating the peak shift to stress found in the literature. The peak intensity was used in silicon samples to calculate the relative phase purity of the material, and the peak width was used to look at the relative crystallinity of the sample.

For area scans, these numbers were then taken to Origin which was used to create color contour maps of these properties. This allowed a visual way to track how material properties changed across the sample's surface.

3.4. "Scratched" Silicon Samples

A scratched single crystal silicon sample was provided by Micro-LAM. This

sample contained scratches made with different conditions with the Micro-LAM

machining process. For this sample, 2 loads were used, a 5g load and a 10g load. These

loads were performed with no laser, and laser powers of 10, 20, and 30% of a 1480nm,

400mW laser.
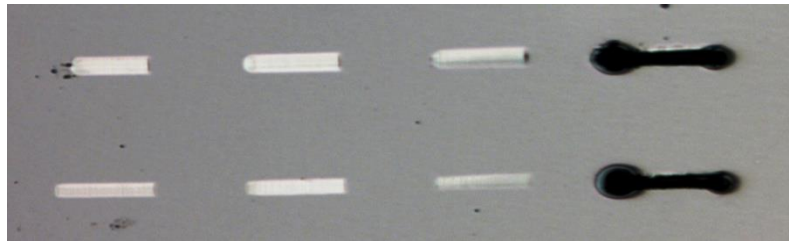
Figure 3.3: Scratches machined at various parameters with the Micro-LAM technique.

The 10g samples are on the top, and the 5g samples on the bottom. From left to right: no

laser, 10% laser power, 20% laser power, and 30% laser power.

Load (g)	Laser Power (W)	Length (µm)	Width (µm)	Depth (µm)
	n/a		21.3	54.6
5	10%		21.7	61.0
	20%	100	21.9	64.0
	n/a		26.9	75.8
10	10%		27.2	79.0
	20%		28.4	86.2

Table 3.1: Machining parameters and scratch dimensions.

The samples were all examined with Raman spectroscopy to look at the residual

stresses and phases present. A line scan running down the center of every scratch was

performed with 2 µm spacing with both the 514nm and 633nm lasers. The spectra were

then fit with the Wire 3.4 software(the software that (is?) associated with the Renishaw spectrometer responsible for running it and for data analysis), and from there the residual stresses were found. These residual stresses were averaged by taking 16 of the stresses in the center of the cut (to avoid any abnormal stresses from loading or unloading the scratch on the ends). Further, the 5 gram load with 10% laser power were mapped over their entirety with both laser settings. Again, the spacing between the points was 2µm.

3.5. Silicon Carbide Roughness Measurements

A Dektat Alpha Profiler was used to measure the surface roughness of the silicon carbide tiles, and the same machine was used to calculate the R_a values of the tiles.

4. Relating Residual Stresses to Machining and Finishing in Silicon Carbide

Benjamin P. Groth[a,b], Sean M. Langan[a], Richard A. Haber[a] and Adrian B. Mann*[a,c]

[a]*Materials Science and Engineering Department, Rutgers University, 607 Taylor Road, Piscataway, NJ08854, USA.*

[b]*Now at: Vesuvius USA, Pittsburgh, Pennsylvania, USA.*

[c]*Biomedical Engineering Department, Rutgers University, 599 Taylor Road, Piscataway, NJ08854, USA.*

*Corresponding author, T:1-848-445-8421; F:1-732-445-3258; email:

abmann@rci.rutgers.edu

Abstract: Machining and surface finishing is essential in the processing of many ceramics, however, it can be detrimental to subsequent performance as it introduces residual stresses and structural defects. Using micro-Raman spectroscopy the residual stress and crystallinity of hot-pressed SiC tiles was examined after finishing with several different methods. 514 nm and 633 nm lasers in both conventional and confocal settings enabled stress as a function of depth to be assessed. Single crystal, electronics grade SiC was used for comparison. Compressive residual stresses were present at the surface and in the sub-surface region in all the samples, but the surface with lowest roughness and a mirror-like finish had the highest residual stress. Crystallinity in SiC is reduced by defects and stacking faults produced during machining and finishing. The finer surface finishes had higher residual stresses, but were actually found to have better crystallinity than the rough surfaces. The dependence of residual stress and crystallinity on surface roughness is attributed to a change in the mode of ceramic removal from energetic and brittle for rough finishes to ductile for the shallow cuts of smooth finishes. The

dependence of stress and crystallinity on roughness means a balance must be struck between smoothness, crystallinity and stresses in choosing the best finish for a given application.

Keywords**:** A. Finishing; B. Spectroscopy; D. SiC; E. Armor.

1 Introduction

1.1 Silicon Carbide

Silicon Carbide is of great importance as a structural ceramic as it is amongst the hardest materials known [1]. As such, machining SiC parts into the required shape and form for a given application can be difficult and may yield unwanted defects. Whether the pieces are machined by grinding and polishing, laser-assisted techniques, or ultrasonic techniques [2], the potential for residual stresses to form at the surface is always present. It is important to know how much stress machining can impart to components, since this stress may be either detrimental, leading to early failure, or advantageous, by helping to toughen the component.

Silicon carbide's crystal structure consists of tetrahedra of either 4 Si atoms and 1 C atom, or 4 C atoms and one Si atom [3]. The tetrahedra can be stacked in either parallel or anti-parallel sequences, and this stacking allows for SiC to take on many different polytypes. The most common polytypes are a cubic structure known as 3C (or beta-SiC) and 2 hexagonal phases 4H and 6H, known as alpha-SiC. Each polytype has slightly different mechanical, optical and electronic properties that make them useful for specific

applications for instance as armor ceramics, power electronic semiconductors or industrial abrasives [4]. As a result of their different structures each polytype has its own unique Raman spectrum. This makes Raman spectroscopy very useful for characterizing variations in polytype within a sample and, significantly for the current study , changes in the Raman peak position can be related to strains (and hence stresses) in the SiC [5,6].

In single crystal SiC, stress concentrators take the form of micropipes [7,8] and dislocations [8]. For some applications what is more detrimental than the increased stress is the fact that these features often impinge on electronic properties and therefore performance when used as single crystal semiconductors. As electronic properties are less important for bulk polycrystalline samples used in structural applications this effect is not so significant, nonetheless when machining SiC it is important to limit the defects so they are not able to act as stress intensifiers. In bulk, polycrystalline samples, stress points can come from processing inclusions and thermal stresses [9,10] created during hot-pressing or heat treating. If the density of defects is large enough, different polytypes with mis-matching lattices are formed or stacking faults are present it can also cause a significant stress in the sample [11,12]. Machining can further augment these stresses by introducing more stacking faults and increasing the defect density.

1.2 Raman Spectroscopy:

Raman spectroscopy is a form of vibrational spectroscopy that relies on inelastic scattering of monochromatic light to provide vibrational, rotational and other low-frequency mode information about a material system [13]. Data obtained from Raman

spectroscopy comes in the form of a vibrational spectra. For a given material system, this spectrum will be unique, and contain information related to bonding between atoms within that system. The theory and fundamentals of Raman have been discussed at great length elsewhere [13-15], as well as the ability to use Raman as a stress measuring tool [16-21]. In the case of silicon carbide the numerous polytypes that can form all have unique Raman spectra. This allows for easy characterization and distinction between polytypes, as seen in Figure 4.1. The use of Raman to measure stress in silicon carbide has been examined quite thoroughly. However, these experiments have been done mostly on the cubic, 3C, polytype [12,22-28] because of its importance and wide usage in the power electronics field. Only a few papers [5,6,29] discuss the use of Raman for stress analysis in 6H-SiC. In the current study we have focused on the equations developed by Liu and Vohra [5,6] for analysis of data as these are widely accepted for use on 6H silicon carbide.
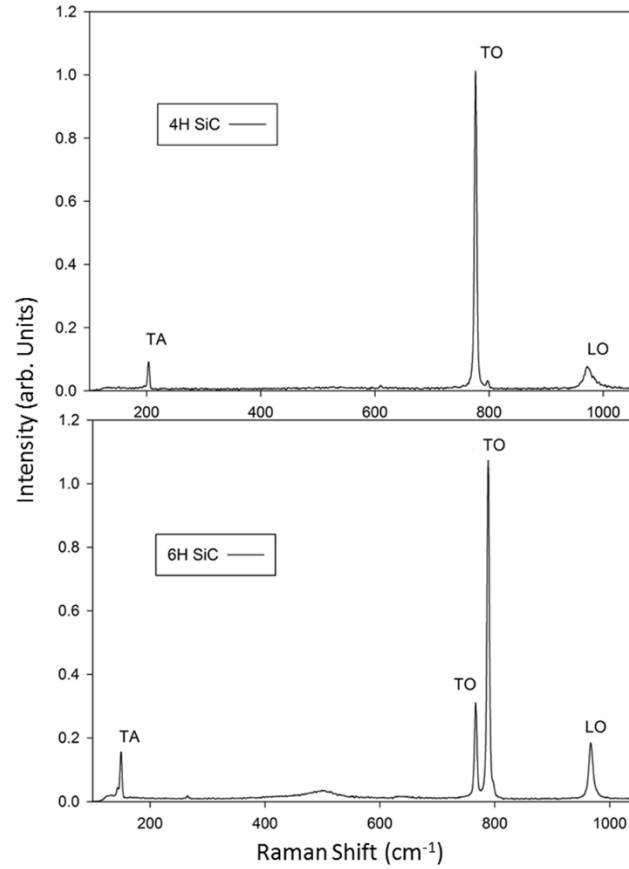
Figure 4.1: Sample spectra for 4H-, and 6H-SiC. The variation in both position of optical phonons and unique acoustic modes allow for characterizing different polytypes. Peaks are designated by their propagation direction, with TO, TA and LO being transverse optical, transverse acoustical and longitudinal optical, respectively.

The micro-Raman system used in the study was an inVia™ from Renishaw Inc (New Mills, Wotton-under-Edge Gloucestershire, GL12 8JR, UK) with 633 nm and 514 nm lasers. The instrument's resolution in terms of deconvoluting overlapping peaks is on the order of 5 wavenumbers with a precision of 0.05 cm^{-1}, and an accuracy of 0.25cm^{-1}. This means that peaks closer than 5 cm^{-1} could not be deconvoluted, however for the peaks of interest in silicon carbide this is not an issue. The penetration of the laser into

the sample and hence the depth from which information is obtained is wavelength dependent and a function of the material being investigated. Penetration depth, D_p, can be estimated from the absorption coefficient, α [19]:

$$D_p = \frac{1}{\alpha(\lambda)}$$

where α depends on the wavelength, λ. In the case of SiC the 514 nm wavelength has a higher absorption coefficient than the 633 nm wavelength, which allows for analysis at different depths [30,31].

Penetration depth can be further tuned by using confocal Raman spectroscopy [32-36]. This involves the beam being focused with a numerical aperture, and then shone onto the sample. A confocal aperture, which can be a physical pinhole or a "virtual" pinhole, acts like a slit to block the path of some of the reflected beam. This allows only photons from a narrow focal plane to be focused on the detector. For non-confocal Raman spectroscopy the beam interacts with the sample at a range of depths and all of these are detected by the Charge Coupled Device (CCD) camera, but with the confocal feature light from only a narrow range of depths below the material's surface is sampled; the confocal aperture excludes light from higher and lower depths. This allows each laser available to the Raman operator to be used for two depths settings: a normal depth setting that goes farther into the sample and a confocal depth setting closer to the sample's surface. By combining multiple lasers in their normal and confocal modes, four depths for each sample have been investigated. These are, in order of increasing penetration: confocal with 514nm laser; confocal with 633nm laser; non-confocal 514nm laser; non-confocal 633nm laser. The approximate, respective, penetration depths for each setting

are given by the absorption properties of sintered SiC [14] as, respectively, 1.5 µm, 2 µm, 3 µm and 3.5 µm.

2 Materials and Methods

2.1 Material Preparation

Four silicon carbide tiles (SiC-N by Cercom®) cut from a larger billet of hot pressed alpha-SiC with 6H structure and grains of ≈ 4.1 □m in size were provided by the Army Research Laboratory, Aberdeen Proving Grounds, MD for this study. The tiles were several millimeters in thickness and had standard, rotary ground, mirror finish and grit-blast surfaces, respectively, on one side. The standard finish, Figure 4.2(a), was obtained after a surface grind and light sand blasting of the hot pressed SiC-N tile. The sand blasting removed any carbon on the tile surface left over from the pressing process which uses a graphite sheet to minimize the interaction with the die. The reverse side of the tiles was finished in the same manner as the standard sample, essentially as-pressed with minimal finishing, and the two were optically similar in appearance. To ensure that the initial states for each of the tile surfaces where consistent the reverse side of the tiles was used as a baseline. The expectation was that each of the reverse sides and the standard finish would have the same initial stress. The grit blast samples were impacted with fine steel shot which, as it can be seen from the SEM image in Figure 4.2(b), gives significant deformation on the machined surface of the tile. The rotary ground samples, Figure 4.2(c), were taken from the as-pressed state to their finished state through the use of diamond grinding wheels, running on a rotary grinder. The mirror polish samples were taken from the as-pressed state to a mirror-like finish through the use of successive

polishing with finer and finer diamond abrasives. The mirror finished sample displayed the lowest amount of surface roughness with $R_a \approx 14\pm3$ nm compared to $R_a \approx 483\pm34$ nm for grit blast, $R_a \approx 264\pm41$ nm for rotary ground and $R_a \approx 236\pm25$ nm for standard finish. Single crystal samples for comparison to the tiles of 6H-SiC (0001) were obtained from MTI Corporation, Richmond, CA 94804, USA. These had roughness of $R_a < 1$ nm and the Raman data suggested that they were essentially stress-free at the depths being studied during the testing.
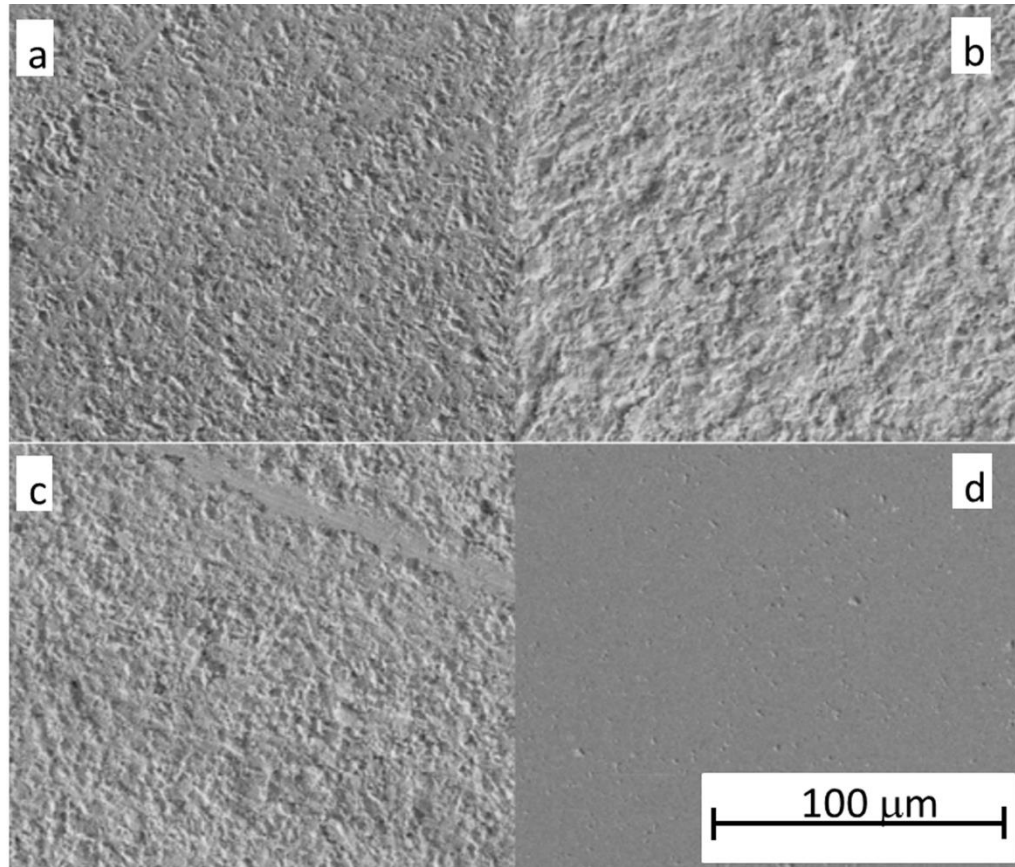
Figure 4.2: SEM images of the machined surfaces for the a) Standard, b) Grit Blast, c) Rotary Ground, and d) Mirror Finish.

In order to evaluate and quantify the stress in each sample due to machining Raman maps were created from measurements obtained at points spaced 2 µm apart over 40 µm x 40 µm areas. This size was set based on the capabilities of the Raman system and to avoid spatial overlap of the Raman signal. The Raman system was equipped with an 1800 l/mm diffraction grating for both the Ar ion 514 nm laser and the HeNe 633 nm laser. The maps acquired were point maps where at each point a full spectrum was obtained and not just one peak as examined in a line focus map. Maps were acquired on several different areas of each sample's surface and stress values were averaged over all maps. Sample maps can be seen in the results section which shows the differences between each of the surface finishes and also the variations with depth for a given finish. Along with the machined surfaces, maps were created of the tiles' reverse (unmachined) sides.

2.2 Micro-Raman Spectroscopy

Variations in stress with depth were examined using the micro-Raman's confocal settings along with the two different excitation wavelengths. The confocal setting enables the Raman spectra to be obtained at a shallower depth into the sample than with the normal setting. It uses a virtual pinhole, created by slits in the spectrometer path and a decreased CCD scan area, as opposed to a physical pinhole in the laser path or in the microscope. The slits spacing is decreased from 50 µm in the regular setup, to 20 µm in the confocal, in order to limit the angle of returning light that is analyzed. Similarly, the CCD area is taken from 15 pixels down to only 3 pixels; this allows for in-depth spatial resolution at a cost of signal-to-noise ratio. In order to achieve intensity counts similar to those in the regular setting, several scan iterations were performed. With regards to

excitation wavelength the absorption coefficient of silicon carbide increases for shorter

wavelengths, so the 514 nm laser penetrates less than the 633 nm laser. Hence, the

different wavelengths enable stress to be examined at different depths.

Averaged stress and peak width values were obtained from all the data in a scan

for the specified depth of penetration. To extract the values for each penetration depth the

data was weighted based on the penetration of the laser used. For example, the 514 nm

confocal setting has a penetration of ~1.5 µm in the polycrystalline SiC tiles, so for this

configuration the stress and peak width values are a weighted average over the first 1.5

µm of depth. For the 633 nm confocal setting the penetration is greater (~2 µm) and the

values of stress and peak width from 1.5-2 µm depth are obtained by subtracting the

values for the 514 nm confocal setting. The other penetration depth values are found

similarly: for the 514 nm regular setting the values at a penetration depth of ~3 µm are

found; for the 633 nm regular setting at a penetration depth of 3.5 µm.

2.3 Analysis of Raman Data

The Raman spectral data was processed using the WiRE3.2 software available

from Renishaw. Spectrum intensities were normalized to the largest intensity peak, the

transverse-optical (TO) peak at $789.2cm^{-1}$, and corrected for baseline. Curve fitting was

performed using the software's curve fit feature, with curve parameters set to allow

mixed Gaussian-Lorentzian behavior. These parameters were saved and applied to each

spectra in the acquired maps, and peak position and width information for the TO peak

was extracted for each map point. These values were used to create a contour plot of peak

shift and an average value for the peak width over the mapped area. Peak shift values were then turned into stresses using:

$$\nu_{TO} = 3.11P + 789.2$$

where P is applied pressure, ν_{TO} is the measured TO peak position, and the value 789.2 is the unstressed peak position for the TO peak in cm^{-1}. This is a modified version of the equation developed by Liu and Vohra [5,6]. They investigated ultrahigh pressures where a quadratic term is needed; this term is negligible for the stresses seen in the current study. The use of this equation to relate stress to shift in a Raman peak assumes that the samples have no preferred crystal orientation; this was confirmed by X-ray diffraction (XRD) studies of the tiles which showed no evidence of texture. A Bruker AXS Inc., WI 53711-5373, USA, HiStar™ system with a 2D array detector, and Cu radiation with a 0.05mm diameter collimator was used for the XRD studies.

3 Results

   3.1 Single Crystal

   Raman maps taken over the unstressed single crystal silicon carbide showed no significant peak shift which is consistent with it being unstressed at the depths of interest. The peak position values obtained were statistically close to the accepted average value of 789.2 cm^{-1}, for the TO peak [5], having deviations less than 0.05cm^{-1} from the average over the mapped section. The penetration depth is large for single crystal 6H-SiC and on the order of 10μm based on absorption coefficients from Werheit and Schwetz [14]. The spectra acquired at each map point are weighted averages from the surface to the

specified depth in each sample. Peak width values were also collected and averaged over the map area to provide a baseline peak width for comparison.

3.2 Machined Samples

Peak shifts due to machining are typically to higher wavenumbers, as shown by the example of Figure 4.3, which corresponds to compressive stress. However, relatively small tensile stress regions are occasionally seen in localized areas. A stress value was found for each of the four surface finishes by averaging over all the data points on all of the Raman maps collected. These average were always relatively large and compressive. For the minimum penetration depth (confocal setting with 514 nm wavelength) the average stresses were: -220 ± 25 MPa for the standard finish; -371 ± 27 MPa for the grit blast sample; -485 ± 33 MPa for the rotary finish; -601 ± 38 MPa for the mirror finish. Raman maps for all 4 samples at each setting (514/633 nm wavelength, confocal/normal setting) are shown in Figures 4.4, 4.5, 4.6 and 4.7. In comparison, the Raman data for the reverse sides of all tiles showed a very uniform average stress of -208 ± 21 MPa with little variation with depth. Within the margin of error this was the same compressive stress as that seen for the sample with the standard finish.
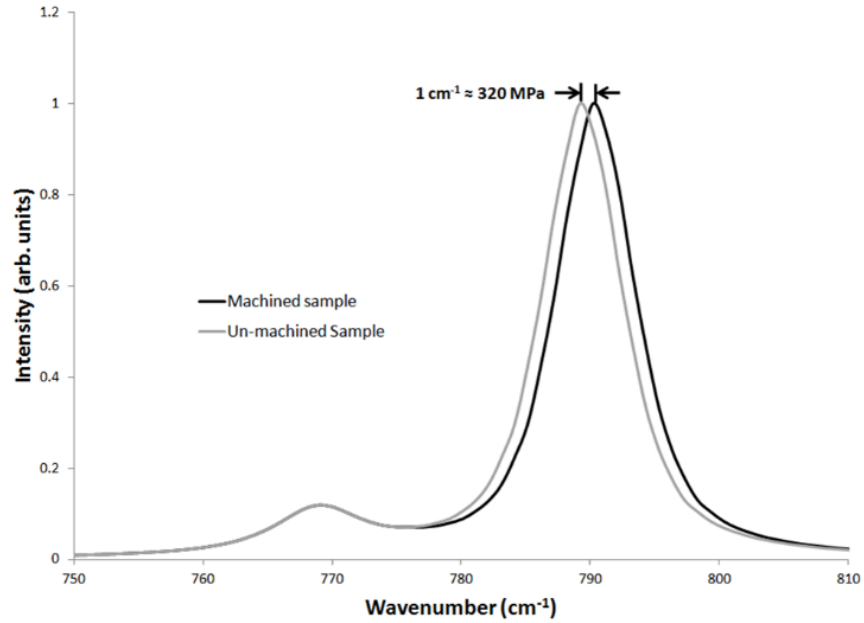
Figure 4.3: Example spectra showing shift in peak position for a machined SiC sample compared to the ideal unstressed (single crystal) Raman spectrum. The peak shift of one wavenumber corresponds to a residual stress of ~320 MPa. In this case it is compressive as the peak shifts to the right.
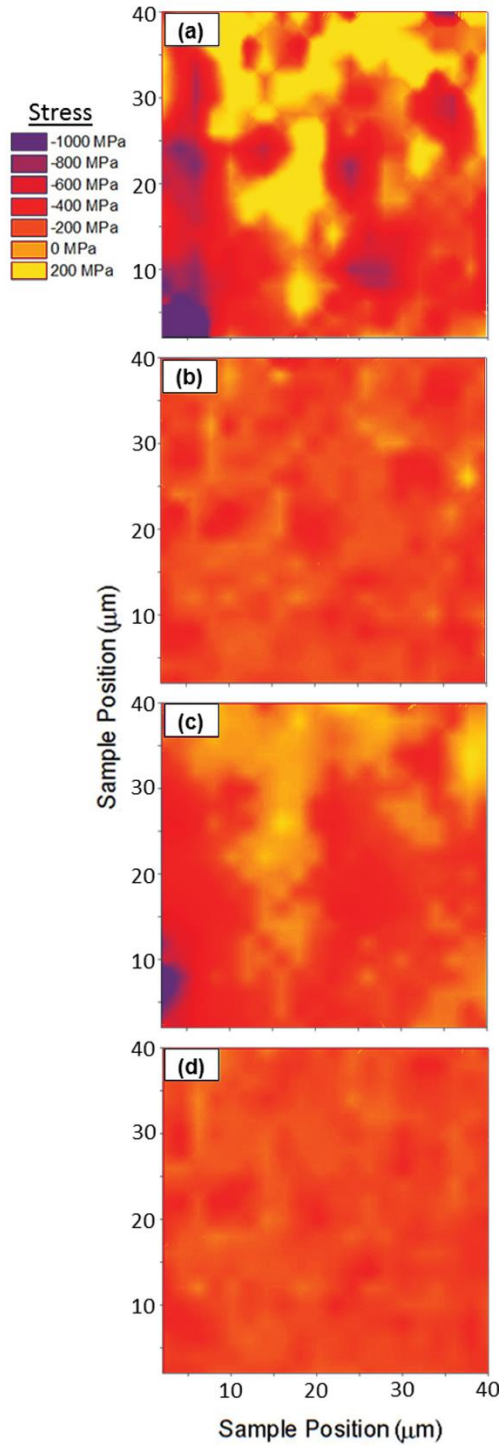
Figure 4.4: Stress maps of the standard finish sample at a) 514nm confocal, b) 633nm confocal, c) 514nm regular and d) 633nm regular settings. The same area is shown in each image.
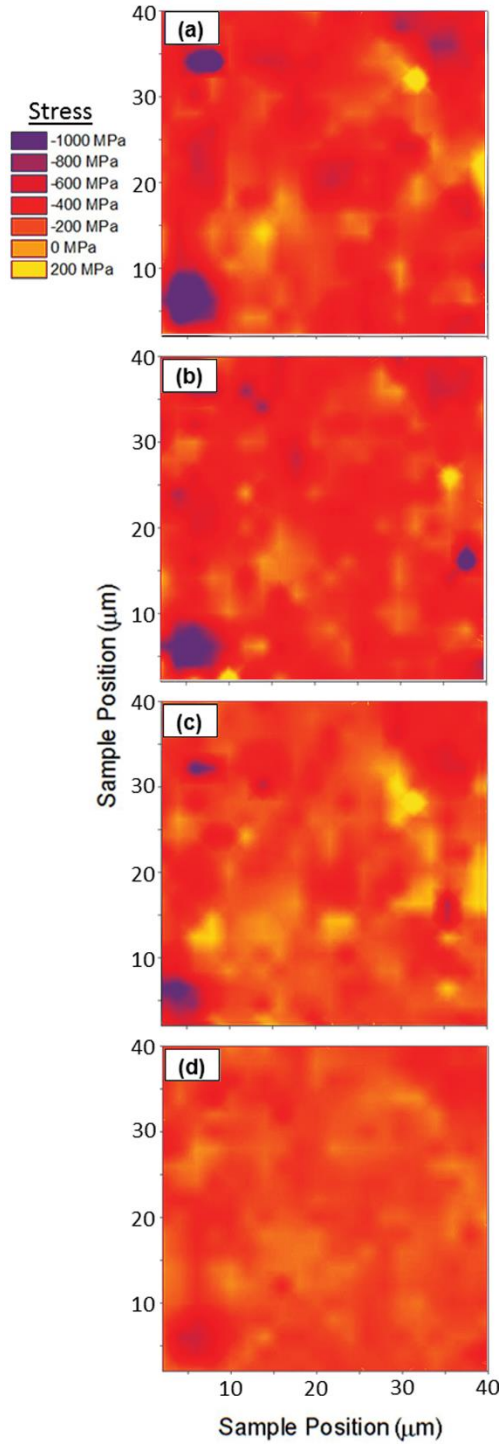
Figure 4.5: Stress maps of the grit blast sample at a) 514nm confocal, b) 633nm confocal,

c) 514nm regular and d) 633nm regular settings. The same area is shown in each image.
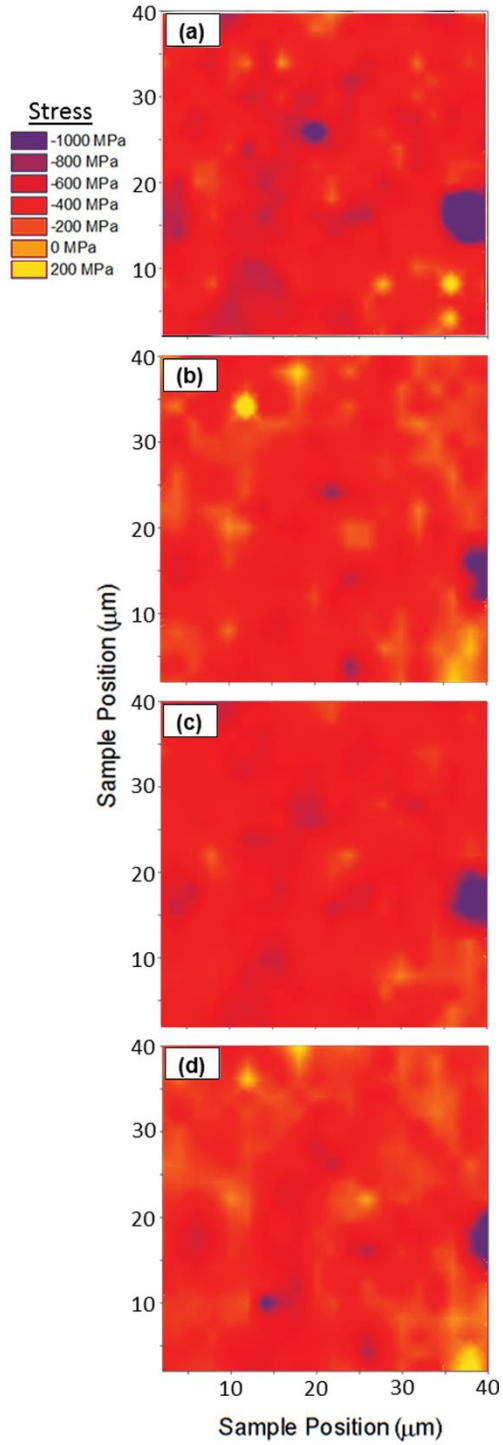
Figure 4.6: Stress maps of the rotary ground sample at a) 514nm confocal, b) 633 confocal, c) 514 regular and d) 633 regular settings. The same area is shown in each image.
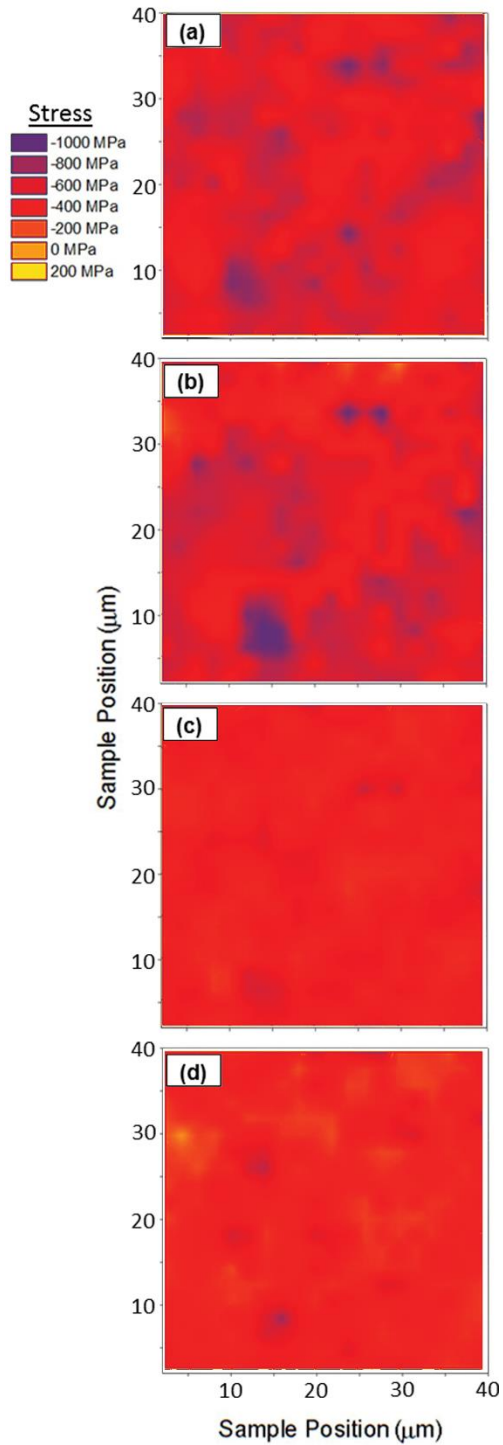
Figure 4.7: Stress maps of the mirror finish sample at a) 514nm confocal, b) 633

confocal, c) 514 regular and d) 633 regular settings. Same area is shown in each image

For each of surface finishes there was considerable variation in stress over each map, though it was least for the standard finish. As the penetration depth increased there was a marked reduction in the range of the stresses measured and also in the average stress over the mapped area. For all of the surfaces except the standard the average stress value dropped by 25-35% between the shallowest confocal setting and the deepest regular setting. This indicates that the machining stresses decrease with depth from the surface. This stress gradient is greatest in the mirror finished sample, but is practically non-existent in the standard finish sample. Figure 4.8 shows the average stress value of each sample at each of the four depth settings. Also plotted on Figure 4.8 is the average stress over the surface for the single crystal SiC (stress $\approx$ 0 MPa). The standard sample and the reverse sides show a consistent stress level with depth (only the standard sample is shown on the Figures as the reverse sides were essentially the same).
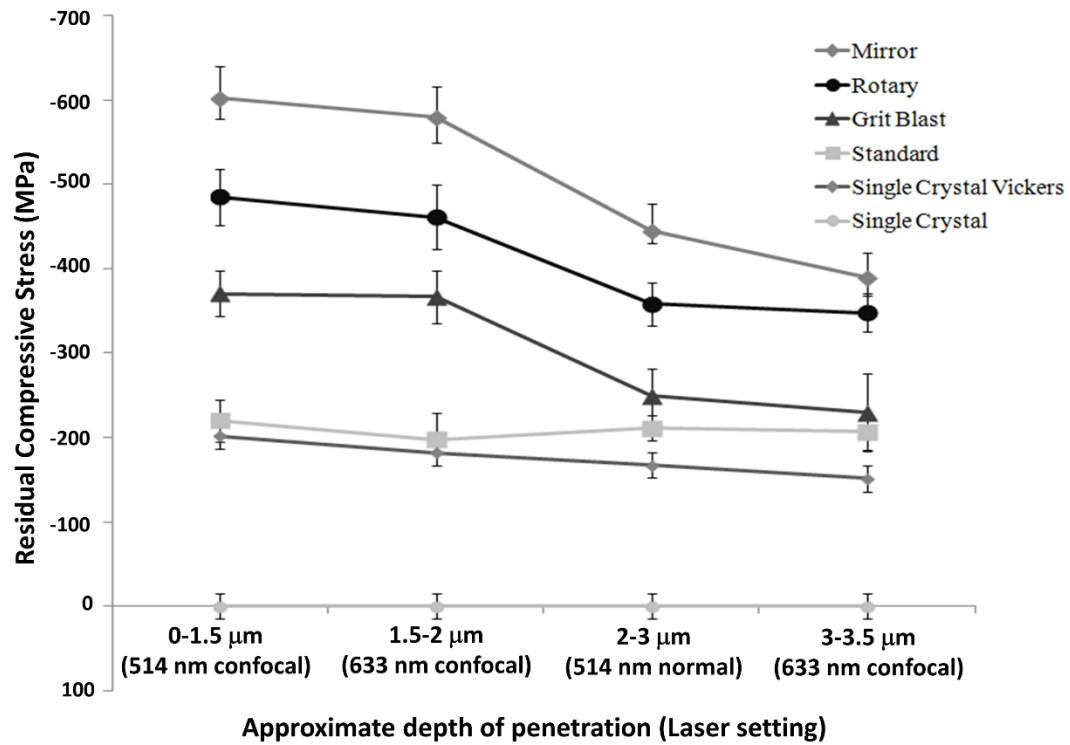
Figure 4.8: Plot of residual stress values in all samples as they vary with depth.

Analyzing the TO peak width (which is related to crystallinity) showed that the samples split into 2 groups: the grit blast and rotary finish showed similar and higher average relative width values of 1.8 cm^{-1} for the shallowest depths (514 nm wavelength and confocal setting); the standard and mirror finish samples showed peak widths of 1.5 cm^{-1} for the shallowest depths. These values were normalized with respect to the average width values of the single crystal SiC, at the respective depth settings. The width values for all of the samples at the different laser and confocal settings can be seen in Figure 4.9. All of the samples tend towards a single relative peak width value as the penetration depth increases. A sample Raman spectrum showing the variation in width, as well as peak position can be seen in Figure 4.10.
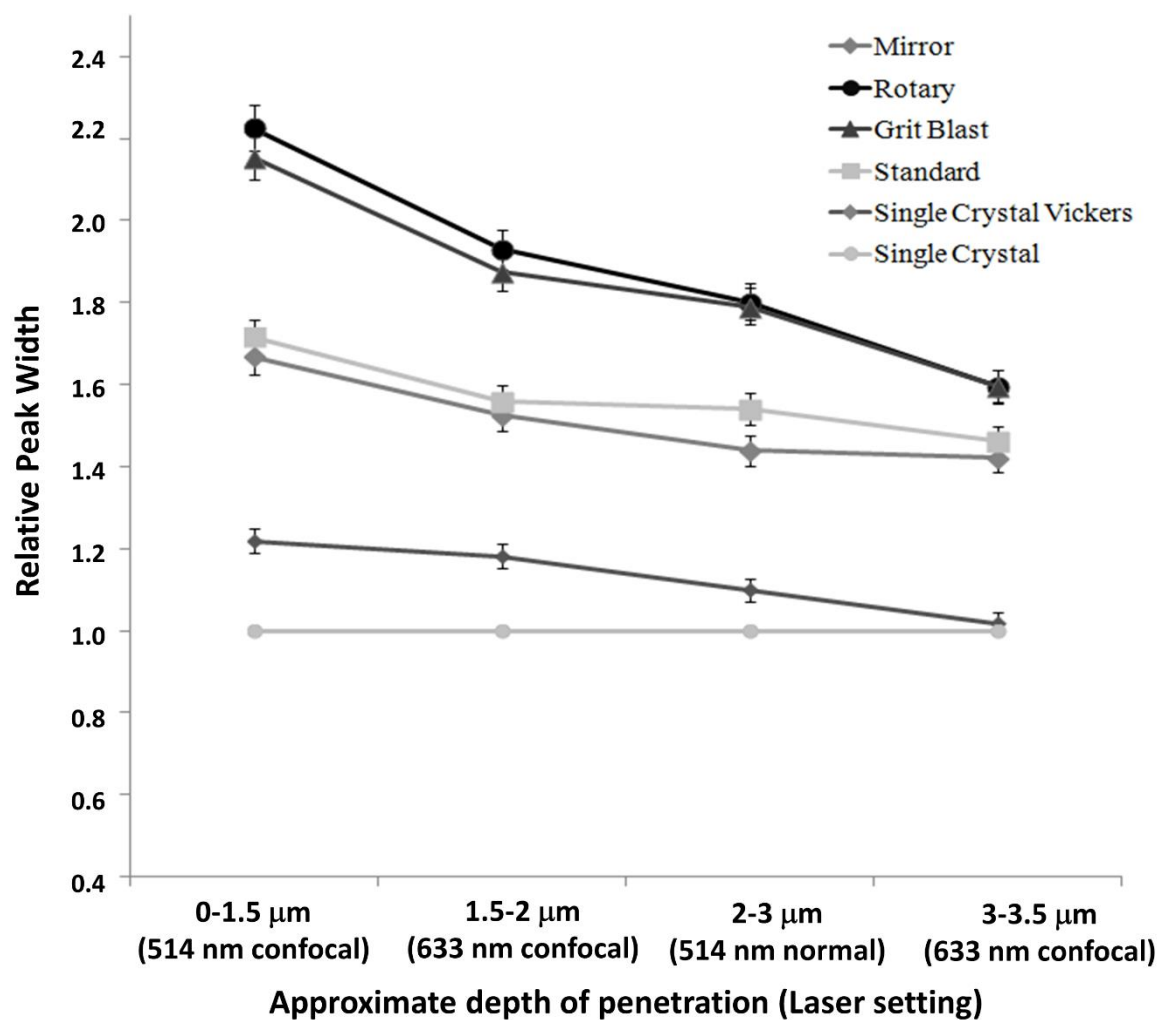
Figure 4.9: Plot of relative peak widths for all samples as they vary with depth.
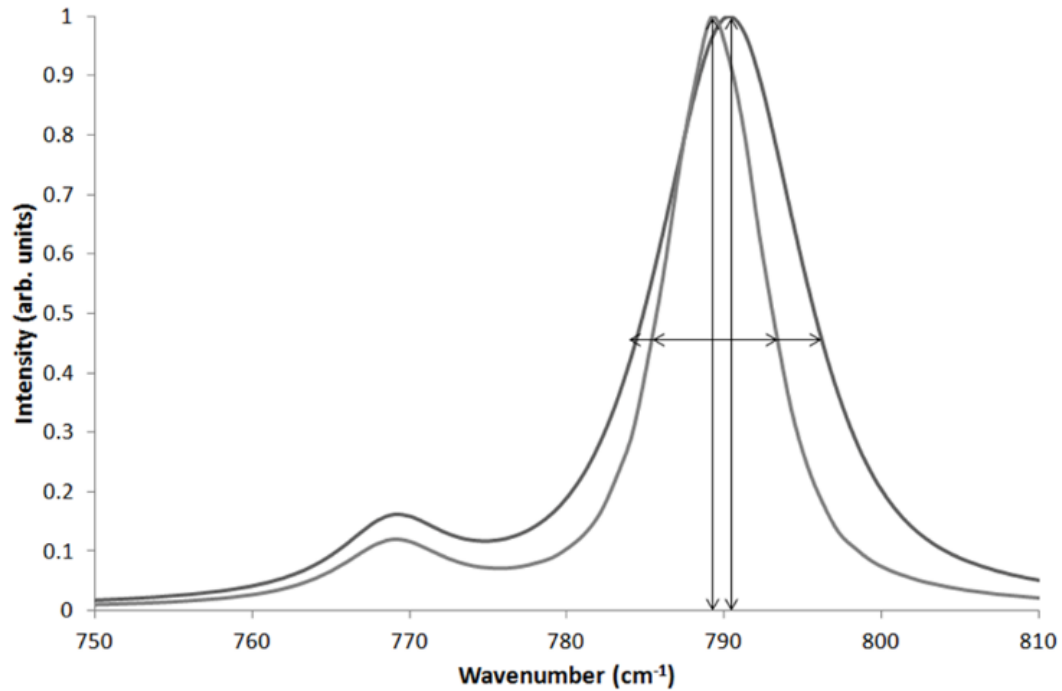
Figure 4.10: Typical spectra showing peak position and peak width variations seen. The peaks located at ~768cm^{-1} are mostly invariant, while the TO peak at 789.2cm^{-1} can both broaden and shift.

4 Discussion

The machined stress values in each sample show a linear trend towards a baseline residual stress value, which is that of the unmachined, reverse sides. The intercept of the trendline with the baseline residual stress value gives an approximate maximum depth at which the machining process has affected the sample. For the higher stressed mirror finish and rotary ground samples, this value is 6.6 ± 0.5μm and 6.6 ± 0.7μm, respectively. In the grit blast sample, this value was lower, at 4.4 ± 0.4μm, indicating that the deformation and stress concentration was much nearer to the surface. In shot peened or grit blasted samples the deformation generally tends to be nearer the surface as the intent is to apply residual compressive surface stresses from densification in the impacted

regions. In single crystal samples it should be noted that given the very low absorption coefficient of 6H-SiC, and the wavelength dependence of this coefficient, there was no wavelength that could be used to analyze the shallowest depths with Raman spectroscopy. There are z-scan techniques that utilize through-focus scanning to get depth resolution, but the depth estimation falls off quickly even with small below-focus step sizes [15].

An analysis of the peak width data shows that all for the machined samples the trend with increasing penetration depth is towards the baseline width value of the unmachined side. There is a relationship between stress and peak width [5,6,38], but in this case the differences in peak width data and stress between the samples do not closely follow each other. Specifically, the mirror finish has less effect on peak width, and therefore crystallinity, than it does on residual stress. Grit blast and rotary ground, however, both increase the peak width considerably, but give less residual stress than the mirror finish; substantially less for the grit blast sample. Thus, it could be misleading to just consider residual stress as an indicator of surface and sub-surface damage and, likewise, it could be misleading to just consider changes in peak width. For a given application either or both could be detrimental to the ultimate performance of the SiC-N.

SiC is anisotropic and for the machined samples studied the stresses introduced are likely to be anisotropic and bi-axial (or possibly even tri-axial). However, the tiles tested consist of randomly-oriented polycrystalline SiC, this eliminates many of the effects on peak shifts due to anisotropy. Consequently, the peak shifts are close to those that would be seen under hydrostatic stress, and any difference in the magnitude of stresses with direction will be relatively small compared to the overall shifts in the

Raman peaks. As a result using equations for isotropic samples under hydrostatic

pressure to obtain stress measurements from Raman is valid for the four surface finishes

studied. In the case of the single crystal sample the material is truly anisotropic

elastically, however the Raman measurements shows no sign of a peak shift in the

pristine surface so the method of quantifying stress does not seem to be an issue in this

case. Though it was not used in the current study a polarized analysis of the Raman

spectra would have given more information on any anisotropy present. Overall, issues

related to anisotropy in the samples might be expected to introduce a small error in the

stress per wavenumber shift (GPa/cm^{-1}) when using the purely hydrostatic stress model.

However, the comparative data, specifically between different machining methods, and

the data with respect to changes in stress with depth remain valid for the samples studied.

There are limits to the ability of micro-Raman as used in this study to characterize

the stress state, in particular whether hydrostatic, biaxial or triaxial stresses are present.

This does not distract from the significance of the results in showing that surface damage

from machining extends many microns below the surface in SiC-N tiles, and the extent of

the damage is a function of the machining methods used. Specifically, the data shows that

there is a tendency for finer surface finishes to result in greater compressive sub-surface

residual stresses, but to give less crystalline disorder when compared to coarser and more

energetic surface finishing methods, such as rotary grinding and grit blasting.

5 Conclusions

The combination of pressure and shear stress inherent in all machining processes

introduces large, compressive residual stresses that persist to a depth of 3.5 µm or more.

The type of machining and finish (grit blast, rotary or mirror finish) was found to affect the magnitude of the average stress at all the depths examined. In this respect the grit blast caused the lowest total increase in stress at all depths, while the mirror finish created the largest stress at all depths, with the rotary finish lying between them. For all the machined samples the average compressive stress was found to be noticeably higher in the first 2 μm below the surface when compared to greater depths. In the case of the mirror finished sample the first 2 μm exhibited extremely high compressive stresses averaging over 600 MPa, with localized peaks close to 1000 MPa. For all the samples there was considerable variation in the magnitude of the stresses over the surface, as shown by the stress maps. This scatter was found to be greater at the shallowest depths examined for all the finishes. The mirror finish gives the most pronounced increase in compressive stress and this is taken to be a result of polishing with fine abrasives.

Silicon carbide 6H has a strong transverse optical peak at 789.2cm^{-1} the width of which can be used as a measure of "crystallinity" or disorder in the crystal structure. This disorder was found to increase with machining, with the increase most pronounced close to the surface. Intriguingly the effect on crystallinity was less pronounced for the mirror finish than for the rotary grind and grit blast surface. Thus, the fine polishing associated with producing a mirror finish gives rise to larger residual stresses, but less disorder in the crystals when compared to the coarser finishes. Fracture mechanics predicts that for finer abrasives with lower depths of removal ductile deformation dominates [39]. The observed differences in residual stress and crystallinity can be explained by, firstly, the transition from brittle deformation for coarser surface finishes to ductile deformation for

finer surface finishes and, secondly, the tendency of more energetic surface finishing methods (rotary grind and grit blast) to introduce defects such as stacking faults in SiC.

Depending on the specific application of the ceramic the changes in crystallinity indicated by the increased peak width may ultimately be as significant in determining the sample's performance as the residual stresses generated by the different machining methods. Thus, the method chosen for finishing the surface should be selected based not only on the roughness required, but also the residual stress and crystallinity that is needed to avoid premature failure.

6 Acknowledgements

7 References

1. K.A. Schwetz, Silicon Carbide Based Hard Materials, in: R. Riedel (ed), Handbook of Ceramic Hard Materials, Wiley-VCH Verlag GmbH, Weinheim, Germany, 2008, pp. 683-748.

2. I.D.Marinescu, Handbook of Advanced Ceramic Machining, Taylor & Francis Group, Boca Raton, 2007.

3. D. Lundquist, On the Crystal Structure of Silicon Carbide and its Content of Impurities, Acta Chem. Scand. 2 (1948) 177-191.

4. S. Saddow, A. Agarwal, Advances in Silicon Carbide Processing and Applications, Massachusetts, Artech House, 2004.

5. J. Liu, Y.K. Vohra, Raman modes of 6H polytype of silicon carbide to ultrahigh pressures: A comparison with silicon and diamond, Phys. Rev. Lett. 72 (26) (1994) 4105–4108.

6. J. Liu, Y.K. Vohra, Raman modes of 6H polytype of silicon carbide to ultrahigh pressures – Reply, Phys. Rev. Lett. 77 (8) (1996) 1661-1661.

7. M. Sasaki, Y. Nishio, S. Nishino, S. Nakashima, H. Harima, Defect Formation Mechanism of Bulk SiC, Mater. Sci. Forum 264-268 (1998) 41-44.

8. M. Tuominen, E. Prieur, R. Yakimova, R.C. Glass, T. Tuomi, E. Janzen. Defect Analysis in Lely-grown 6H SiC, J. Cryst. Growth 165 (3) (1996) 233-244.

9. M. Hundhausen, R. Pusche, J. Rohrl, L. Ley, Characterization of defects in silicon carbide by Raman spectroscopy, Phys. Stat. Sol. B 245 (7) (2008) 1356-1368.

10. W. Wesch, Silicon carbide: synthesis and processing', Nucl. Instrum. Methods Phys. Res. Sect. B 116 (1-4) (1996) 305–321.

11. J. Zhu, S.Y. Liu, J.W. Liang, Raman study on residual strains in thin 3C-SiC epitaxial layers grown on Si(001), Thin Solid Films 368 (2) (2000) 307-311.

12. C. Genzel, A. Klaus, I. Denks, H.G. Wulz, Residual stress fields in surface-treated silicon carbide for space industry—comparison of biaxial and triaxial analysis using different X-ray methods, Mater. Sci. Eng. A 390 (1-2) (2005) 376-384.

13. J.R. Ferraro, K. Nakamoto, C.W. Brown, Introductory Raman Spectroscopy (2nd ed.), Academic Press, San Diego, 2003.

14. H. Werheit, K.A. Schwetz,: Comparative optical investigations of sintered and monocrystalline black and green silicon carbide (SiC), J. Solid State Chem. 177 (2) (2004) 580-585.

15. J.L. Bruneel, J.C. Lassegues, C. Sourisseau, In-depth analyses by confocal Raman microspectrometry: experimental features and modeling of the refraction effects, J. Raman Spectrosc. 33 (10) (2002) 815-828.

16. B. Dietrich, and K. Dombrowski, Experimental challenges of stress measurements with resonant micro-Raman spectroscopy, J. Raman Spectrosc. 30 (10) (1999) 893–897.

17. P. Colomban, Analysis of Strain and Stress in Ceramic, Polymer and Metal Matrix Composites by Raman Spectroscopy, Adv. Eng. Mater. 4 (8) (2002) 535-542.

18. L.A. Falkovsky, J.M. Bluet J. Camassel, Strain-fluctuation effect on Raman spectra, Phys. Rev. B: Condens. Matter 55 (22) (1997) R14697-14700.

19. G. Gouadec, P. Colomban, Raman spectroscopy of nanomaterials: How spectra relate to disorder, particle size and mechanical properties, Prog. Cryst. Growth Charact. Mater. 53 (1) (2007) 1-56.

20. E.M. Anastassakis, Morphic effects in lattice dynamics: in G.K. Horton, A.A. Marahudin (eds.), Dynamical Properties of Solids, North Holland Publishing Company, Amsterdam, Netherlands, 1980, pp. 158-373.

21. L. Colombi Ciacchi, G. Gregori, V. Lughi, A. Rossi, V. Sergo, Piezo-spectroscopy: a materials science perspective: in M. Pandalai (ed.), Recent Research Developments in Applied Spectroscopy 2, Research Signpost, Kerala, India, 1999, pp. 243-272.

22. A. Debernardi, C. Ulrich, K. Syassen, M. Cardona, Raman line widths of optical phonons in 3C-SiC under pressure: First-principles calculations and experimental results, Phys. Rev. B: Condens. Matter 59 (10) (1999) 6774-6783.

23. Z. Feng, W. Choyke, J. Powell, Raman determination of layer stresses and strains for heterostructures and its application to the cubic SiC/Si system, J. Appl. Phys. 64 (12) (1988) 6827–6835.

24. D. Ghosh, G. Subhash, N. Orlovskaya, Measurement of scratch-induced residual stress within SiC grains in ZrB2–SiC composite using micro-Raman spectroscopy, Acta Mater. 56 (11) (2008) 5345-5354.

25. C.J. Lee, G. Pezzotti, Y. Okui, S. Nishino, Raman microprobe mapping of residual microstresses in 3C-SiC film epitaxial lateral grown on patterned Si(111), Appl. Surf. Sci. 228 (1-4) (2004) 10-16.

26. D. Olego, M. Cardona, Pressure dependence of Raman phonons of Ge and 3C-SiC, Phys. Rev. B: Condens. Matter 25 (2) (1982) 1151-1160.

27. H. Mukaida, H. Okumura, J. H. Lee, H. Daimon, E. Sakuma, S. Misawa, K. Endo, S. Yoshida, Raman scattering of SiC: Estimation of the internal stress in 3C-SiC on Si, J. Appl. Phys. 62 (1) (1987) 254–257.

28. D. Matsuoka, H. Yamamoto, S. Nishino, N. Hasuike, K. Kisoda, H. Harima, Raman scattering study of stress distribution around dislocation in SiC, Mater. Sci. Forum 600-603 (2009) 337-340.

29. K. Grodecki, A. Wysmolek, R. Stepniewski, J.M. Baranowski, W. Hofman, E. Tymicki, K. Grasza, Raman piezospectroscopy of phonons in bulk 6H-SiC, Acta Phys. Pol. A 116 (5) (2009) 947-949.

30. S. Nakashima, H. Harima, Raman investigation of SiC polytypes, Phys. Status Solidi A 162 (1) (1997) 39–64.

31. S. Nakashima, Raman imaging of semiconductor materials: characterization of static and dynamic properties, J. Phys.: Condens. Matter 16 (2) (2004) S25-S37.

32. N. Everall, Depth profiling with confocal Raman microscopy, part I, Spectrosc. 19 (10) (2004) 22-27.

33. N. Everall, Depth profiling with confocal Raman microscopy, part II, Spectrosc. 19 (11) (2004) 16-27.

34. N. Everall, Confocal Raman microscopy: Performance, pitfalls, and best practice, Appl. Spectrosc. 63 (9) (2009) 245A-262A.

35. P. Vicente, D. David, J. Camassel, Raman scattering as a probing method of subsurface damage in SiC, Mater. Sci. Eng. B 80 (1-3) (2001) 348-351.

36. D.M. Lipkin, D.R. Clarke, Sample-probe interactions in Spectroscopy: Sampling microscopic property gradients, J. Appl. Phys. 77 (5) (1995) 1855-1863.

37. A.M. Gigler, A.J. Huber, M. Bauer, A. Ziegler, R. Hillenbrand, R.W. Stark, Nanoscale residual stress-field mapping around nanoindents in SiC by IR s-SNOM and confocal Raman microscopy, Opt. Express 17 (25) (2009) 22351-22357.

38. I. DeWolf, Micro-Raman spectroscopy to study local mechanical stress in silicon integrated circuits, Semicond. Sci. Technol. 11 (2) (1996) 139–154.

39. T.G. Bifano, T.A. Dow, R.O. Scattergood, Ductile-regime grinding: a new technology for machining brittle materials, J. Eng. Ind. 113 (2) (1991) 184-189.

5. "Scratched" Silicon Sample

As previously mentioned, we were supplied with several samples scratched with the Micro-LAM technique. These samples were subjected to Raman spectroscopy to examine how they withstood the machining process. They were examined with the 514 nm and the 633 nm lasers, which have penetration depths of 762 nm and 3000 nm [49] respectively. In the literature for silicon, the convention is to give compressive stresses positive values, and tensile stresses negative values, and we will follow that convention for silicon.

As shown in Table 5.1 and Figure 5.1, several patterns emerge from the data. As could be seen in Figure 3.3, the 30% LP samples appear physically different from other samples, and they have very different residual stress values than the other samples. These scratches have large tensile residual stresses, much larger than the other scratches. These scratches also have significant amounts of fluorescence when viewed under the 633 nm laser, and either had no readable spectra or very few, and as such no residual stress is reported.

Sample Section	514nm Residual Stress (MPa)	633nm Residual Stress (MPa)
10g load, no laser	24 +/- 3	72 +/- 1
10g load, 10% laser power	53 +/- 2	108 +/- 1
10g load, 20% laser power	-4 +/- 3	111 +/- 1
10g load, 30% laser power	-213 +/- 13	n/a
5g load, no laser	-63 +/- 2	1 +/- 1
5g load, 10% laser power	-39 +/- 4	27 +/- 2
5g load, 20% laser power	-45 +/- 2	-32 +/- 2
5g load, 30% laser power	-246 +/- 18	n/a

Table 5.1: Residual stress values for the scratched silicon regions.

The scans with 10g force applied feature almost entirely compressive stresses, with the 514 nm laser on the 20% LP being the exception as it features a small tensile stress. None of the stresses are large, the largest being around 100 MPa. What is interesting is that the 514 nm scans feature smaller stresses than the 633 nm scans, even though they are closer to the surface. It was postulated in [20] that the laser anneals the surface during the cut, which could cause the reduction in stress closer to the surface.
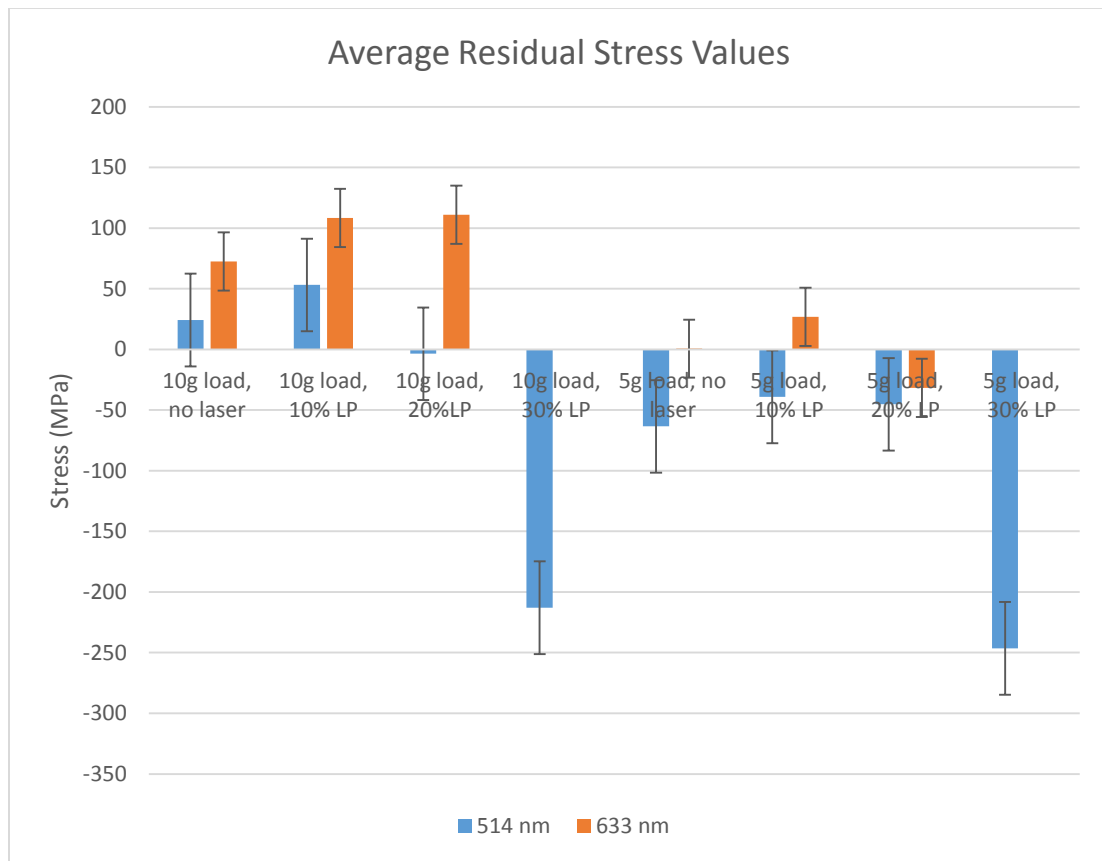
Figure 5.1: Graph of residual stress values for scratched samples.

The stresses from the 5g samples are smaller than the stresses in the 10g samples, and also follow the more predictable pattern of larger stresses closer to the surface, and

smaller stresses away from the surface. The 5g load samples, however, were found to

have mostly tensile stresses. It is possible that under the smaller loads, the thermal

softening causes the diamond stylus to "pull" the sample, causing some tensile stress.

The larger force on the 10g cuts could cause this, but more testing would have to be done

to see if this hypothesis was valid.

Sample	Silicon Phases Present on 514 nm Scans	Silicon Phases Present on 633 nm Scans
5g load, no laser	I, amorphous	I
5g load, 10% LP	I, III, XII, amorphous	I, III, XII, amorphous
5g load, 20% LP	I, III, XII, amorphous	I, III, XII, amorphous
5g load, 30% LP	I, IV	n/a
10g load, no laser	I, III, XII, amorphous	I, III, XII, amorphous
10g load, 10% LP	I, III, XII, IV (possibly)	I, III, XII
10g load, 20% LP	I, III, XII, amorphous	I, III, XII
10g load, 30% LP	I, IV	n/a

Table 5.2: Phases present in the scratched silicon samples.

        From the line scans shown in Figures 5.2 and 5.3 it appears that stress is highest at

the ends of the scratches. This is probably caused by the loading/unloading of the

diamond tip. Within the line scans there are often large variances in the stress present.
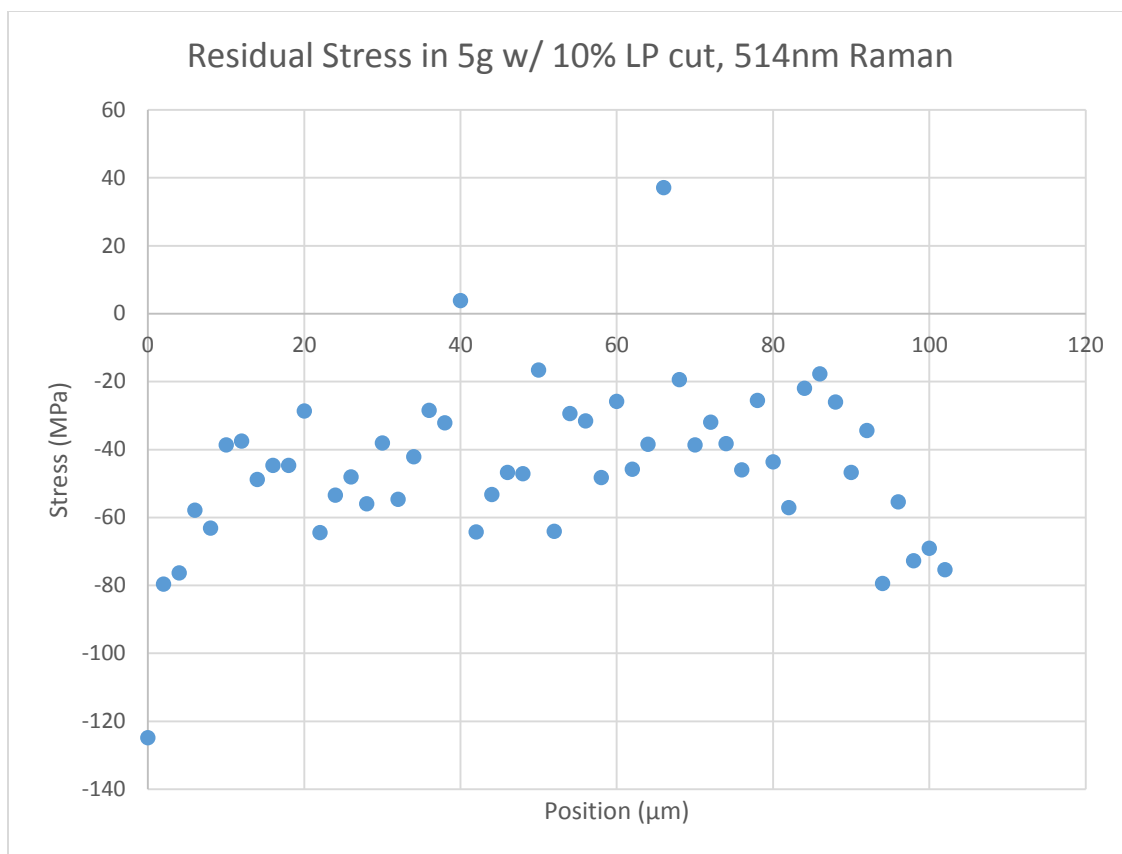
Figure 5.2: Stress vs. position along silicon scratch with 514nm laser
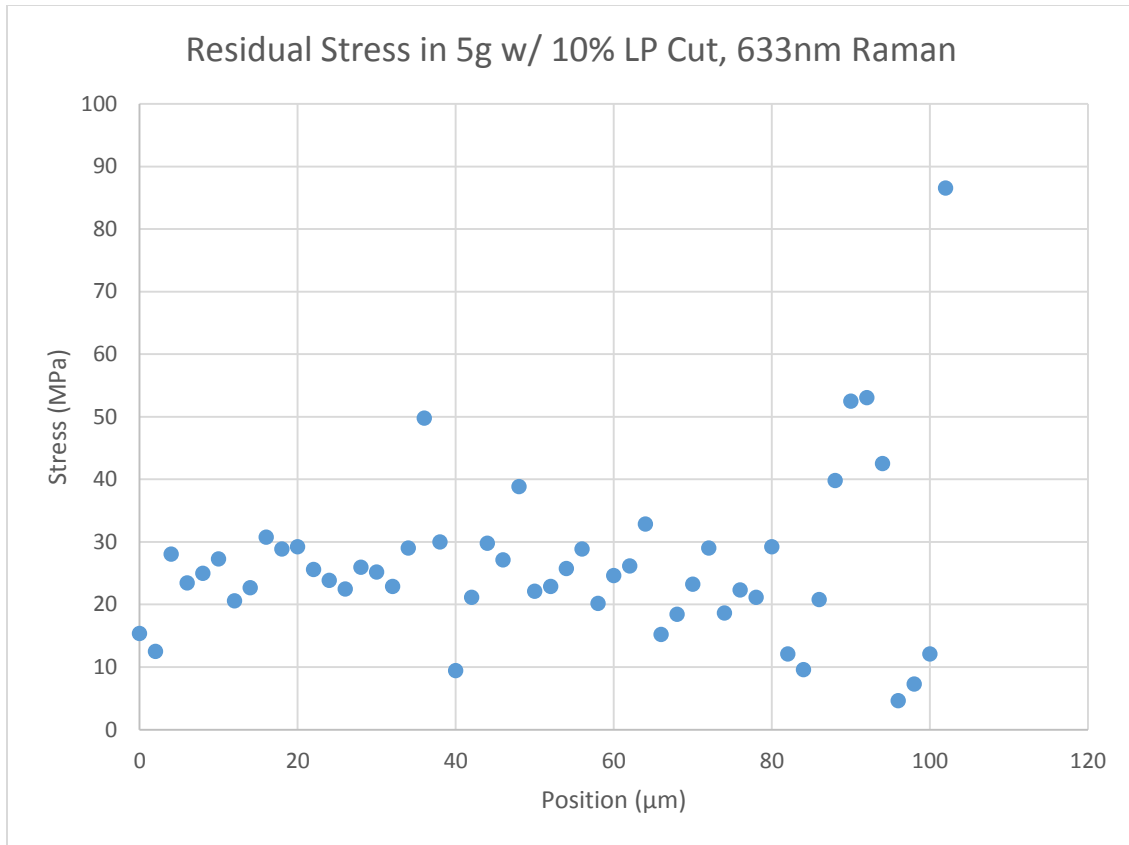
Figure 5.3: Stress vs. position along silicon scratch with 633nm laser

It is also important to examine any additional phases that have been introduced by the machining process. Table 5.2 shows what silicon phases are present in which of the scratches. It would be possible for a machining technique to create so many additional phases that the original phase would not be detected by Raman, which is not the case here, though it can be observed several times in the scratches with no laser and with 10% LP Si-I is no longer the primary phase. Almost all the machining processes leave Si-III and Si-XII as residual phases, though in the samples with 20 and 30 percent laser power they are are present only in very small amounts. Many machining conditions create amorphous silicon as well. Though the two loads at 30% LP create some of the more

phase pure material out of all the scratched samples, it is done with large residual stresses. It is interesting that the 5 gram load with no laser produces very phase pure material. Though none of the scratches receiving the Micro-LAM are completely phase pure, some are close.

Mapping scans were also performed on the entirety of the 5 gram load, 10% LP scratch with both the 514 nm and 633 nm lasers, seen in Figures 5.4 and 5.5 respectively. The 633 nm sample features larger stresses than the 514 nm sample, the 633 nm sample being 125.21 MPa while the 514 nm sample being -73.80 MPa. Another interesting feature is the spacing of the high stress regions on the 633 nm scan. Sometimes, the cutting tool will "skip" or "jump" along the cut as a way to release energy during the cutting process. We believe that is the cause of these high stress regions in the sample. It would be good to see if this happens on other cuts, or to see if it is present on pieces of silicon where the whole surface is turned. Perhaps by changing machining settings, such as feed rate or cutting force, this can be reduced or even eliminated. These maps are inconsistent with the line scans of the same scratch, which have smaller stresses further away from the sample surface. The smaller sample size of the line scan may be over-emphasizing some of the more anomalous stress values, but it is worth examining in the future.
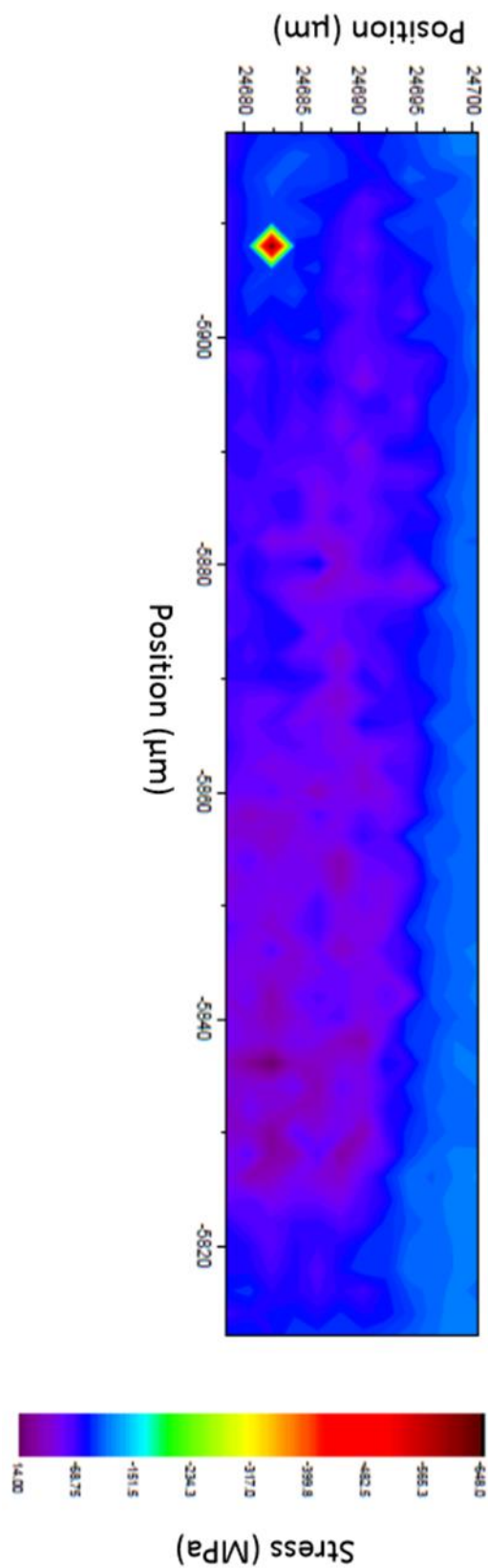
Figure 5.4: Stress map of the 5 gram load, 10%LP scratch with the 514nm laser.
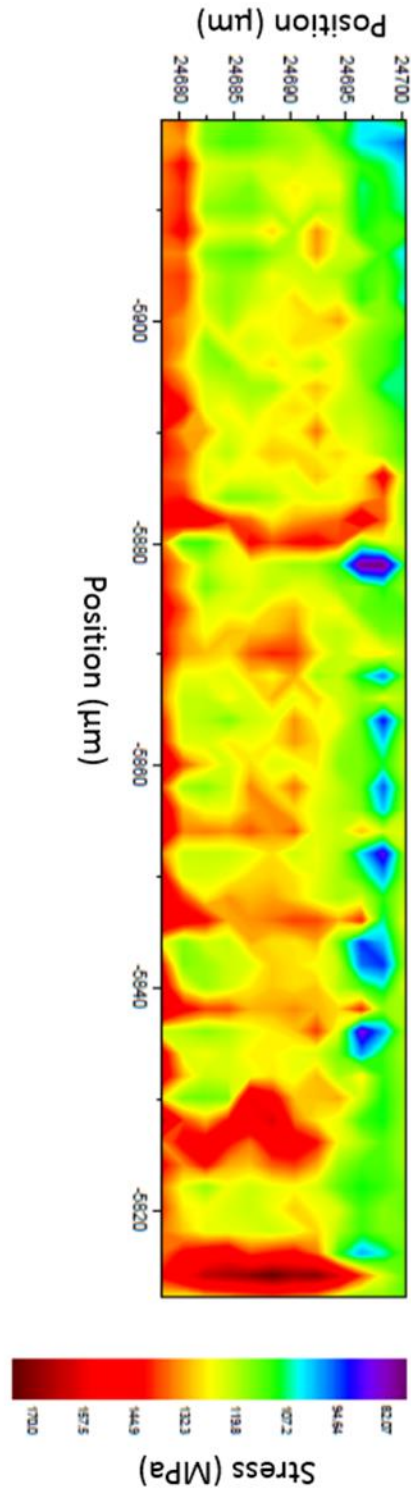
Figure 5.5: Stress map of the 5 gram load, 10%LP scratch with the 633nm laser.

6. Evaluation and Optimization of Micro-Laser Assisted Machining of Silicon

S.M. Langan[a], D. Ravindra[b], A.B. Mann[a]

[a] Materials Science and Engineering, Rutgers University, Piscataway, NJ 08854, USA.

[b] Micro-LAM, Inc., 5960 S. Sprinkle Rd., Portage, MI 49002, USA.

Abstract

Traditional machining of brittle materials like silicon is expensive and frequently leads to detrimental damage. New techniques are essential to improving the efficacy of the machining process; one possible method is using traditional single point diamond turning with laser assistance. The method, termed Micro-Laser Assisted Machining (Micro-LAM), reduces the likelihood of fracture by increasing the ductility of the material during the machining process. Raman microspectroscopy has been used to examine silicon subject to forty-one different combinations of Micro-LAM machining parameters. Raman provided information on residual stress, additional phases, and relative crystallinity, which enabled the optimal Micro-LAM parameters to be identified. With the use of laser assistance with several machining conditions, the results show a clear improvement in the silicon's quality, giving silicon with low residual stress, high phase purity, and good relative crystallinity.

Keywords: Ductile, machining, Raman, silicon, stresses, Micro-LAM, laser, assistance

Introduction

Machining of brittle materials has become a more important topic in recent years as the technological and structural uses of ceramic and semiconductor single crystals have increased. During the production process, the raw part frequently requires machining to meet the desired dimensional tolerances or surface finish. However, the machining can incur a severe penalty in terms of both damage to the material [1] and additional expenditure that can account for 60-90% of the product's final cost [2]. The damage can lessen the material's performance and lifetime by leading to premature material failure.

Given the drawbacks of traditional machining, new methods that are more cost effective and cause less damage are needed. One such method is Micro-Laser Assisted Machining, or Micro-LAM (Micro-LAM Technologies, Battle Creek, MI), which has been applied to the machining of silicon in this study. It is based on Single Point Diamond Turning (SPDT), which uses a diamond stylus to put high pressure on a brittle material with the intent of causing it to behave in a ductile fashion [3]. If it can be machined in the ductile region it allows for many of the difficulties of traditional machining, such as micro-cracking, to be avoided [4].
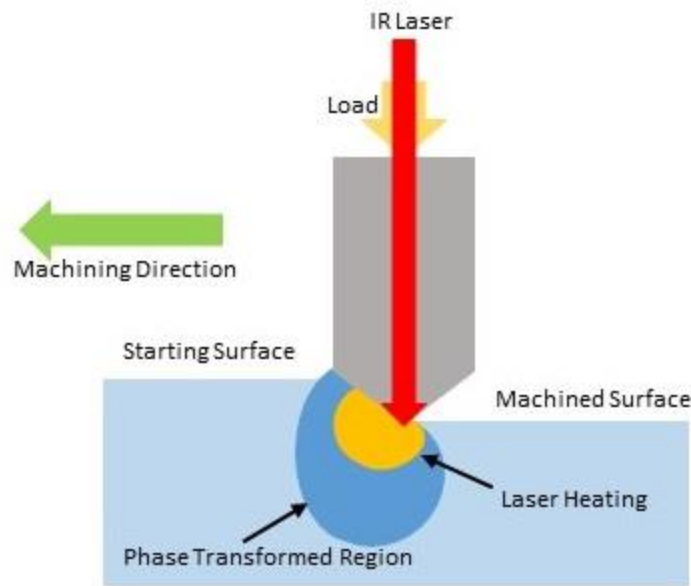
Figure 6.1: Depiction of the Micro-LAM process. As with SPDT, a diamond stylus is used to induce a brittle to ductile transition; however with the Micro-LAM process a laser shines through the stylus to thermally assist the machining process. Figure based on [5].

With the Micro-LAM process, *in situ* laser assistance is used to augment the ductility of the material and potentially enhance phase transitions which aid in the machining, and is seen in Figure 6.1. The diamond stylus is attached to an infra-red laser by fiber optics [5] which enables the laser's energy to be transmitted through the diamond stylus onto the sample. This thermally softens the material, promoting the brittle to ductile transition [6] and lowering the apparent hardness of the machined material by as much as 50% [7].

Silicon is valuable for optical and electrical applications, and its brittle nature makes the Micro-LAM process a promising method to machine it. As reported by

Jasinevicius et al. [8], based on the work of [9] silicon can undergo several phase transformations during the mechanical loading and unloading associated with machining. There are two different sequences of phase transformations possible during the unloading dependent upon the unloading rate [9]; both sequences can give rise to amorphous silicon, which must be annealed to give the Si-I phase. Since the various phases occur as a result of mechanical loading and unloading it is possible for various combinations of the phases to be present when a silicon surface is finished using SPDT.

The surface finish for silicon when using the Micro-LAM process has been studied in earlier work which found a reduction in the silicon wafers' roughness, R_a, from 0.85 μm (unpolished) to 0.23 μm after machining with a minimal number of passes [10]. With more passes the Micro-LAM method was found to give an improved finish with R_a of 5 nm [11], making it a better reflective surface than conventionally finished wafers. It has also been shown [12] that when machining parameters are optimized, the Micro-LAM process has the potential to keep the Si-I phase pure. However, if these parameters are not optimized,several other silicon phases have been found to be present. It is suggested in this study that annealing of the high pressure phases back to the Si-I phase by the laser used for assisting machining is vitally important.

Raman microspectroscopy (microRaman) which combines Raman spectroscopy with optical microscopy has the ability to look at a variety of near-surface properties with a high degree of spatial resolution [13]. In silicon, microRaman can be used to look at residual stresses, different crystal phases, and relative crystallinity, and, hence, offers a valuable insight into the effect of machining on the quality of a silicon surface beyond simply measuring roughness. Raman can be used to quantify residual stress as changes

in a Raman peak's position follow a linear function relating stress to changes in peak position. This is seen in many materials including ceramics and single crystal semiconductors [13]. The dependence of Raman peaks on stress stems from the lattice vibration modes that give rise to the peaks. A local stress causes a change in bond length (strain) which modifies the energy of the vibrational modes, hence changing the Raman spectral peak positions in ways that can be quantified.

Materials and Methods

Micro-LAM method with a range of different machining parameters was used to produce machined surface on (100) single crystal silicon. The Micro-LAM system used a modified universal micro-Tribometer as shown in Figure 6.2 A 10 μm diameter fiber optical cable was used to connect a 1064 nm wavelength, 100W infrared laser to the micro-Tribometer. The turning tool is made up of a diamond tip (stylus) with a 5 μm radius, that was connected with a transparent epoxy to the optical fiber, hence allowing the laser's energy to pass through the diamond stylus directly onto the silicon at the point of contact.
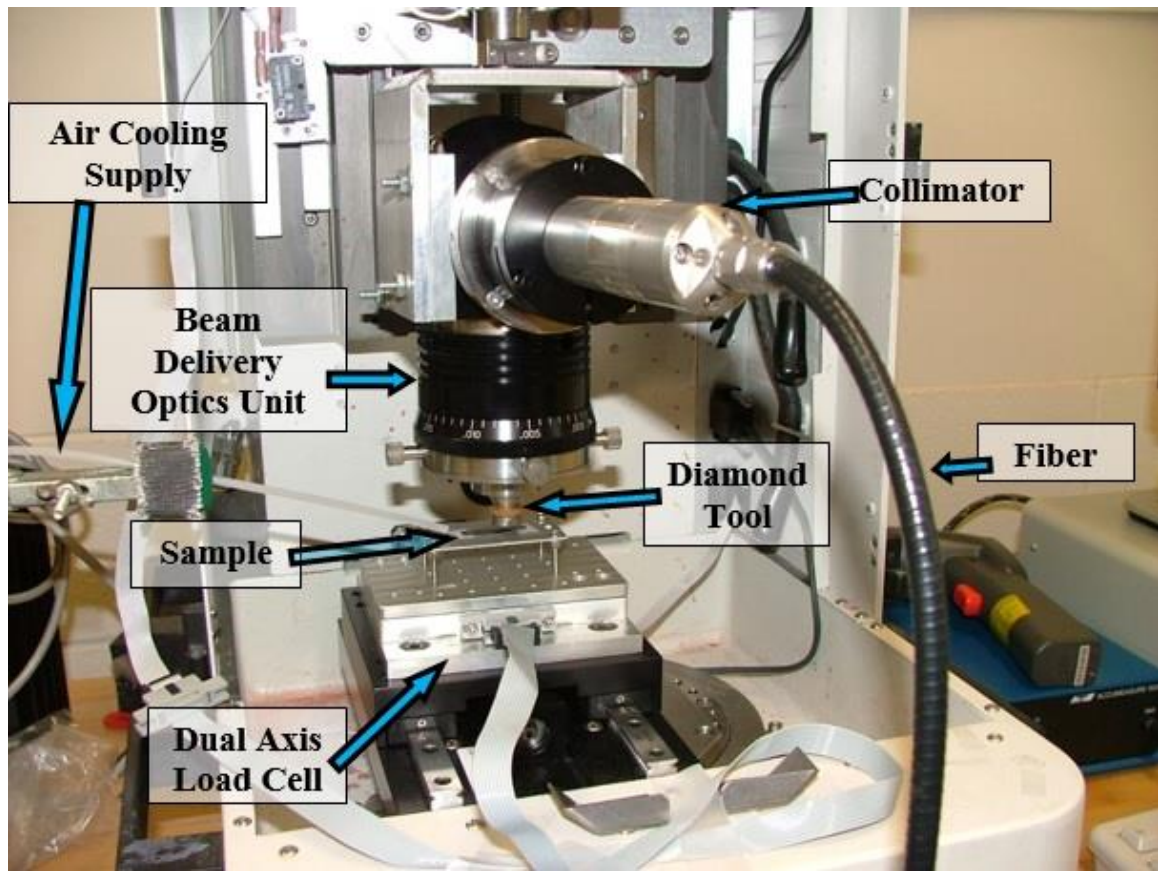
Figure 6.2: The modified universal micro-Tribometer used for the Micro-LAM machining.

Three wafers of silicon, each subject to multiple different machining conditions, were examined. Various machining conditions were used in concentric rings on these wafers. In total, forty-one different combinations of machining parameters were examined, the specifics of which are given in Table 6.1.

Machining Conditions

Sample Number	Laser Power (W)	Feed Rate (µm/ rev)	Maximum Cutting Speed (m/s)	Sample Number	Laser Power (W)	Feed Rate (µm/ rev)	Maximum Cutting Speed (m/s)
1	8.2	30	$2.44\,\mathrm{e}^{-2}$	22	8.8	10	$1.92\,\mathrm{e}^{-2}$
2	8.2	10	$2.34\,\mathrm{e}^{-2}$	23	8.8	2	$1.80\,\mathrm{e}^{-2}$
3	8.2	2	$2.23\,\mathrm{e}^{-2}$	24	9	10	$1.64\,\mathrm{e}^{-2}$
4	5.28	30	$2.07\,\mathrm{e}^{-2}$	25	9	2	$1.53\,\mathrm{e}^{-2}$
5	5.28	10	$1.96\,\mathrm{e}^{-2}$	26	4	10	$1.34\,\mathrm{e}^{-2}$
6	5.28	2	$1.85\,\mathrm{e}^{-2}$	27	4	2	$1.23\,\mathrm{e}^{-2}$
7	9	30	$1.68\,\mathrm{e}^{-2}$	28	6.8	10	$1.07\,\mathrm{e}^{-2}$
8	9	10	$1.58\,\mathrm{e}^{-2}$	29	6.8	2	$0.96\,\mathrm{e}^{-2}$
9	9	2	$1.46\,\mathrm{e}^{-2}$	30	6.5	10	$0.81\,\mathrm{e}^{-2}$
10	8	30	$1.29\,\mathrm{e}^{-2}$	31	6.5	2	$0.70\,\mathrm{e}^{-2}$
11	8	10	$1.18\,\mathrm{e}^{-2}$	32	9	10	$0.54\,\mathrm{e}^{-2}$
12	8	2	$1.07\,\mathrm{e}^{-2}$	33	9	2	$0.42\,\mathrm{e}^{-2}$
13	8	30	$0.91\,\mathrm{e}^{-2}$	34	0	30	$1.91\,\mathrm{e}^{-2}$
14	8	10	$0.80\,\mathrm{e}^{-2}$	35	0	30	$1.44\,\mathrm{e}^{-2}$
15	8	2	$0.68\,\mathrm{e}^{-2}$	36	0	10	$1.27\,\mathrm{e}^{-2}$
16	0	10	$0.51\,\mathrm{e}^{-2}$	37	0	2	$1.16\,\mathrm{e}^{-2}$
17	0	2	$0.40\,\mathrm{e}^{-2}$	38	0	10	$1.00\,\mathrm{e}^{-2}$
18	8.2	10	$2.51\,\mathrm{e}^{-2}$	39	0	2	$0.91\,\mathrm{e}^{-2}$
19	8.2	2	$2.39\,\mathrm{e}^{-2}$	40	0	10	$0.72\,\mathrm{e}^{-2}$
20	6	10	$2.22\,\mathrm{e}^{-2}$	41	0	2	$0.61\,\mathrm{e}^{-2}$
21	6	2	$2.10\,\mathrm{e}^{-2}$				

Table 6.1: Machining conditions examined in this study. The maximum cutting speed refers to the speed at the outer edge of the ring containing the specific machining conditions.

Samples were examined with a Renishaw InVia™ Raman spectrometer. Line scans with a spacing of 2 µm were performed on each machining condition using two different Raman excitation lasers with wavelengths of 514 nm and 633 nm respectively. Different volumes at the surface are sampled with the two lasers as there is dependence between wavelength and the depth of penetration, which for these lasers into silicon are 762 nm and 3000 nm respectively [14]. The Raman spectra obtained during the line

scans were fitted with Renishaw's Wire 3.4 software. Spectra that oversaturated the Raman's CCD did not contain enough Si-I for stress measurements so were removed. Furthermore, scans that contained excessive nanocrystalline material or peak splitting were removed as the standard Si-I peak is not present in these cases, as demonstrated in [14] for nanocrystalline silicon and [15] for peak splitting.

Fitting the peaks in the Raman spectra to identify the peaks' positions, relative sizes and widths enables the residual stress, relative phase purity, and crystallinity (from the normalized curve width) to be examined. The residual stress was found from the peak shift when compared to the unstressed peak position using the formula below from Jasinevicius et al. [16]:

$$\omega = \omega_o + 0.52P \qquad (1)$$

where ω is the shifted peak position in wavenumbers (waves per centimeter, cm^{-1}), ω_o is the unstressed peak position, and P is the hydrostatic stress in Kilobar. This formula assumes stress is hydrostatic and gives a value for stress averaged over different directions in the machined silicon. It is important to note that by convention due to silicon's positive phonon potentials, compressive stresses are denoted as positive in these calculations rather than positive for tensile (which is more typical for mechanical measurements).

To find the relative phase purity, the equation below which is similar to the one used by *Gogotsi, et al* [17] was used:

$$P_{rel} = \frac{I_{515-525}}{I_{350-515}+I_{515-525}} \qquad (2)$$

where P_{rel} is the relative phase purity (maximum value 1 for pure Si-I). $I_{350-515}$ is

obtained from the Raman spectra by totaling the intensity of all peaks in the range of 350-

515 cm^{-1} and $I_{515-525}$ is the total intensity of all peaks in the range of 515-525 cm^{-1},

which is the range for the Si-I peak however it is shifted. Thus, if the sample only

contains Si-I there will be a single peak in the range 515-525 cm^{-1} and P_{rel} will be 1,

while if there is no Si-I peak present P_{rel} would be 0. If peaks had a negative intensity

(an anomaly of the Wire 3.4 software curve fitting process) then the peak intensity was

set to zero.

To find the normalized phase width, the full width at half-maximum (FWHM) for

the fitted Si-I peak was divided by the value for the FWHM for an unstressed, single

crystal piece of silicon. In Raman spectroscopy this is widely used as a measure of

crystallinity [18].

Results and Discussion

The micro-Raman with two different wavelength lasers was used to examine each

of the forty-one different machining conditions. For each of these the raw Raman data

was analyzed to give the residual stress, relative phase purity, and normalized curve

width (crystallinity). Average values over the Raman line scans for each set of conditions

were obtained. To provide a standard for the ranges of the properties obtained when the

samples were machined with laser assistance the results were compared to those

machined without laser assistance. Machining, by its nature, is expected to give a

scattering of residual stress, relative phase purity, and crystallinity, but comparing the

range of values with and without laser assistance allows for a greater understanding of the laser's effect on the machining process.

Across all the samples, the average residual stress results (seen in Figure 6.3) when using laser assistance during machining are almost entirely positive in terms of reducing the magnitude of residual stresses. For the 514 nm Raman laser (relatively shallow penetration depth) the range of average stresses was much smaller with laser assistance than without, and had a smaller tensile stress. The laser assistance did, however, make for a higher compressive residual stress than when no laser assistance was used. For the 633 nm scans, the sample machined with the laser assistance had a higher range, as well as higher maximum stresses (compressive). It should be noted, that while the range is larger, the average residual stress obtained with the 633 nm Raman laser scans is 179.8 MPa with laser-assisted machining, compared to 224.5 MPa without laser assistance.
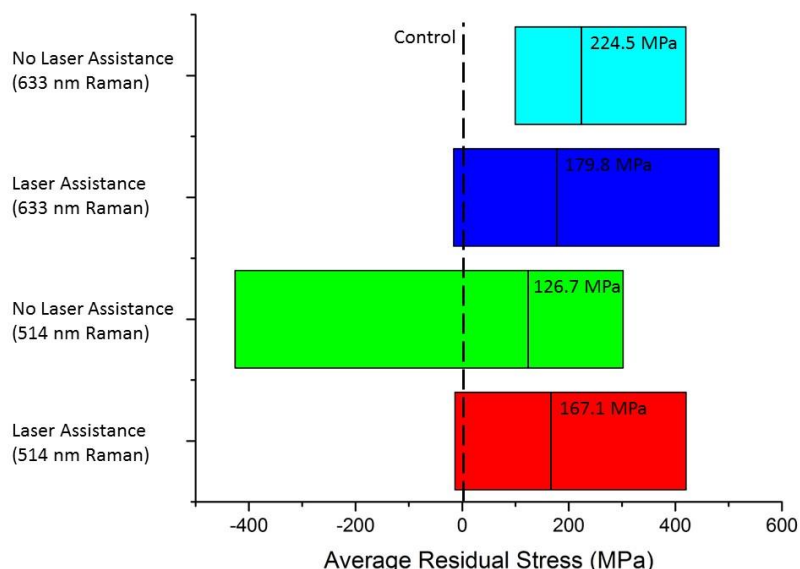
Figure 6.3: Ranges of average residual stress across all the samples machined with and without laser assistance. The values obtained using both Raman laser wavelengths (633 nm and 514 nm) are shown. The control, or point of zero residual stress, for an unmachined Si-I sample is shown as well. The solid lines on each bar demonstrate the average residual stress of all individual scans in that dataset, and that stress is noted next to the line. Note that for silicon the convention is to plot compressive stress as positive.

Across all the samples the relative phase purity with laser assistance during machining shows a marked improvement over those machined without laser assistance. As seen in Figure 6.4, the range of values for the samples machined with laser assistance is smaller than the range seen without laser assistance. Furthermore, the minimums and maximums of phase purity with laser-assisted machining are closer to those of the control than the values seen without laser assistance. This applies when both the 514 nm and 633

nm Raman lasers are used. Generally speaking, machining with laser assistance is giving more phase pure material than without it.

Similar results were seen for the average normalized curve width, seen in Figure 6.5, which is a measure of crystallinity. That very narrow peak width implies a large single crystallinity with few defects, while a wider peak implies more defects and a polycrystalline material with small grains (even nanocrystalline if the peak is very wide). The range of peak widths is smaller with laser assistance, as well as being closer to the control, showing that using laser-assisted machining generally results in better quality crystals. When the peak width data is looked at together with the other data, it is seen that using laser assistance generally gives better results than not using it.

Figure 6.4: Ranges of average relative phase purity across all the samples machined with and without laser assistance. The values obtained using both Raman laser wavelengths (633 nm and 514 nm) are shown. The control value of 1 is for an unmachined, phase pure Si-I sample. The solid lines on each bar demonstrate the average relative phase purity of all individual scans in that dataset, and that phase purity is noted next to the line.
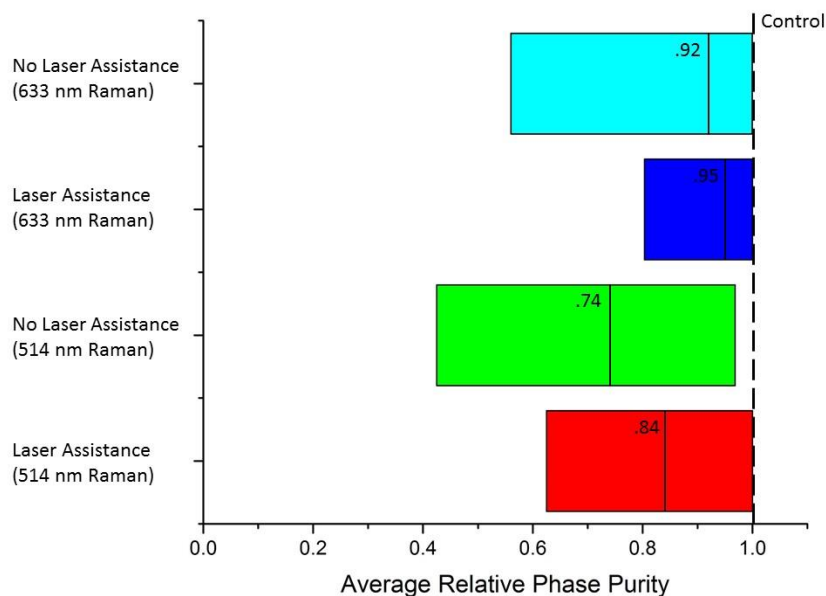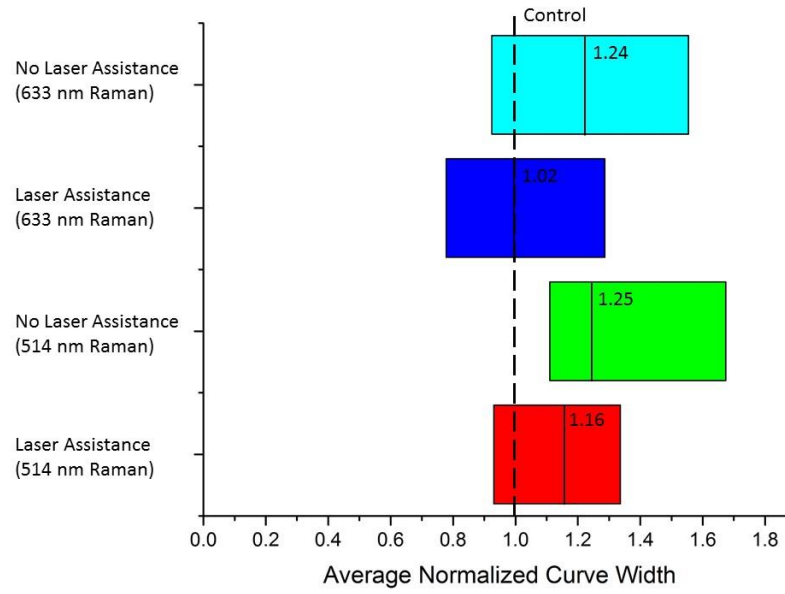
Figure 6.5: Ranges of average normalized curve width across all the samples machined

with and without laser assistance. The values obtained using both Raman laser

wavelengths (633 nm and 514 nm) are shown. The control, or the normalized width of

the single crystal silicon standard, is shown as well. The solid lines on each bar

demonstrate the average normalized curve width of all individual scans in that dataset,

and that width is noted next to the line. Some of the results have a better (lower) value

than the control, and it is possible that the laser assistance is annealing the sample giving

a more defect free Si-I phase than that seen in the standard single crystal sample.

The overall results shown on Figure 6.3, 6.4, and 6.5 give a clear indication that

adding the infra-red laser during the machining process can provide for good results.

Also, the averages of the datasets are better with laser assistance for all material

properties, except for stress measured with the 514 nm laser, further showing the value of

laser assistance during machining. However, the overlap in the ranges between the

settings with laser assistance and those without shows that poor results are also possible with the wrong settings. This shows the need for the process to be optimized to give a machined surface that has low residual stress, low additional amounts of phases other than Si-I, and good crystallinity.

An example of a Raman spectrum of a highly phase pure Si-I material after machining with near-optimal parameters can be seen in Figure 6.6. When the process is not optimized, it is often readily apparent in the Raman spectra of the material. Figure 6.7 shows one such spectrum where various crystalline and amorphous phases are present in greater amounts than the primary Si-I phase.

Figure 6.6: A Raman spectrum of a silicon sample machined using laser assistance with a laser power of 8 W and a 2 µm/rev feed rate. The spectrum was obtained using a Raman excitation laser of 514 nm wavelength. Only one peak which corresponds to the Si-I phase is present indicating good phase purity.
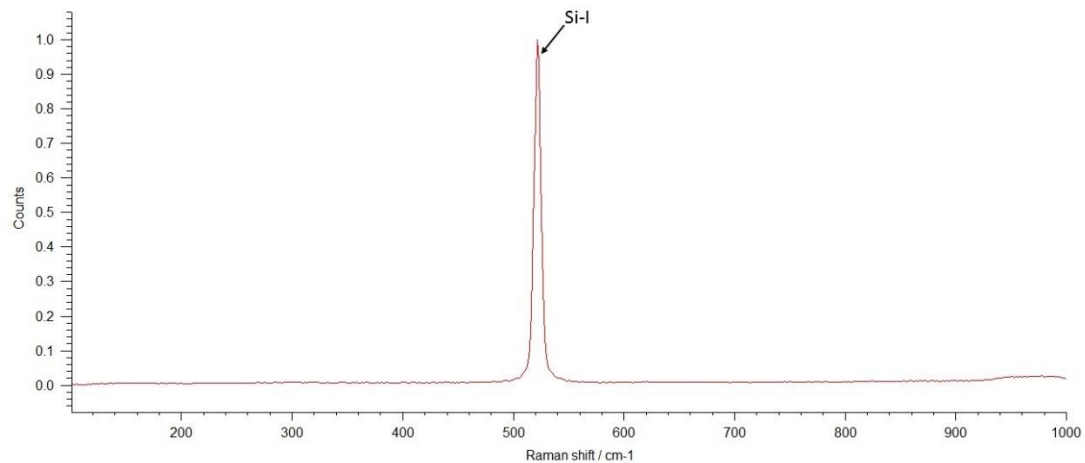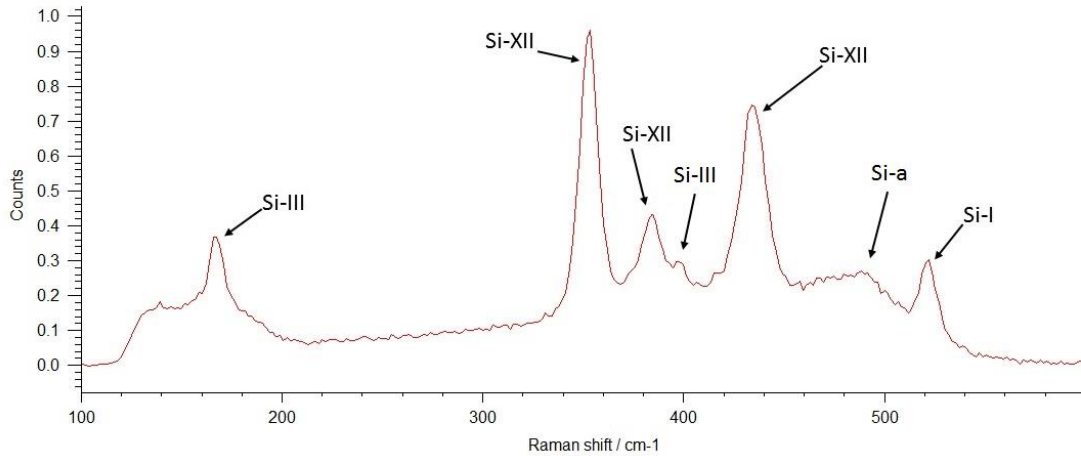
Figure 6.7: A Raman spectrum of a silicon sample machined using laser assistance with a laser power of 9 W and 2 μm/rev feed rate. The spectrum was obtained using a Raman excitation laser of 514 nm wavelength. This sample shows many extra phases as well as a large amount of amorphous material.

There are other dangers with using non-optimal parameters during the machining process one of which results in significant peak splitting as can be seen in the spectrum of Figure 6.8. This split represents a breakdown in the degeneracy of the phonon modes from a triplet with two transverse optical and one longitudinal optical mode all with the same Raman peak to a singlet and doublet peak. The splitting of the peak is due to stress having a different effect on one of the optical phonon modes compared to the effect on the other two modes [9, 17]. Distinguishing the split peaks and fitting them in order to find the stresses acting is difficult and requires assumptions to be made about the relative amplitudes of the peaks. For this reason, no residual stress analysis was performed on spectra exhibiting splitting. Nonetheless, the presence of these spectra does show that there are areas of the sample that are under a more complex stress state (not simply

hydrostratic as assumed by equation (1)),which is generally not a desirable result of the machining process. With laser assistance during the machining, splitting was found to have occurred only in 0.06% of the spectra obtained with the 514 nm Raman laser, while without laser assistance it was almost ten times as likely at 0.61%. Interestingly, the reverse was seen with the 633 nm Raman laser with 3.06% of the spectra showing peak splitting time after laser-assisted machining compared to 0.90% of peaks splitting without laser assistance. The extra depth that the 633 nm Raman laser penetrates into the surface compared to the 514 nm Raman laser suggests that the use of laser assistance during machining can impact the stresses several microns below the surface.
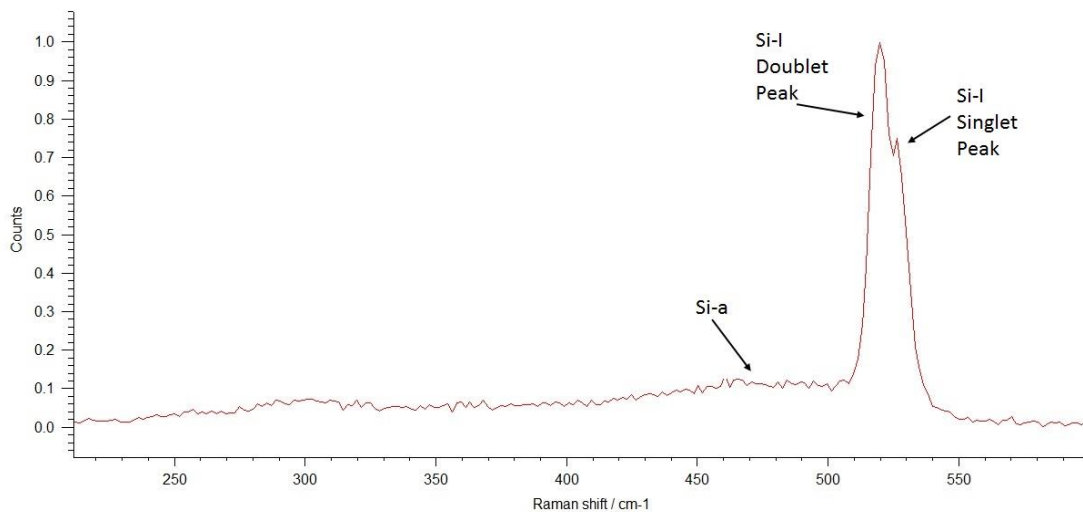

Figure 6.8: A Raman spectrum of a silicon sample machined using laser assistance with a laser power of 5.28 W and 2 μm/rev feed rate. The spectrum was obtained using a Raman excitation laser of 633 nm wavelength. While a small amount of amorphous material is present, a complex stress state has led to the 520 cm^{-1} peak splitting into a double and singlet.

Laser-assisted machining can also give rise to significant amounts of nanocrystalline silicon if the parameters are not properly optimized. This gives a markedly different Raman spectrum [9] which can be seen in Figure 6.9. This transformation to nanocrystalline silicon should be avoided if machining is intended to retain the original single crystal silicon. The current study found that an excessive amount of nanocrystalline silicon (enough that stress readings could not be trusted) was seen in 0.58% of the Raman spectra obtained with the 514 nm Raman laser (that is at shallow depths) when laser assistance was used during machining. For deeper depths (using the 633 nm Raman laser) there was 0% of the spectra exhibiting nanocrystalline silicon. Given that the 633 nm Raman laser probes shallow as well as deeper depths it is likely that nanocrystalline silicon is confined to a region close to the surface with the Raman for single crystal silicon at deeper depths giving a much stronger peak at 520 cm^{-1}. On samples machined without laser assistance a high fraction (19.1%) of the spectra showed evidence of nanocrystalline silicon using the 514 nm Raman laser. Again the deeper penetrating 633 nm Raman laser showed no evidence of nanocrystalline silicon. Raman spectra showing significant amounts of nanocrystalline silicon were excluded from analysis of residual stress, additional phases, and curve width.
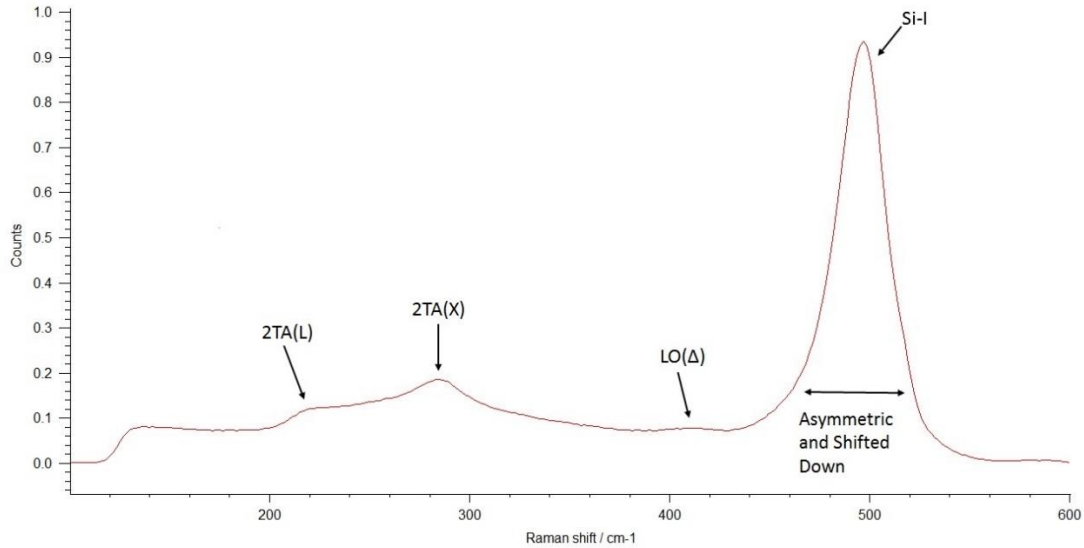
Figure 6.9: Raman spectra of a silicon sample machined with no laser assistance and 30 μm/rev feed rate. The spectrum was obtained with the 514 nm Raman laser. The spectrum shows nanocrystalline silicon, with the peaks of visible phonon modes labeled. The main Si-I peak is shifted to a lower wavenumber and becomes asymmetrical when the silicon is nanocrystalline [9].

The combinatorial approach used in this study examined forty-one different combinations of machining parameters, and the Raman was performed with two excitation laser wavelengths sampling different depths into the silicon. This enabled the effect of machining on three different properties (residual stress, phases present and crystallinity) to be examined as a function of machining conditions and, hence, gives an excellent baseline for optimizing the process. This can be done by looking at plots of the average relative phase purity versus average residual stress for each set of machining parameters (see Figure 6.10). Similar plots can be done for the average normalized curve width versus average residual stress, and average relative phase purity versus average

normalized curve width (see Figures 6.11 and 6.12, respectively). On each plot, the most desirable location combining the better of the two physical properties indicates the machining conditions closest to the optimum. When all three plots are looked at for commonalities the best overall machining conditions can be found.

Figure 6.10: Graph of average relative phase amount vs average residual stress for each set of machining parameters. The data was obtained with a Raman laser of either 514 nm or 633 nm wavelength. The machining conditions that give the best results, representing low stresses and high phase purity, are in the bottom right corner;this is expanded for clarity. 38 is not included in this graph as its large tensile stress, -425 MPa, skews the graph.

Figure 6.11: Graph of average normalized curve width vs average residual stress for each set of machining parameters. The data was obtained with a Raman laser of either 514 nm or 633 nm wavelength. The machining conditions that give the best results , representing low stresses and good crystallinity, are in the bottom left corner; this part is expanded for clarity. 38 is not included in this graph.
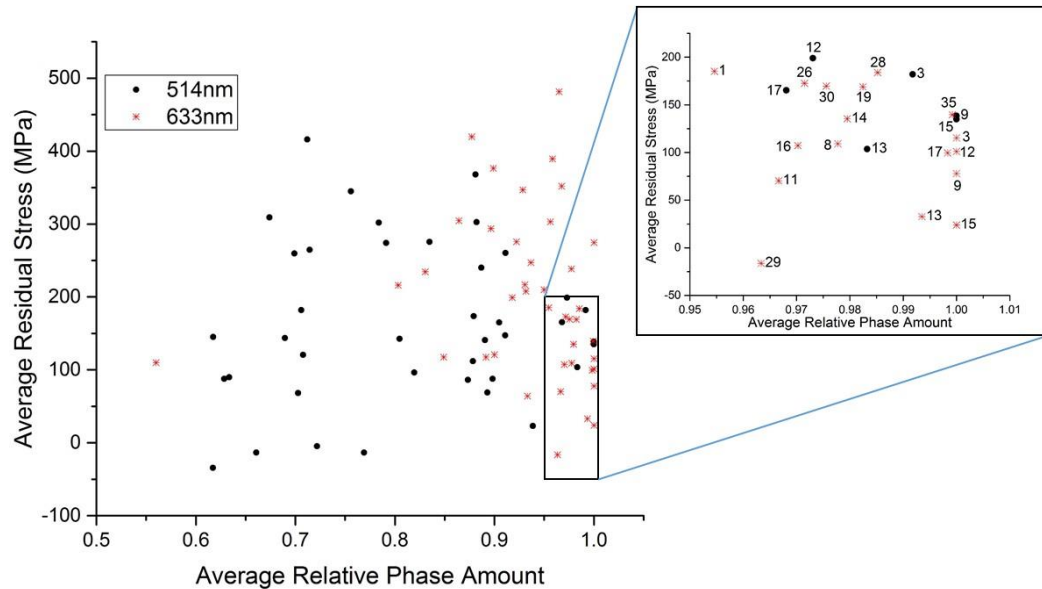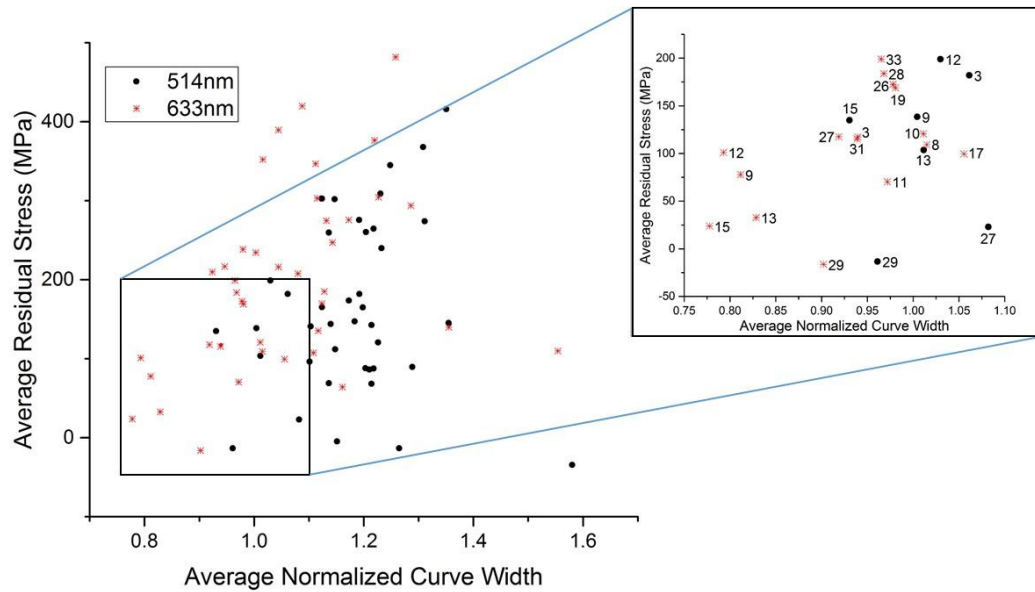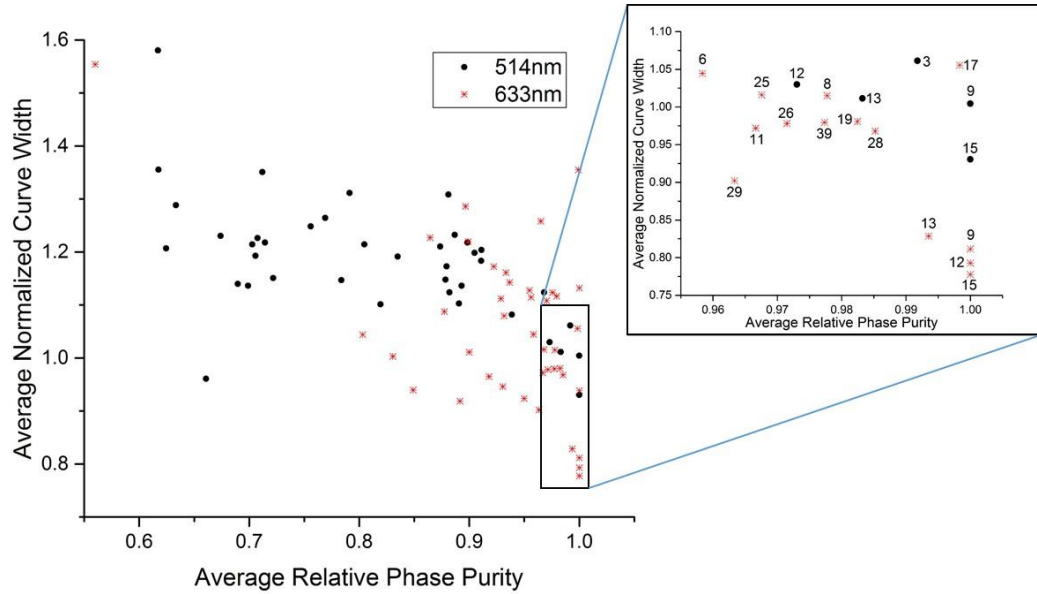
Figure 6.12: Graph of average relative phase purity vs average normalized curve width

for each set of machining parameters. The data was obtained with a Raman laser of either

514 nm or 633 nm wavelength. The machining conditions that give the best results,

representing high relative phase purity and good crystallinity, are in the bottom right

corner; this part is expanded for clarity. 38 is not included in this graph as it skews the

graph.

Considering all the data for each of the machining conditions there were four

settings for the various parameters that all had stresses below 200 MPa, relative phase

purities greater than 0.95, and normalized curve widths (crystallinity) below 1.1 when

examined with both the 514 nm and 633 nm Raman lasers. These conditions and the

corresponding Raman measurements are given in Table 6.2.

Optimal Machining Conditions

Sample Number	Machining Condition	514nm Average Residual Stress (MPa)	514nm Average Relative Phase Purity	514nm Average Norm. Curve Width	633nm Average Residual Stress (MPa)	633nm Average Relative Phase Purity	633nm Average Norm. Curve Width
3	8.2 W, 2 μm/rev, 2.23e^{-2} m/s	182	0.99	1.06	115	1	0.94
9	9 W, 2 μm/rev, 1.46e^{-2} m/s	138	1.00	1.00	78	1	0.81
12	8 W, 2 μm/rev, 1.07e^{-2} m/s	199	0.97	1.03	101	1	0.79
13	8 W, 30 μm/rev, 0.91e^{-2} m/s	104	0.98	1.01	33	.99	0.83

Table 6.2: The four machining conditions that gave the best results in terms of the

Raman measurements when using both the 514 nm and 633 nm Raman lasers

These machining conditions meet high standards for the three material properties

tested. All of them feature high laser power for the laser assistance, and three of the four

have the feed rate of 2 μm/rev. Of the machining conditions examined, it appears that in

order to get a good balance of material properties a large amount of energy needs to be

put into the material. For the most part, this is accompanied by a low feed rate, allowing

the laser to pass over the sample many times. This gives greater opportunity for the laser-

assistance to anneal any damage caused by the earlier passes.

The optimal parameters of Table 6.2 have good results in terms of all three

Raman measurements, but depending on the design needs of the final product this may or

may not be the best machining conditions. For instance, there may be situations where phase purity and crystallinity are more important than low residual stress, or in other applications it may be a different property that is of greatest importance. While the machining conditions in Table 6.2 were excellent overall, some machining conditions gave excellent values for one or two of the measurements at the expense of the third. For example, 27 with the 514 nm Raman laser had a residual stress of 23 MPa and a normalized curve width of 1.08, but the phase purity was 0.94. If phase purity is not a high priority for a particular application, these may be better machining conditions than any in Table 6.2.

It should be noted that one condition with no laser assistance, 17, was almost good enough to make it into the optimized samples. Its curve width for the 514 nm laser excitation was just above the necessary threshold. This was an unexpected result, and it would appear it is possible to get good results without laser assistance during machining, but achieving good results is easier with laser assistance.

Conclusions

This study examined the differences in the surface quality of silicon machined with traditional SPDT and with the Micro-LAM process. The study looked at optimizing the results of the Micro-LAM process by finding conditions that minimized residual stress, while maintaining relative phase purity and crystallinity. Using micro-Raman to assess the silicon's surface and varying a range of machining parameters, a pattern

emerged for how to achieve optimal machining. Of the four optimal conditions identified all were found to have a high laser power, and three of them also had a low feed rate.

The consistency observed in the optimal conditions, combined with the fact that some of the worst results were obtained with a low laser power, or even no laser assistance, shows the necessity of putting a sizeable amount of energy into the silicon during machining to achieve the thermal softening and annealing needed to increase ductility and to alleviate machining damage. This is essential for maximizing the quality of the machined silicon's surface. The good results for low feed rates with high laser powers further support this, since the low feed rate allows for more passes over the sample and therefore more laser energy being put into a given volume at the surface.

While it is difficult to discern if a lack of thermal softening or annealing is responsible for the poor results for samples machined with low laser power or no laser assistance, it is clear that without laser assistance, annealing is unlikely. There is evidence for this in the large amount of unwanted phases present when traditional methods are used. Separating the effects of the lack of annealing from those due to thermal softening during machining on the resultant stresses and reduced crystallinity is difficult, but it is unlikely annealing does not play a role as it relieves stresses and improves a sample's crystallinity. However, due to silicon's complex transformations during loading and unloading, thermal softening undoubtedly plays a role in easing the machining process. Further research needs to be done to understand how the two effects of the laser interact and impact the machining outcome.

This current study has shown both the benefits of the Micro-LAM method and the necessity of using a high laser energy to obtain the best results. When the machining

conditions are optimized, the resulting surface of the silicon showed low residual stresses, high relative phase purity, and high relative crystallinity. In summary, the work shows a substantial and significant benefit from using high laser energy with the Micro-LAM method when machining silicon compared to the results obtained with traditional SPDT.

Acknowledgements:

References

1. Zhang, B.; Zheng, X.L.; Tokura, H.; Yoshikawa, M. Grinding Induced Damage in Ceramics. *Journal of Materials Processing Technology* **2003**, *132*, 353-364. doi: 10.1016/S094-0136(02)00952-4

2. Chinn, R. E. *Ceramography: Preparation and Analysis of Ceramic Microstructures*. 1st edition, Wiley-American Ceramic Society: Malden, Massachusetts, USA, 2002; 230pp.

3. Patten, J.; Gao, W.; Yasuto, K. Ductile regime nanomachining of single-crystal silicon carbide. *Journal of Manufacturing Science and Engineering* **2005**, *127*, 522–532. doi: 10.115/1.1949614

4. Kovalchenko, A. M. Studies of the ductile mode of cutting brittle materials (A review). Journal of Superhard Materials **2013**, *35*(5), 259–276. doi: 10.3103/S1063457613050018

5. Patten, J.; Ghantasala, M.; Ravindra, D.; Poyraz, H.; Virkar, S. The Effects of Laser Heating on the Material Removal Process in Si and SiC Nanomachining; in *Proceedings of 2011 NSF Engineering Research and Innovation Conference*, Atlanta, Georgia, USA, 2011.

6. Ravindra, D.; Virkar, S.; Patten, J. *Ductile Mode Micro- Laser Assisted Machining of Silicon Carbide*. 1st Edition, In *Properties and Applications of Silicon Carbide*, Gerhardt R., Ed., InTech: Croatia, 2011; 546pp.

7. Shayan, A.; Poyraz, H.; Ravindra, D.; Patten, J. Pressure and Temperature Effects in Micro-Laser Assisted Machining (µ-LAM) of Silicon Carbide; In *North American Manufacturing Research Conference (NAMRC)*, Greenville, South Carolina, USA; Dearborn, Michigan, USA, 2009.

8. Jasinevicius, R. G.; Duduch, J. G.; Pizani, P. S. Structure Evaluation of Submicrometre Silicon Chips Removed by Diamond Turning. *Semiconductor Science and Technology* **2007**, *22*(5), 561-573.

9. Domnich, V.; Gogotsi, Y.; Phase Transformations in Silicon Under Contact Loading. *Reviews on Advanced Materials Science* **2002**, *3*, 1-36. doi: 10.1007/978-94-011-5050-7_30

10. Mohammadi, H.; Poyraz, H.; Ravindra, D.; Patten, J. An Experimental Study on Single Point Diamond Turning of an Unpolished Silicon wafer via Micro-Laser Assisted Machining. *Advanced Materials Research* **2014**, *1017*, 175-180. doi: 10.4028/www.scientific.net/AMR.1017.175

11. Ravindra, D.; Ponthapalli, S.; Patten, J. Micro-Laser Assisted Single Point Diamond Turning Feasibility Tests of Single Crystal Silicon. In *American Society for Precision Engineers (ASPE) 28th Annual Meeting*, St. Paul, Minnesota, USA; Raleigh, North Carolina, USA, 2013.

12. Ravindra, D.; Ghantasala, M.; & Patten, J. Ductile Mode Material Removal and High-Pressure Phase Transformation in Silicon During Micro-Laser Assisted Machining. *Precision Engineering* **2012**, *36*; 364-367. doi: 10.1016/j.precisioneng.2011.12.003

13. Colomban, P. Analysis of Strain and Stress in Ceramic, Polymer and Metal Matrix Composites by Raman Spectroscopy. *Advanced Engineering Materials* **2002**, *4*, 535-542. doi: 10.1002/1527-2648(20020806)4:8<535::AID-ADEM535>3.0.CO;2-E

14. Strain Measurements of a Si Cap Layer Deposited on a SiGe Substrate Determination of Ge Content. (n.d.). Horiba Scientific.

15. Poborchii, V., Tada, T., & Kanayama, T. Observations of the Forbidden Doublet Optical Phonon in Raman Spectra of Strained Si for Stress Analysis. *Applied Physics Letters* **2010**, *97*, 041915. doi: 10.1063/1.37272604

16. Jasinevicius, R., Duduch, J., Montanari, L., & Pizani, P. Phase Transformations and Residual Stress Probed by Raman Spectroscopy in Diamond-Turned Single Crystal Silicon. *Proceedings of the Institution of Mechanical Engineers, Part B: Journal of Engineering Manufacture* **2008**, *222,* 1065-1073. doi: 10.1243/09544054JEM1161

17. Gogotsi, Y.; Baek, C.; Kirscht, F. Raman Microspectroscopy Study of Processing-Induced Phase Transformations and Residual Stress in Silicon. *Semiconductor Science and Technology* **1999**, *14*, 936-944.

18. What is Raman Spectroscopy? http://www.nanophoton.net/raman/raman-spectroscopy.html Accessed 7/5/17.

7. Minimizing Surface Damage in Silicon with Micro-Laser Assisted Machining

S.M. Langan[a], D. Ravindra[b], A.B. Mann[a]

[a] Materials Science and Engineering, Rutgers University, Piscataway, NJ 08854, USA

[b]Micro-LAM, Inc., 5960 S. Sprinkle Rd., Portage, MI 49002, USA.

Abstract

Machining of ceramics and crystalline semiconductors is often a necessary processing step, but is both expensive and potentially damaging to the surface. Micro-Laser Assisted Machining (micro-LAM) adds *in situ* laser assistance to traditional single point diamond turning to increase throughput, hence lowering cost, while simultaneously reducing the damage caused by machining. Micro-Raman spectroscopy was used to examine residual stress, changes in relative crystallinity, and creation of additional phases when using different settings the machining of silicon. Low residual stress, high relative crystallinity, and a high relative phase purity are all achieved with optimal machining parameters, laser power, and feed rate, but non-optimal settings have detrimental effects on the surface properties.

Introduction

Ceramics and single crystal semiconductors are frequently produced with dimensions and morphologies that do not conform to those required for their intended application. As a result, some form of surface finishing and machining is almost always

necessary in order to reach the required tolerances for size and surface finish. This processing step is often a major source of damage during production as shown by Zhang et al (2003) and can account for 60-90% of a part's cost as described by Chin (2002). Despite not always being apparent, the damage due to machining can lead to early failure as well as a decrease in the functional performance of the material.

Due to the damaging and expensive nature of "traditional" machining new techniques are constantly being sought that can bring down the cost and improve the quality of the machined material. Micro-Laser Assisted machining, or Micro-LAM, is one of the most promising of these techniques. It uses a method that is similar to Single Point Diamond Turning (SPDT) based on the principle that high pressures can cause brittle materials to behave in a ductile fashion during removal (as described by Patten et al., 2005). When machining is done in the ductile regime it alleviates many of the hazards of "traditional" machining, such as microcracking, (as described in Kovalchenko, 2013).
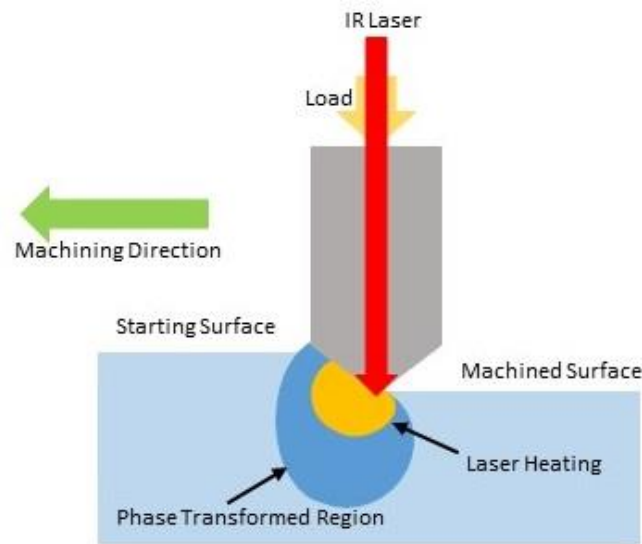
Figure 7.1: The Micro-LAM process (figure adapted from Patten et al., 2011) which is similar to SPDT, but a laser is shone through the diamond stylus to thermally soften the material and augment the phase transformed region.

The Micro-LAM process involves the use of a laser to assist the phase transformation and subsequent machining. The diamond stylus is connected to a laser through fiber optics (as seen in Patten et al., 2011) which enables the laser to shine through the stylus onto the sample. This gives thermal softening of the material and makes the brittle to ductile transition more favorable, (as described in Ravindra et al., 2011). This can be seen in terms of mechanical properties as a lowering of the apparent hardness of the material by as much as 50%, (see Shayan et al., 2009).

The current study focuses on silicon because of its importance as a material for optical and electric applications, and because it is an excellent candidate for machining via Micro-LAM. Silicon undergoes a complex phase change under pressure (shown in Jasinevivius et al., 2007). During loading, the Si-I transforms to Si-II. If the unloading

rate is slow, this transforms into Si-XII, then Si-III and finally Si-IV/Si-XIII. If the unloading rate is fast, it goes from Si-II to Si-IX and then to amorphous. With annealing both routes can give amorphous Si, which transforms to Si-I. The uniqueness of the brittle to ductile transition in silicon, and its dependence on pressure and rate, often give multiple phases that are not present with other materials. It has also been found that at smaller cut depths more amorphous Si is present while at deeper cuts more Si-XII, Si-III and Si-IV are found. It was postulated that the smaller cuts had less stress associated with them, which leads to faster unloading, hence the amorphous Si. The amorphous phase is almost always present when silicon undergoes this kind of process, and it can be an issue in terms of the silicon's subsequent performance.

Previous studies have looked at the effect of the Micro-LAM process on the surface finish of silicon. Preliminary work by Mohammadi et al. (2014) showed a reduction in the roughness, R_a, of unpolished wafers from 0.85μm to 0.23μm with as few as two passes using the Micro-LAM process. With closer to optimal conditions, an even better value of R_a (around 5nm) was reported by Ravindra et al. (2013); this level of smoothness allows for a more reflective surface than conventionally polished wafers. However, it has been found that if the Micro-LAM parameters are not correct, large amounts of additional phases such as Si-III, Si-IV, and Si-XII, as well as the original Si-I phase, can be present. Optimizing the machining parameters gives a final material that can be close to phase pure (as shown by Ravindra, et al., 2012). None of these previous studies have examined the residual stresses, crystallinity, and phases present after the Micro-LAM process, all of which contribute to the subsequent performance and potential failure of the material.

Here, Raman spectroscopy coupled to optical microscopy (micro-Raman) is employed to look at residual stress, relative phase purity, and relative crystallinity in silicon before and after machining with the Micro-LAM process. Raman looks at shifts in an incident laser's wavelength due to excitation of lattice vibrational modes in a crystalline material. As such, Raman can be used to look at residual stresses that strain the lattice, giving rise to changes in bond length and vibrational modes. The shift in a Raman spectral peak between a stressed and an unstressed state is a well-documented method for measuring stresses. It is applicable to many materials (Colomban, 2002), with the stress being linearly related to the change in peak position for many ceramics and single crystal semiconductors, such as the silicon of interest here.

Experimental

Single crystal silicon samples finished using the laser assisted machining method combined with an ultraprecision diamond turning machine were provided by Micro-LAM Inc., Portage, MI, USA. The samples were machined on a Precitech N250 using the Micro-LAM Optimus setup. The laser assistance came from a 1064nm diode laser. The machining parameters are described in Table 7.1.

Sample	Depth of Cut (μm)	Feed Rate (μm/rev)	Laser Power
A	5	2	10% of 200W
B	5	0.5	10% of 200W
C	5	2	30% of 200W
D	5	0.5	30% of 200W

Table 7.1: Machining conditions for single crystal silicon samples machined with the ultraprecision diamond turning machine.
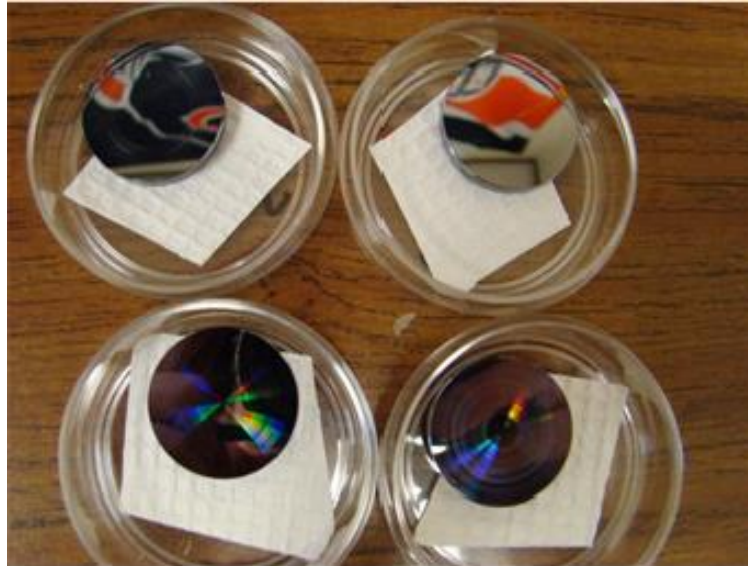

Figure 7.2: Highly reflective single crystal silicon samples machined with the Micro-LAM technique on an ultra-high precision diamond turning machine.

Raman micro-spectroscopy of all the samples were undertaken with a Renishaw InVia™ Raman spectrometer. All samples were examined with Raman excitation lasers of 514 nm and 633 nm, which penetrate 762 and 3000 nm respectively as seen in "Strain

Measurements of a Si Cap", and areas of 40 x 40 μm were mapped with scans taken every 2 μm.

The Raman spectra were then fitted with the Renishaw Wire 3.4 software, which comes with the spectrometer. From this fitting, the peak shift from the unstressed peak (taken from a piece of single crystal silicon) was found, and the stress was found using the following formula from Jasinevicius et al. (2008).

$$\omega = \omega_o + 0.52P \qquad (1)$$

where ω is the peak position, ω_o is the unstressed peak position, and P is the stress in Kilobar. For single crystal Si-I there is a single strong peak at 520 cm^{-1}, which corresponds to ω_o. Note that by convention for silicon compressive stress is given as positive and tensile stress as negative.

Results

Figure 7.3 shows the average residual stress values obtained using the 514 nm and 633 nm Raman lasers on the samples. It should be noted that no residual stress could be obtained using the 514 nm laser for sample C (feed rate of 2 μm/rev and 30% laser power). This does not mean the surface was stress free, rather that strong Raman peaks (due to the presence of additional phases) prevented the calculation of a residual stress.
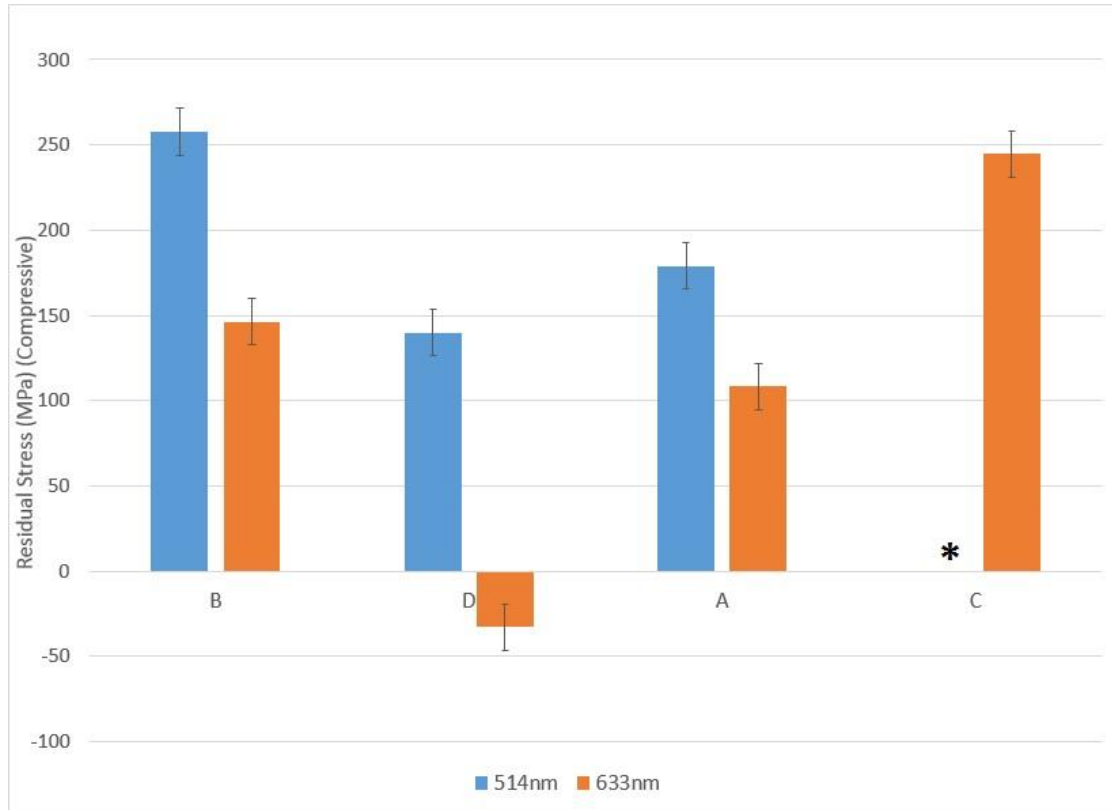
Figure 7.3: Average residual stress values in the high precision turned samples. 514nm and 633nm data is presented along with the feed rate and the laser power during the machining.   Error bars found by propagating errors. *For sample C, the 2 μm/rev feed rate with 30% laser power, using a Raman laser of 514 nm there is insufficient Si-I to measure the residual stress.

Sample B (0.5 μm/rev, 10% laser power) has the highest residual stress of 258 ± 13.6 MPa when measured with the 514 nm Raman laser. It also has the second highest stress when the Raman with the 633 nm laser is used. The largest stress with the 633 nm Raman laser is with sample C (2 μm/rev, 30% laser power). Sample D (0.5 μm/rev, 30% laser power) has the lowest residual stresses for both the 514 nm and 633 nm Raman lasers, though it is of note that at 633 nm, the average residual stress is tensile. For both the 514 nm and 633 nm lasers the average stresses are very low at 140 ± 13.6 MPa and -

33 ± 13.6 MPa , respectively. For a sample polished with a high quality mirror finish, these low stresses are very good.

Maps of the Raman peak shift for the samples (Figures 7.4, 7.5, 7.6, 7.7) show how much residual stress varies over the surface. As well as the maximum values, consistency of the residual stress over the surface is desirable as it avoids stress concentration "hot spots" that could lead to early failure. For this reason, it is good to look at the stress maps for each machining condition. These reinforce the view that the conditions for sample D, Figure 5, gives the best results in terms of residual stresses. The stress maps obtained with the 514 nm and 633nm Raman lasers also give insight into how the stress changes with depth as the two lasers probe different volumes at the surface (633 nm penetrating deeper than 514 nm).
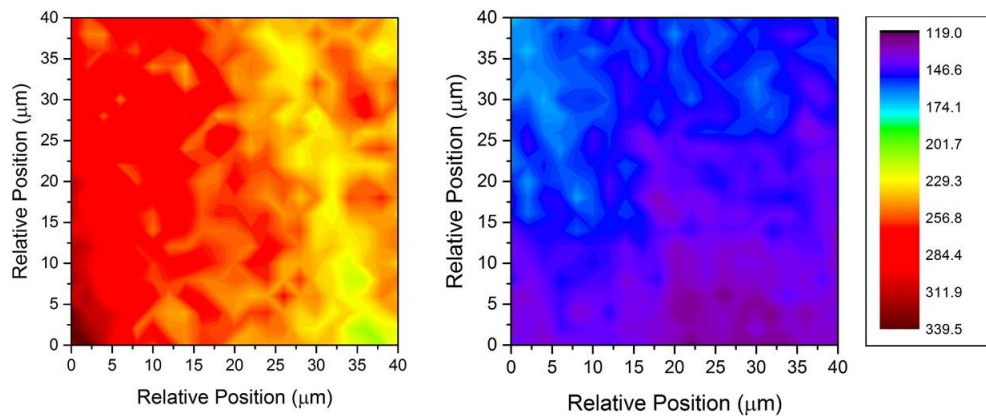

Figure 7.4: Stress maps of sample B (machined at 0.5 µm/rev and 10% laser power) obtained using the 514 nm Raman laser (left) and the 633 nm Raman laser (right). The bar on the far right represents stress, in MPa.

Figure 7.5: Stress maps of sample D (machined at 0.5 μm/rev and 30% laser power) obtained using the 514 nm Raman laser (left) and the 633 nm Raman laser (right). The bar on the far right represents stress, in MPa.

Figure 7.6: Stress maps of sample A (machined at 2 μm/rev and 10% laser power) obtained using the 514 nm Raman laser (left) and the 63 3nm Raman laser (right). The bar on the far right represents stress, in MPa.
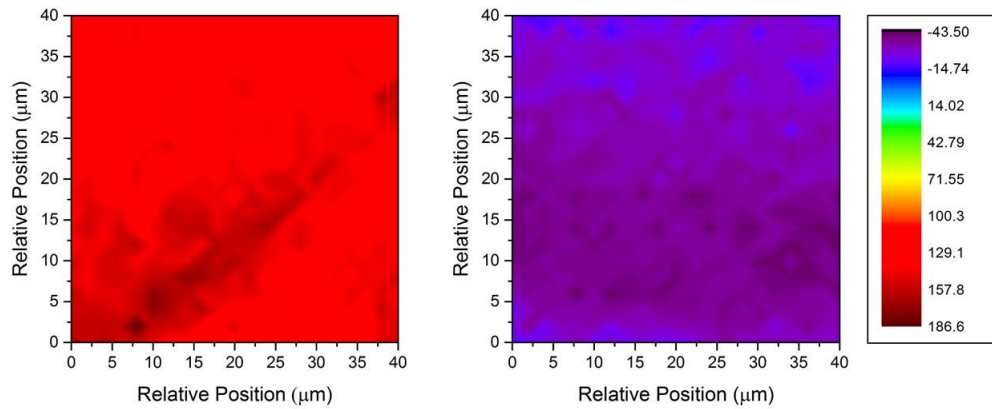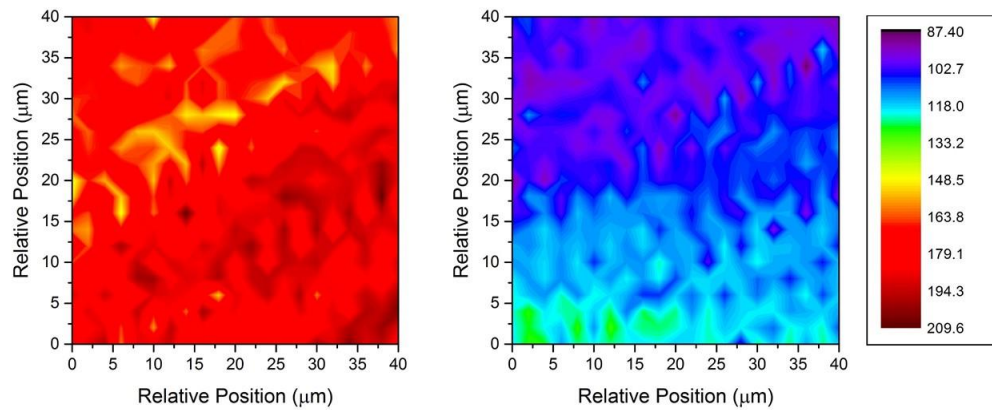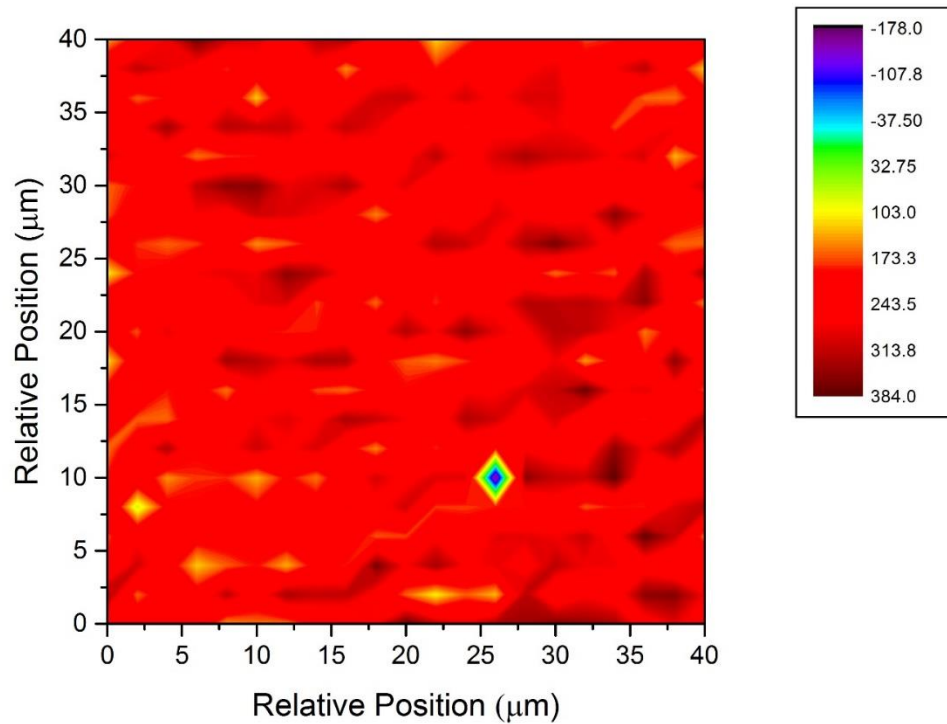
Figure 7.7: Stress map of sample C (machined at 2 μm/rev and 30% laser power)

obtained using the 633nm Raman laser. The bar on the right represents stress, in MPa.

Note that the stress could not be measured using the 513 nm laser to due to the many

phases present.

In terms of uniformity of the residual stress, relatively little scatter is seen for

most of the samples and Raman laser wavelengths and the values only vary over a range

of 80 MPa. The anomaly is the map for sample C (feed rate 2 μm/rev and 30% laser

power) taken with the 633 nm Raman laser, which has a range of 500 MPa in stress,

including several spots which differ from the average by hundreds of MPa. This is

probably because of the presence of many phases at the surface when it has finished using these machining conditions. For the better samples (notably sample D) a good finish is obtained with desirably low residual stress and a small range of stresses. Figures 7.4, 7.5, 7.6 show that the stresses measured for samples A, B, and C using the 514 nm Raman laser are uniformly higher than those measured with the 633 nm Raman laser. This reflects the fact that the 633 nm penetrates further and samples volumes deeper in the sample. At deeper depths below the surface the impact of the Micro-LAM process is expected to be less pronounced. This is also true for sample D, but in this instance the machining results in many phases being present at the shallow depths measured with the 514 nm Raman laser.

Other information can be obtained from the Raman data including the relative full width at half maximum (FWHM) of the Raman spectral peaks. This is generally used as a measure of crystallinity, and can be used to assess how machining distorts the crystal lattice in single crystal silicon. While Raman cannot give the rigorous data about crystallinity provided by X-ray diffraction (XRD), it does give an idea of how "good" the crystal structure is for a material. Narrower Raman peaks are taken to be a sign of better crystallinity. Figure 7.8 gives the relative peak widths (crystallinity) for the machined samples and the two Raman lasers give an indication of how crystallinity changes with depth.
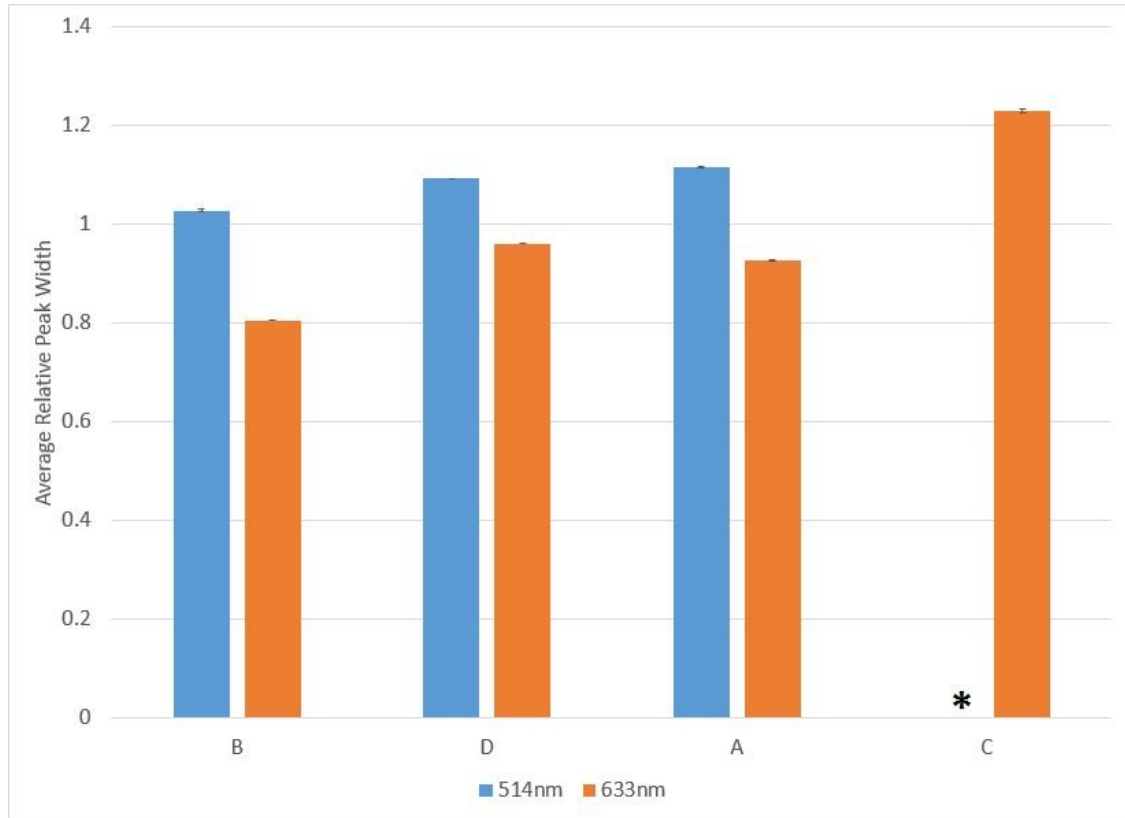
Figure 7.8: Average Relative Peak Widths in the high precision turned samples. 514 nm

and 633 nm Raman laser data is presented along with the feed rate and the laser power

during the machining. Error bars represent standard error. *The 514 nm Raman laser data

for sample C (feed rate of 2 μm/rev, 30% laser power) is not zero, but the Si-I peak was

too weak to measure due to the presence of other phases.

As would be expected of each machining condition, the peaks for the 633 nm

Raman laser are narrower than the peaks for the 514 nm Raman laser. This reflects the

greater penetration into the less damaged interior of the sample using the longer

wavelength Raman laser. Sample B (with a feed rate of 0.5 μm/rev, and 10% laser power)

had the narrowest peaks, showing it has the best relative crystallinity out of all the

machined samples. It should be noted that some results have a lower value than the control's of 1, which could be due to annealing from the laser assistance that makes for better machining quality than the standard.

The same mapping that was used to examine residual stress in the material was also used to look at the distribution of the peak widths in the sample. All of the machined samples showed very uniform peak widths over the mapped areas, as seen in Figures 7.9, 7.10, and 7.11. As with residual stress, consistent relative crystallinity avoids localized spots that can become as points of failure. Only sample C (feed rate of 2 μm/rev and 30% laser power) had a large range for peak width of 0.62 cm^{-1} as shown in Figure 7.12 for the 633 nm Raman laser. Sample C has the largest stress, the widest peaks, and as will be seen, the most additional phases as well.

Figure 7.9: Peak width maps for sample B, machined with a feed rate of .5 μm/rev and 10% laser power. Two penetration depths with the 514 nm Raman laser (left) and the 633nm Raman laser (right) show a small range in crystallinity. The bar on the far right represents the normalized peak width.

Figure 7.10: Peak width maps for sample D, machined with a feed rate of .5 μm/rev and 30% laser power. Two penetration depths with the 514 nm Raman laser (left) and the 633nm Raman laser (right) show the uniformity of the crystallinity. The bar on the far right represents the normalized peak width.
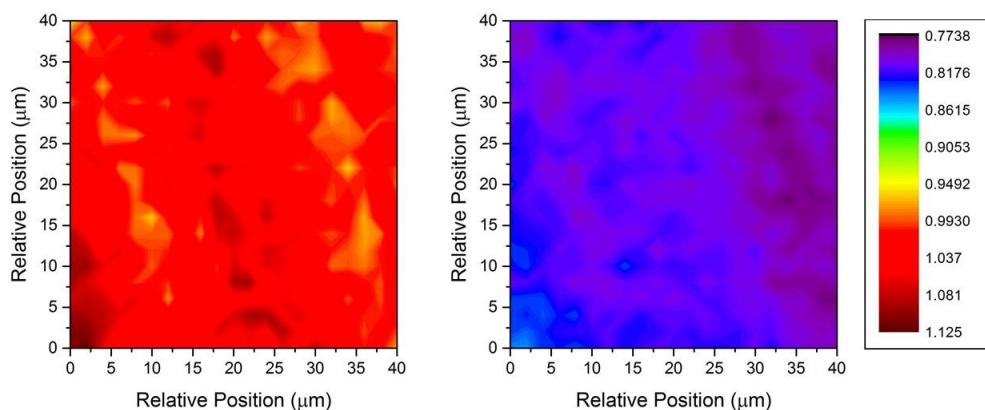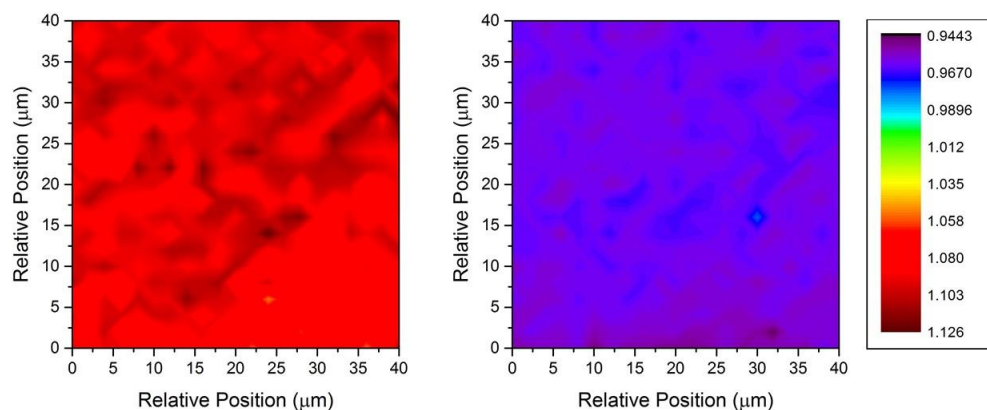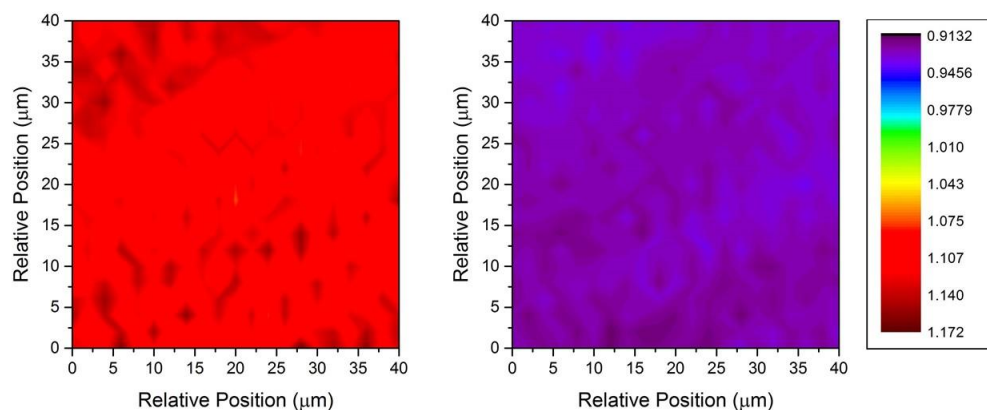
Figure 7.11: Peak width maps for sample A, machined with a feed rate of 2 μm/rev and 10% laser power. Two penetration depths with the 514 nm Raman laser (left) and the 633nm Raman laser (right) show the uniformity of the crystallinity. The bar on the far right represents the normalized peak width.
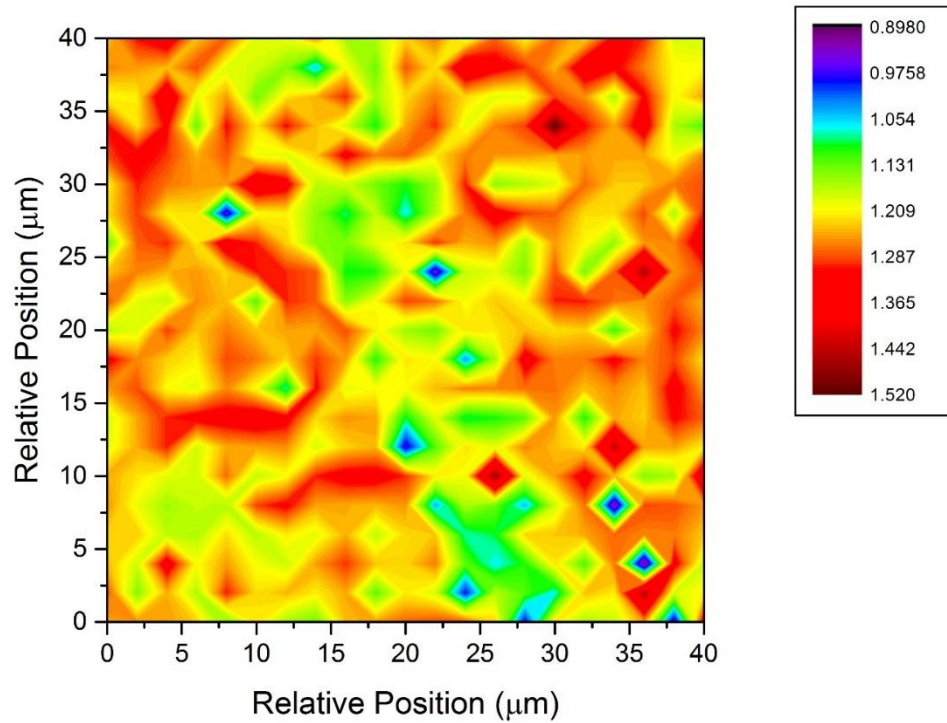
Figure 7.12: Peak width map for sample C machined with a feed rate of 2 μm/rev, and 30% laser power obtained using the 633 nm Raman laser. The bar on the right represents peak width.

Since silicon can form different phases under pressure, and the Micro-LAM process exerts pressure on the sample, it is important to examine the additional phases in these silicon samples. Additional phases can cause differences in the mechanical, electrical, and optical properties of the machined silicon in comparison to pure Si-I, therefore minimizing the presence of these phases after the machining is desirable. To judge the overall performance of the Micro-LAM process it is vital that the presence of multiple phases be considered along with the residual stresses and crystallinity already

discussed. As shown in Figures 7.13 and 7.14, the Raman spectra shows the presence of

many phases after machining, in this case for sample C.

Figure 7.13: Raman spectra for sample C (feed rate of 2 μm/rev and 30% laser power)

taken with the 514 nm Raman laser. Si-III, Si-IV, Si-XII, and amorphous silicon are

present, while no Si-I peak at 520 cm^{-1} is seen.

Figure 7.14: Raman spectra for sample C (feed rate of 2 μm/rev and 30% laser power) taken with the 633 nm Raman laser. Si-III, Si-IV, Si-XII, and amorphous silicon are present, along with a small Si-I peak.

A significant number of additional Raman peaks for sample C are seen with both the 514 nm and 633 nm Raman lasers as shown in the spectra of Figures 7.13 and 7.14. This indicates a significant quantity of additional phases in the surface region, which is highly undesirable in terms of optical and electronic applications of silicon. However, when the Micro-LAM process is optimized, phase pure materials can be made, as is evident in Figure 7.15 and 7.16 for sample A. In these figures, it can be seen that there is very little amorphous silicon, and no peaks for crystalline silicon phases aside from Si-I.
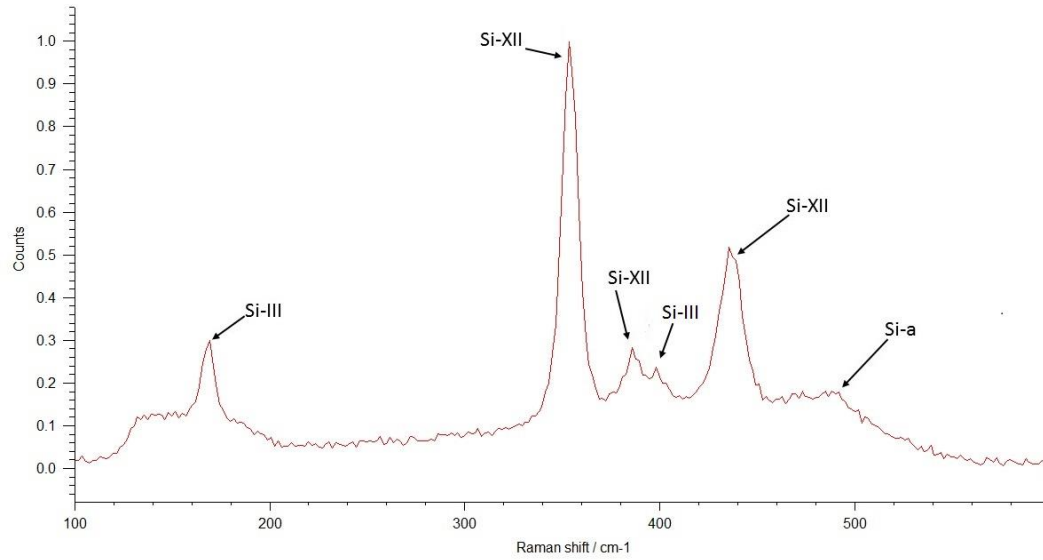
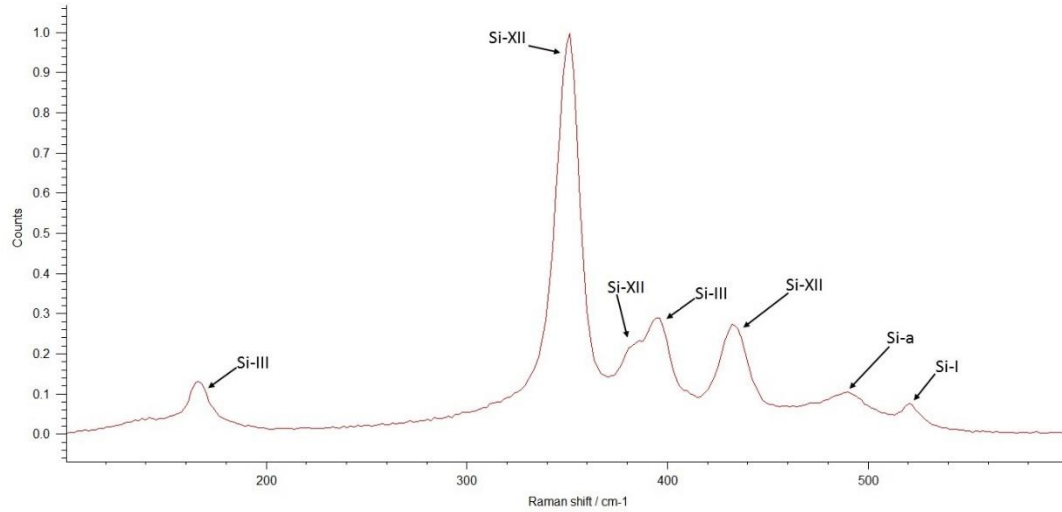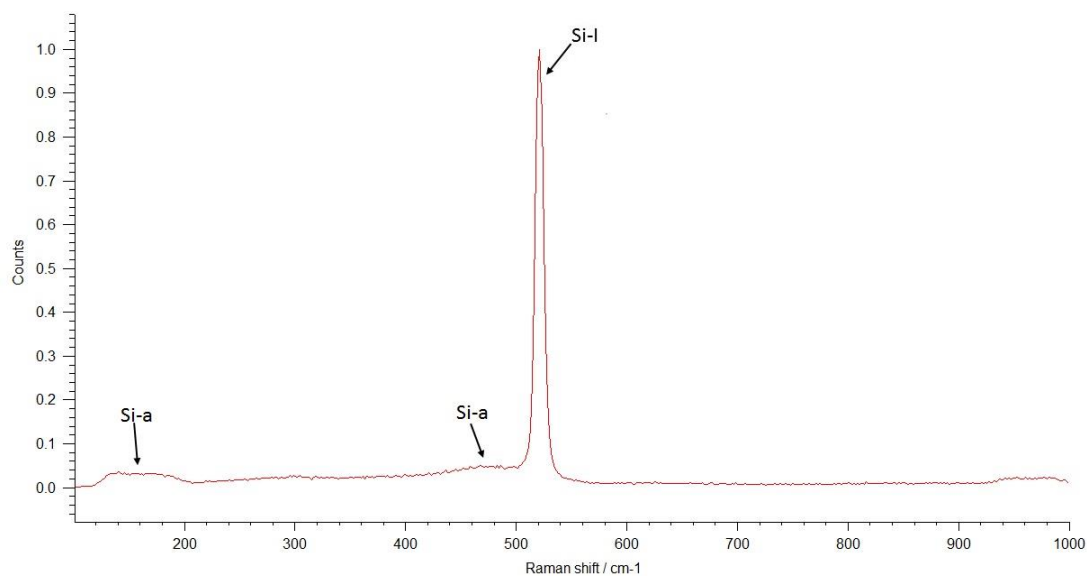Figure 7.15: Raman spectra for sample A (feed rate of 2 μm/rev and 10% laser power) taken with the 514 nm Raman laser. Only a small amount of amorphous phase is present.
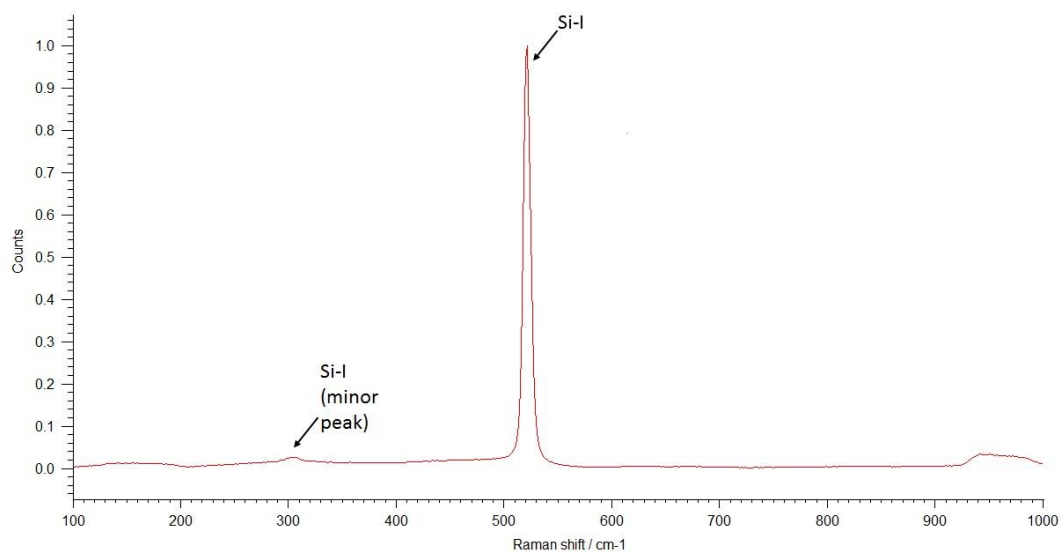
Figure 7.16: Raman spectra for sample A (feed rate of 2 μm/rev and 10% laser power) taken with the 633 nm Raman laser. Virtually no amorphous phase is present.

To quantify the amounts of the additional phases as best as possible, an approach similar to that taken by Gogotsi, et al (1999) was taken, using the equation

$$P_{rel} = \frac{I_{515-525}}{I_{350-515}+I_{515-525}} \qquad (2)$$

where P_{rel} is the relative phase purity, $I_{350-515}$ is the total intensity of all peaks in the range of 350-515 cm^{-1}, and $I_{515-525}$ is the intensity of any peak in the range of 515-525 cm^{-1}, which is the Si-I peak, however, it is shifted. Thus, if the sample only contains Si-I, P_{rel} would be 1, and if there is no Si-I peak present it would be 0. The results of this analysis are plotted in Figure 7.17.
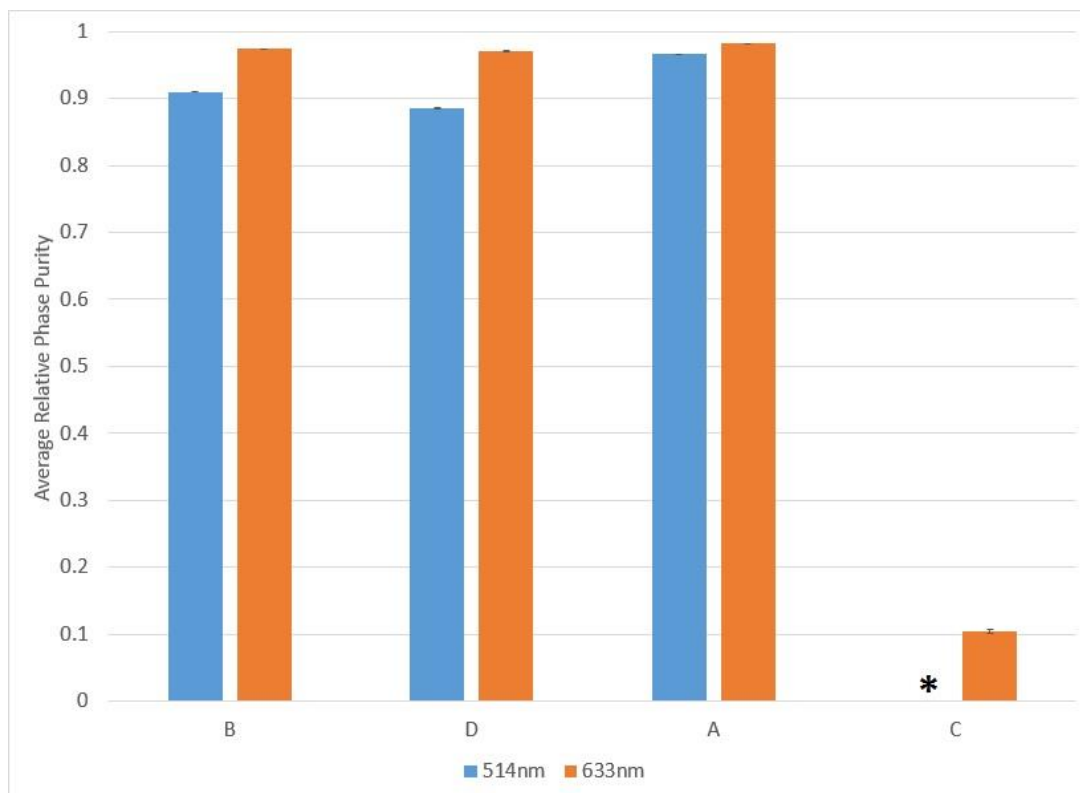
Figure 7.17: Relative phase amounts for the various machining conditions performed

with Micro-LAM with the 514 nm and 633nm Raman lasers. Error bars represent

standard error. *The 514 nm Raman laser data for sample C (feed rate of 2 μm/rev, 30%

laser power) is not zero, but the peak due to Si-I was not present so it could not be used

as a measure of relative phase purity.

As expected, in general there is a stronger Si-I peak in the scans obtained with the

633 nm Raman laser when compared to the scans with the 514 nm Raman laser, because

the longer wavelength penetrates deeper into the sample. The data shown does not

include the 514 nm Raman laser scans for sample C, because the Si-I peak at 520 cm^{-1}

was not present.

Overall, the Micro-LAM process resulted in surfaces with good phase purity, with the exception of sample C (feed rate of 2 μm/rev, 30% laser power). The best phase purity was with sample A (feed rate of 2 μm/rev, 10% laser power). Even at the shallower depths probed with the 514 nm Raman laser, sample A exhibited phase purity comparable to the other samples phase purity for the 633 nm Raman laser. Sample C's very low phase purity (0.1 for the 633 nm Raman laser) contrasts strongly with the other Micro-LAM machined samples. The next lowest was sample D (feed rate of 0.5 μm/rev, 30% laser power), with a relative phase purity of 0.89 taken with the 514 nm Raman laser.

As with residual stress and crystal quality, it is valuable to examine the maps to see if there are "hot spots" where there are significantly higher amounts of additional phases when compared to the phase pure silicon. The lattice mismatch between phases could decrease performance under stress, so it is important to see the distribution of stresses left by the various machining conditions.

As can be seen in Figures 7.18-7.21, there are generally only small variations in the relative phase purity. All of the scans have ranges less than 0.07, except the 633 nm Raman laser scan of sample C (feed rate of 2 μm/rev, 30% laser power) with a range of 0.33, and the 514 nm Raman laser scan of sample D (feed rate of 0.5 μm/rev, 30% laser power) with a range of 0.10. It is notable that the maps have "bands" that are present for both the 514 nm Raman laser and 633 nm Raman laser. These are most likely formed during the machining process, and reflect the variations in pressure that occur under the point of contact for the diamond tip.
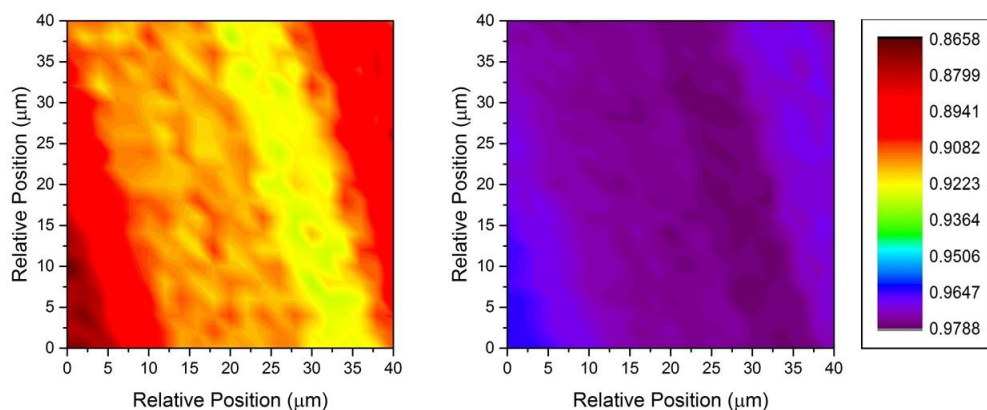
Figure 7.18: Phase purity maps of sample B (feed rate of 0.5 μm/rev, and 10% Laser power) taken with the 514 nm Raman laser (left) and the 633nm Raman laser (right). The bar on far right represents the relative phase purity.
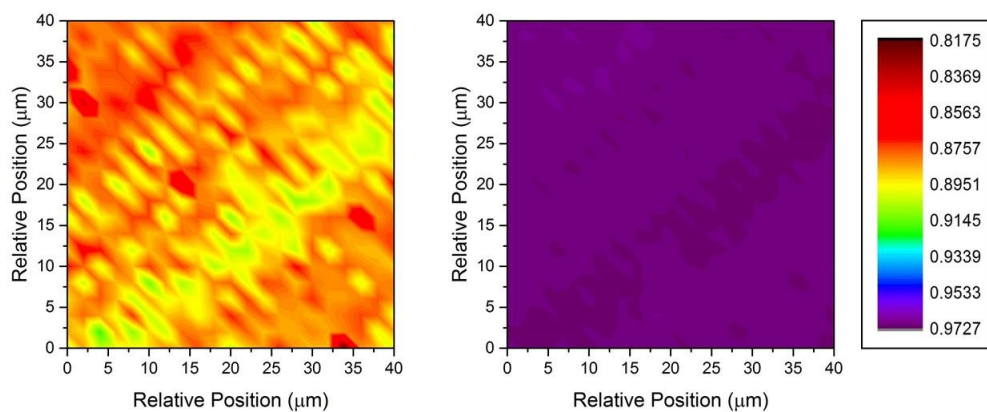
Figure 7.19: Phase purity maps of sample D (feed rate of 0.5 μm/rev, and 30% Laser power) taken with the 514 nm Raman laser (left) and the 633nm Raman laser (right). The bar on far right represents the relative phase purity.
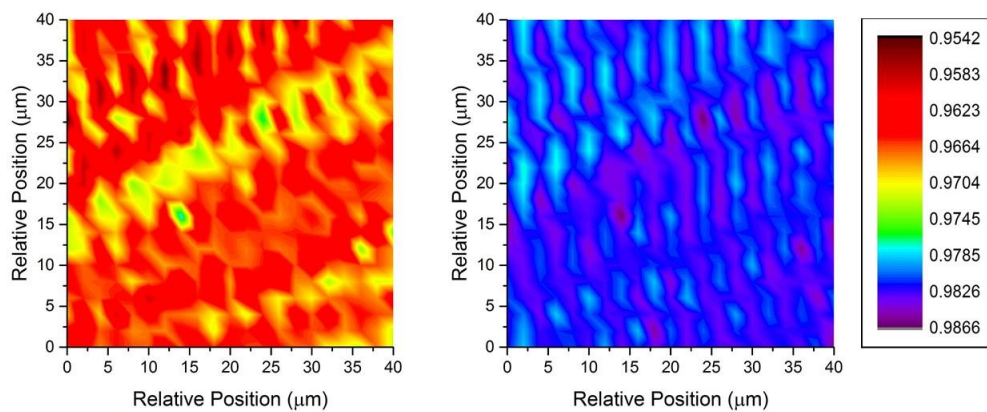
Figure 7.20: Phase purity maps of sample A (feed rate of 2 μm/rev, and 10% Laser power) taken with the 514 nm Raman laser (left) and the 633nm Raman laser (right). The bar on far right represents the relative phase purity.
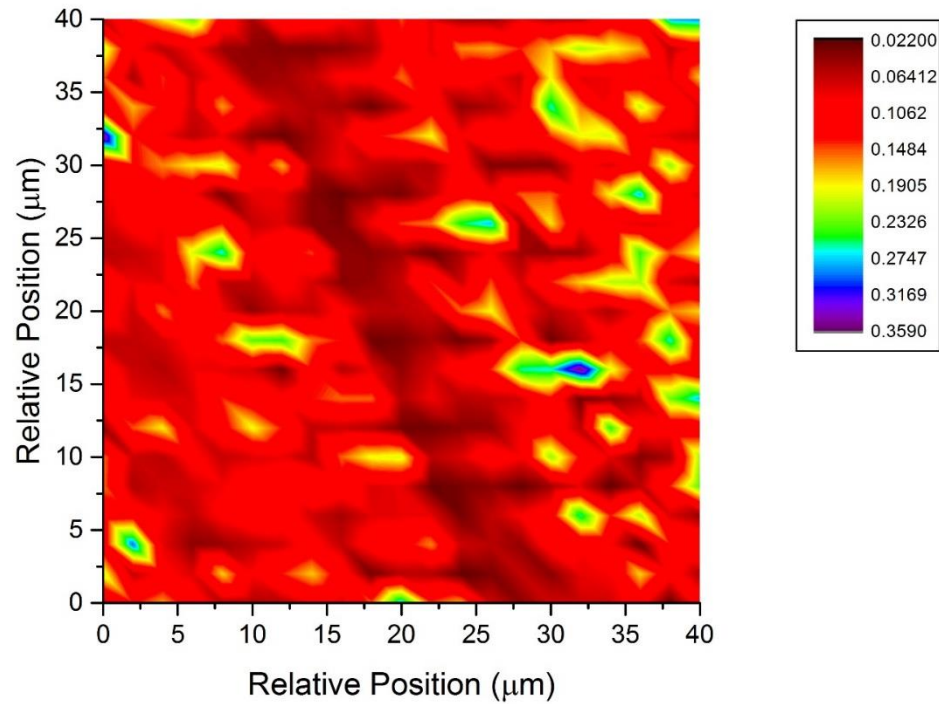
Figure 7.21: Phase purity map of sample C (feed rate of 2 μm/rev, and 30% Laser power) taken with the 633nm Raman laser. The bar on the right represents the relative phase purity.

Conclusion

When the Micro-LAM process is applied to machining silicon with optimal settings the results are excellent with low stress, high relative crystallinity, and good phase purity. However, the incorrect settings can give entirely the opposite results with high stress, low relative crystallinity and phase purity. In this study, two different feed rates and two different laser powers were combined in four samples, and the results were examined. The different results in the samples correlate strongly with how much total

energy (mechanical and laser) is put into the sample. That is, sample C (feed rate of 2 μm/rev, and 30% Laser power) with the highest machining rate and highest laser power gave the worst results in terms of residual stress, additional phases present, and relative crystallinity. The high rate of deformation and the laser power combine to give phase transformations that are not reversible without subsequent annealing.

One of the advantages of Micro-LAM over traditional SPDT is that the laser gives the user another factor to "tweak". For example, sample B (with a feed rate of 0.5 μm/rev and 10% laser power) has high residual stress, but when the laser power is increased for sample D the residual stress is reduced possible through in situ annealing. Similarly, the settings of sample C (feed rate of 2 μm/rev, and 30% Laser power) yield poor results, but a lower laser power of 10% (sample A) gives lower residual stresses along with the most phase pure material of all the samples examined.

Machining is a complex process, and it is difficult to predict how it will affect a material. The Micro-LAM method offers additional parameters that can be changed and optimized to achieve a desirable surface finish. The method combines the benefits of traditional SPDT and enables easier material removal and the elimination of microcracks and chipping, that are often evident in brittle material removal. The laser assistance thermally softens the material being machined and reduces the material's apparent hardness. Varying the laser power allows for machining to be optimized. This added parameter allows for residual stress to be reduced and additional phases largely eliminated when machining silicon. In this study, optimal conditions were found where residual stresses are low (<150 MPa) with good relative crystallinity and high phase

purity. This combined with prior work highlighting the excellent surface finish that can be obtain indicate that the Micro-LAM process is invaluable for machining silicon.

References

Chinn, R. E. (2002) Ceramography: Preparation and Analysis of Ceramic Microstructures. 1st edition, Wiley-American Ceramic Society: Malden, Massachusetts, USA.

Colomban, P. (2002) Analysis of Strain and Stress in Ceramic, Polymer and Metal Matrix Composites by Raman Spectroscopy. Advanced Engineering Materials, 4; 535-542.

Gogotsi, Y.; Baek, C.; & Kirscht, F. (1999) Raman Microspectroscopy Study of Processing-Induced Phase Transformations and Residual Stress in Silicon. Semiconductor Science and Technology, 14; 936-944.

Kovalchenko, A. M. (2013). Studies of the ductile mode of cutting brittle materials (A review). Journal of Superhard Materials, 35 (5): 259–276.

Jasinevicius, R. G.; Duduch, J. G.; & Pizani, P. S. (2007) Structure Evaluation of Submicrometre Silicon Chips Removed by Diamond Turning. Semiconductor Science and Technology, 22 (5): 561-573.

Jasinevicius, R.G; Duduch, J.G.; Montanari, L.; & Pizani, P.S. (2008) Phase Transformation and Residual Stress Probed by Raman Spectrosopy in Diamond-Turned Single Crystal Silicon. Proceedings of the Institution of Mechanical Engineers, Part B: Journal of Engineering Manufacture, 222; 1065-1073.

Mohammadi, H.; Poyraz, H.; Ravindra, D.; & Patten, J. (2014) An Experimental Study on Single Point Diamond Turning of an Unpolished Silicon wafer via Micro-Laser Assisted Machining. Advanced Materials Research, 1017: 175-180.

Patten, J.; Gao, W.; & Yasuto, K. (2005) Ductile regime nanomachining of single-crystal silicon carbide. Journal of Manufacturing Science and Engineering, 127: 522–532.

Patten, J.; Ghantasala, M.; Ravindra, D.; Poyraz, H.; & Virkar, S. (2011) The Effects of Laser Heating on the Material Removal Process in Si and SiC Nanomachining. Proceedings of 2011 NSF Engineering Research and Innovation Conference, Atlanta, Georgia, USA.

Ravindra, D.; Ghantasala, M.; & Patten, J; (2012) Ductile Mode Material Removal and High-Pressure Phase Transformation in Silicon During Micro-Laser Assisted Machining. Precision Engineering, 36; 364-367.

Ravindra, D.; Ponthapalli, S.; & Patten, J. (2013) Micro-Laser Assisted Single Point Diamond Turning Feasibility Tests of Single Crystal Silicon. American Society for Precision Engineers (ASPE) 28th Annual Meeting, St. Paul, Minnesota, USA; Raleigh, North Carolina, USA.

Ravindra, D.; Virkar, S.; & Patten, J. (2011) Ductile Mode Micro Laser Assisted Machining of Silicon Carbide. 1st Edition, In Properties and Applications of Silicon Carbide, Gerhardt R., Ed., InTech: Croatia.

Shayan, A.; Poyraz, H.; Ravindra, D.; & Patten, J. (2009) Pressure and Temperature Effects in Micro-Laser Assisted Machining (µ-LAM) of Silicon Carbide. In North American Manufacturing Research Conference (NAMRC), Greenville, South Carolina, USA; Dearborn, Michigan, USA.

Strain Measurements of a Si Cap Layer Deposited on a SiGe Substrate Determination of Ge Content, Horiba Scientific.

Zhang, B.; Zheng, X.L.; Tokura, H.; & Yoshikawa, M. (2003) Grinding Induced Damage in Ceramics. Journal of Materials Processing Technology, 132: 353-364.

8. Mitigation of Damage During Surface Finishing of Sapphire Using Laser-Assisted Machining

Sean M. Langan[a]*, Deepak Ravindra[b], Adrian B. Mann[a]

[a]Materials Science and Engineering, Rutgers University, Piscataway, NJ 08854, USA

[b]Micro-LAM, Inc., 5960 S. Sprinkle Rd., Portage, MI 49002, USA.

*Corresponding Author: sean.langan@rutgers.edu

Abstract

Machining of hard, crystalline ceramics is time-consuming, expensive and vital in many industries, but getting good results is challenging because of the surface damage it can cause. For sapphire machining damage can be especially detrimental because it can create significant stresses in the surface and sub-surface regions. Worst case, the stresses are relieved by crack propagation, fracture, and chipping at the surface. Conventional machining with a single point diamond-turning machine was compared to the same method with a laser simultaneously focused through a diamond stylus. The laser makes ductile machining more favorable and provides *in situ* annealing of damage. Micro-Raman spectroscopy was used to quantify residual stresses and optical microscopy was used to identify cracking. A reduction in the residual stresses was achieved when using the laser. This is seen most dramatically at higher laser powers, where fracture, cracking and chipping can be alleviated.

KEYWORDS: Ductile Mode Machining, Micro-Laser Assisted Machining, Sapphire

1. Introduction

Machining of ceramic and single crystal materials is a difficult, but necessary, step in the processing of materials for a variety of applications including optics [1], electronics [2], and MEMs [3]. The as-synthesized parts almost never fall within engineering dimensional requirements, and/or do not have the necessary surface finish, so machining is virtually always necessary. Yet this machining is also one of the primary sources of damage to the material during production [4]. This damage can lead to inferior material performance, as well as early failure. Furthermore, this essential machining step in the processing can account for 60-90% of the final cost of the product [5]. These difficulties with traditional machining have led researchers to seek alternative machining methods.

One machining technique that has been developed to reduce machining times and surface damage is Micro-Laser Assisted Machining, or Micro-LAM (Micro-LAM, Inc., Kalamazoo, MI). This process is based on Single Point Diamond Turning (SPDT) and aims to cause a high-pressure phase transformation at an elevated pressure in material under the point of contact. These conditions allow plastic yielding and ductile removal of the material during machining [6] without the damage associated with traditional machining, such as chipping or microcracking [7].
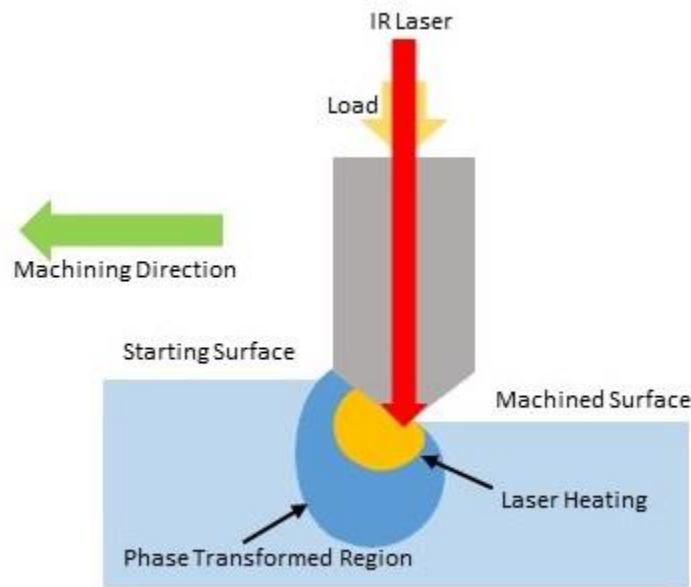
Figure 8.1: Diagram of the Micro-LAM process adapted from [8]. A diamond stylus is dragged across the material, creating a ductile phase through a high-pressure transformation. During this, a laser shines through the stylus, thermally softening the material.

The Micro-LAM process adds laser assistance to machining. A diamond stylus is embedded in an epoxy and connected to a laser via optical fibers [8]. The laser's light is guided through the fiber, then through the stylus and focused onto a sample. The laser provides thermal softening of the material, making the brittle-to-ductile transition more favorable by reducing the material's brittle nature and creating a more ductile response [9]. This thermal softening has been shown to lower the hardness of the material by as

much as 50% [10], allowing for better machining than similar diamond turning processes without the laser. The localized heating may also help to alleviate damage by providing in situ annealing during the machining process.

Sapphire is a material that is notoriously difficult to machine, and where the Micro-LAM process could prove particularly useful. Sapphire has high strength and hardness at 9 Mohs, and good wear resistance [11], which combined with its optical clarity make it an excellent material for windows and domes [12], as well as for lenses [13] and LEDs. Sapphire's exceptional physical properties mean it can perform in environments that many traditional transparent materials cannot [13]. Unfortunately, the physical properties that make it exceptional also make it a difficult and time-consuming material to machine. Due to its ability to reduce a material's hardness during the machining process, the Micro-LAM approach avoids many of the pitfalls of traditional machining, and offers a potential route to efficient machining of sapphire.

While there has been extensive work published on using the Micro-LAM method for machining silicon [14-16] and silicon carbide [9, 10, 17], as well some work on soda-lime glass [18] and quartz [19], only one preliminary study has been published on Micro-LAM of sapphire [20]. The study found that Micro-LAM machining of sapphire was possible, and that the addition of a laser to the SPDT process allowed for deeper cuts to be made on the material while preserving the cutting tool tip.

In the current study, Raman spectroscopy was used to examine residual stress in sapphire that has been subjected to both conventional SPDT and using the Micro-LAM

technique. Raman is a vibrational spectroscopy technique that looks at lattice

vibrational modes. These modes originate from the oscillation of atoms and molecules

in the crystal lattice. When a material is stressed, the spacing between atoms and

molecules is modified (strained), which in turn changes the frequency or energy of the

vibrational modes. This gives shifts in the peak positions of the Raman spectra of the

material. The relationship between Raman peak position and stress is well known for a

variety of materials [21]. With small strains, the relationship is typically linear, and the

stress in the material is directly proportional to the Raman frequency shift from the

unstressed state.

2. Experimental method

Samples were machined with a modified universal micro-Tribometer, seen in

Figure 8.2. The machine is adapted to accommodate the Micro-LAM system. An infra-

red laser was attached to the diamond turning tool with a 10 µm fiber optical cable. The

tool has two parts; a ferrule and a diamond tip with a 5µm radius, connected/coupled

with an UV curable epoxy to the fiber and, hence, the laser. The diamond, fiber, and

epoxy are all transparent to light of the laser's wavelength.
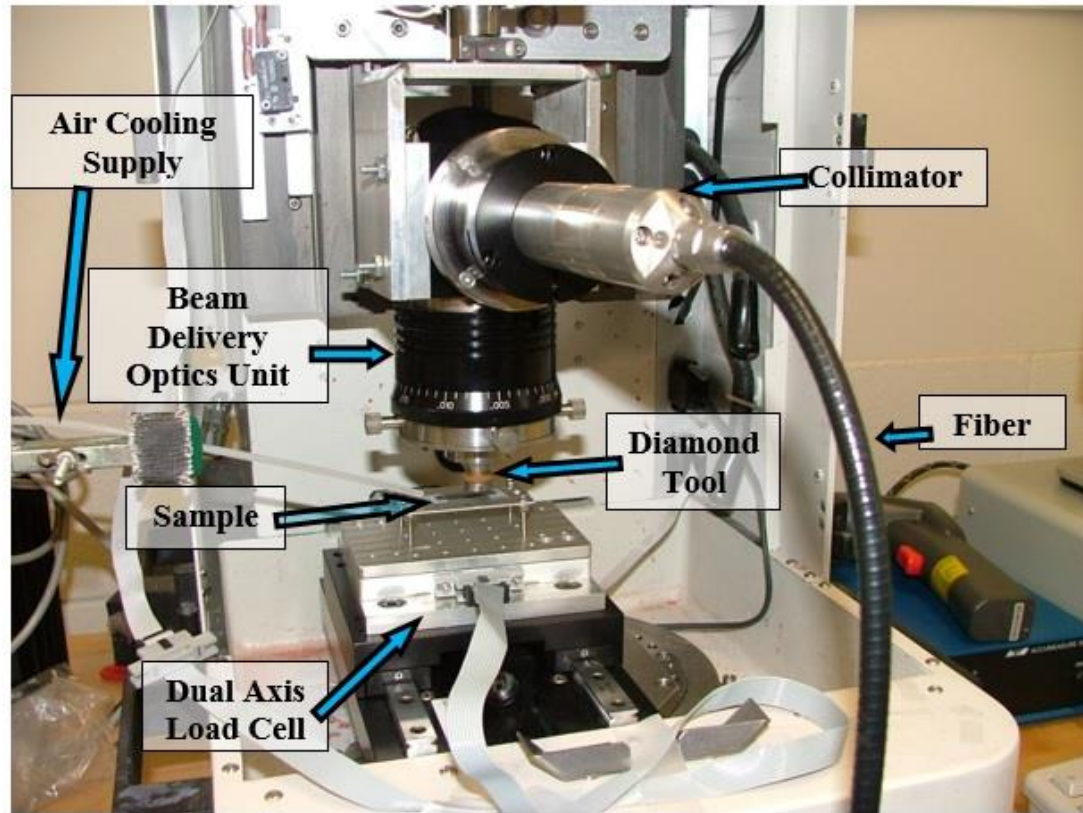
Figure 8.2: The Micro-LAM setup.

Three kinds of cuts were made with the Micro-LAM method on polished

sapphire, with low, medium, and high laser assistance. The "low" cuts were made with a

normal thrust force of 10, 20, and 50mN, and as a control all had corresponding cuts

made without laser assistance. The laser used with these cuts was a 1480nm laser with

the maximum power of 400mW used. The cuts made with "medium" and "high" laser

assistance were done at a different load, and also have corresponding cut made without

laser assistance. The "medium" laser was a 976nm laser with the maximum power of

10W used, while the "high" laser was a 1070nm laser with a maximum power of 100W

with 20-30% of the power used.

All samples were then examined with a Renishaw InVia[TM] Raman spectrometer. Two different lasers of 514 nm and 633 nm wavelength were used during the Raman studies, and each of these was used with the Raman system set for either "high" or "regular" confocality. Thus, four different Raman laser settings were used. In terms of penetration into the sample the approximate depth of field [22] for each of the settings ranged from the 514 nm wavelength laser in confocal setting with the shallowest ($\approx$ 1.3 µm), to 633 nm confocal ($\approx$ 1.6 µm), to 514 nm regular ($\approx$ 1.8 µm), to 633 nm regular, which had the deepest ($\approx$ 2.3 µm). The samples were mapped on each setting to look at variations in stress across the machined area. The maps were along the center of the cut for the "high" and "medium" cuts, and both along the center of the cut and in the surrounding area for the smaller cuts, due to their narrow size.

The Raman spectra obtained from the analysis were fitted with the Wire 3.4[TM] software from Renishaw. From this fitting, the peak shift from the unstressed peak was found, and the stress calculated using (1) from [23].

$v = 0.0022\ \sigma + v_o$ 　　　(1)

Where v is the peak position, v_o is the unstressed peak position (found from another area on the sample far from the Micro-LAM cuts), and σ is the stress in MPa.

3. Results and discussion

The sapphire sample machined with the lowest laser power had machining cuts that were approximately 2 μm wide. Raman shift, and thus stress, was mapped in and across the cuts using the Renishaw invia[TM] mapping capability. The Raman system's optical microscope has a lateral resolution of 1-2 μm and sample translation stage motors have a similar positioning limit so a large area must be examined to ensure the cut and surrounding stressed region are mapped, see Figure 8.3.
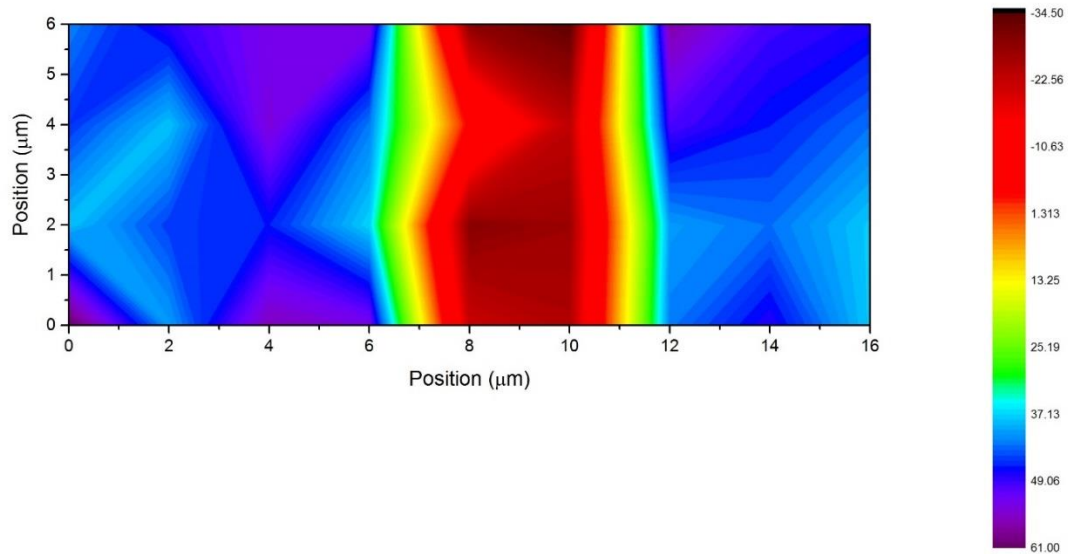
Figure 8.3: A stress map of sapphire machined with the Micro-LAM technique with a 20 mN thrust/applied force and low powered laser assistance. This map was taken with the 633nm laser in the confocal setting. Stresses are in MPa.

As Figure 8.3 shows, there is an area of compressive stress (negative values) inside and along the cut. This region is approximately 2-3 µm wide with a fairly uniform stress. Moving away from the cut, the stress changes sharply from compressive to tensile. This occurs over a narrow distance of 1-2 µm with the highest tensile stress occurring around 5 µm from the cut's center. The narrowness of the transition from compressive to tensile is at the limit of the system's resolution so it is possible that it is even sharper than it appears in Figure 8.3. The compressive region within the cut is due to the normal thrust force and the lateral cutting force resulting from the machining process, consequently the compression is expected to be present with or without the addition the Micro-LAM laser. Outside the cut the stress tends to be tensile, due to the flexing of the surface outside the contact region. This is well-known in the field of contact mechanics [24], there can also be extrusion (pushing up) of material outside the area of contact that can create tensile regions at the surface.

The magnitude of the compressive stress is a key area of assessment in how much damage a cut is causing. Given the maps of stress around the cuts and the wide range of stresses observed, a consistent method for assessing the magnitude of the compressive stress is needed. To find the average residual stress of an individual cut, the map was divided into a series of horizontal line scans, and the highest stress for each line averaged to give a mean magnitude for the compressive stress.
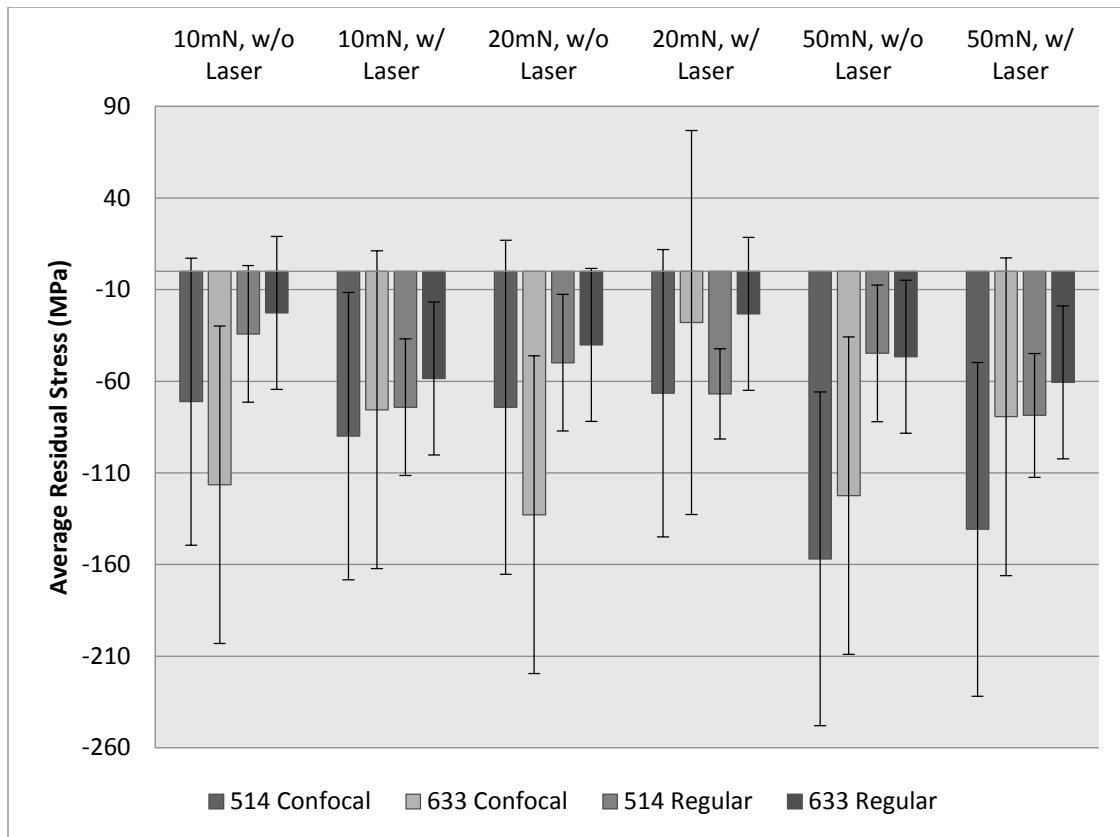
Figure 8.4: Average residual compressive stress values for samples machined with the low laser. Error bars are calculated from propagation of error of the equation used to find residual stress.

As shown in Figure 8.4, in many cases there is little difference between the magnitude of the compressive stresses in the cut made with and without laser assistance if the laser is used at low power. This is not surprising, as sapphire has a high transmittance (around 85%) for the wavelength of the laser used to assist in the machining [13]. Consequently, the laser should have minimal impact at low power because the absorption of photons is essential for the localized heating required to

thermally soften the sapphire. The extent of the heating depends on both the optical absorption and the thermal conductivity; both of which for sapphire depend on the local temperature and hydrostatic pressure. At many different temperatures and wavelengths the optical absorption coefficient of sapphire has been found to increase with temperature [13]. In contrast, the thermal conductivity of sapphire decreases with temperature [25]. This suggests that an increase in temperature at the point of contact can lead to a positive feedback mechanism where the temperature increase raises absorption while reducing thermal conduction of heat away from the point of contact. There is the additional impact of high pressures and phase transformations occurring during the machining process [26, 27] which can increase absorption at the laser's wavelength.

With regard to the thrust force, there is little difference between the 10mN and 20mN sample, as both have approximately the same average residual stresses. However, there is a marked increase in the residual stress for the sample machined with 50mN force. This is seen most significantly for the Raman settings with the shallowest penetration (514 nm confocal), suggesting that the higher cutting force generates greater stress close to the surface. This clearly shows that the force used to machine the sapphire has a significant impact on the magnitude of the resulting stresses and surface damage. For low laser powers, the load is likely to be the major factor in determining the extent of the residual stresses.

From the magnitude of the stresses at different Raman penetrations the conditions that give least residual stress is a 20 mN thrust force when using a low power

laser during the Micro-LAM process. With these settings the stress is compressive in the range of 20-70 MPa. For a hard ceramic material such as sapphire these low residual stresses after machining are very good. This is a very encouraging sign that the micro-LAM process can give significant improvements when machining sapphire.

Micro-Raman evaluation was also performed on damaged regions caused by repeated cuts, which give a larger machined area. During this part of the study higher laser powers were also used. Examples of these larger machined regions are shown by the optical micrographs of 5. Note that larger machined regions with low laser power were not investigated due to the tendency for cracking and chipping to occur. This is also seen when no laser is used (Figure 8.5, left).
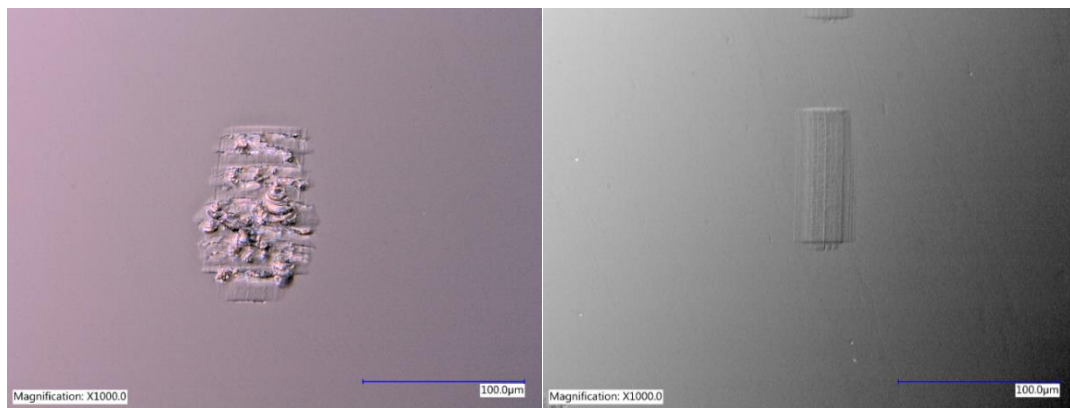
Figure 8.5: Optical micrograph of Micro-LAM cuts on sapphire with no laser assistance (left) and with medium laser assistance (right) at 1000X magnification.

The optical microscope images (Figure 8.5) of the cuts with and without laser assistance show a dramatic difference in the quality of the two machined surfaces. The cut without laser assistance (seen on the left in Figure 8.5 and in Figure 8.6) shows

significant cracking and chipping all over the machined region. For any real application

of machined sapphire (the field of optics, for instance) this would be unacceptable. The

surface damage in this case was so bad that the cracked sapphire surface may act as the

starting site for failures, due to fracture that lead to the total loss of structural integrity.

Machining with laser assistance, however, alleviates all optical evidence of cracking and

chipping, giving a much better surface finish without potential failure sites, as seen in

Figure 8.5.
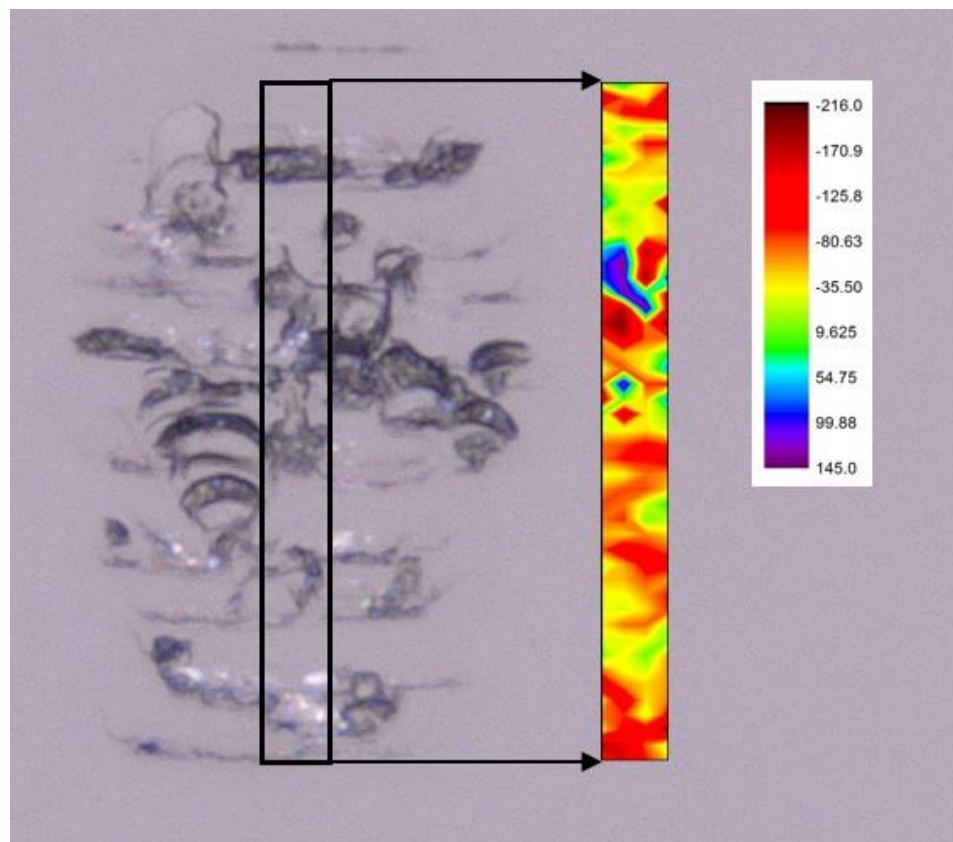
Figure 8.6: Optical microscope image of sapphire machined with the Micro-LAM

technique with no laser assistance, and the corresponding stress map taken with the

514nm confocal laser. Stresses are in MPa.

Examining the residual stresses at the surface of machined samples with and without laser assistance highlights the dramatic differences been the two finishes. Figure 8.6 shows the cut performed with no laser assistance, as well as its corresponding stress map from the 514nm confocal laser. The most obvious effect of the machining is the large peak stresses, both tensile and compressive, and the large heterogeneity of the stresses. The range in residual stresses is very large over the region, ranging from 145 MPa to -216 MPa. There is a strong correlation between the pattern of the stresses and the chips and cracks in the surface. For example, the areas of high tensile stress (seen in blues and purples) correlate with prominent chips in the material, suggesting that compressive stresses are relieved by the chipping, but at the expense of generating tensile stresses. Elsewhere there are large, but variable compressive stress, shown in shades of red.

To gain greater insight into the damage caused without the laser when compared to that when the laser is used, the magnitude of the stresses for each case can be examined. The average residual stresses over the machined area for the two cases are shown in Figure 8.7. It should be noted that though these larger machined areas are much wider than those of Figure 8.3, the same method for finding the magnitude of the average residual stress was used. It was seen that there are larger compressive stresses with laser assistance for the Raman setting of 514 nm confocal (shallowest) and 633 nm regular (deepest). For the other Raman settings the stresses were in general lower, with a noticeable tensile stress for the no laser 633 nm confocal.

It is important to note that the sample machined without laser assistance has a lower or tensile residual stress at some depths because of the cracking and chipping. These cracks provide stress relief, at the cost of material performance. Indeed, for a sample as hard as sapphire to achieve, as the laser-assisted process did, the relatively low stresses and excellent surface finish is very impressive. Furthermore, as the stresses obtained with the laser are small and compressive, they will likely provide a toughening mechanism for the material, which is desirable. It is not easy to machine a material as hard as sapphire, and to do so with these kinds of results is highly desirable.
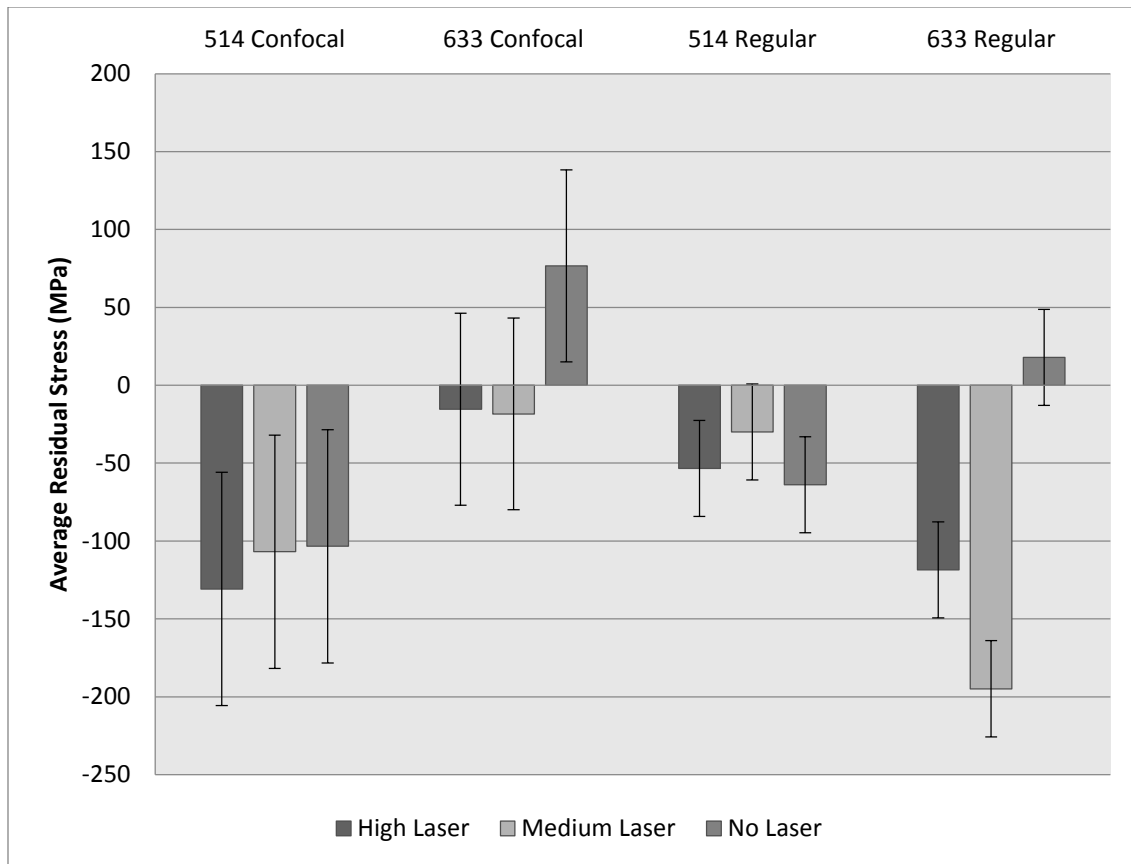
Figure 8.7: Average residual stress for cutting performed with high and medium laser powers, as well as without laser assistance (which results in cracking). Error bars are calculated from propagation of error of the equation used to find residual stress.

4. Conclusion

In this study it was shown that the Micro-LAM process can be successfully used in machining a hard, transparent material like sapphire. The apparent transparency of sapphire for the laser wavelength used is intriguing since it would imply the laser should have little impact on the machining process. However, during the laser assisted machining several different factors can affect the optical absorption and the local increase in temperature at the point of contact. Effectively a small increase in temperature can be magnified by decreasing thermal conductivity

and increasing optical absorption for sapphire as it is heated. In addition, the mechanical process of machining can change the alumina phase present and, hence, increase its absorption. The net effect is that laser assistance can have a significant impact on the machining if the laser's power is sufficient to cause even minimal local heating.

Without the laser assistance of the Micro-LAM process, machining sapphire has been shown to be a very damaging, and results in large compressive stresses developing, which if present in a finished material could lead to early failure. These high stresses are often relieved by severe surface damage in the form of chipping and cracks. When laser-assisted machining is used a largely damage free surface (no chipping or cracking) is obtained. Because the presence of chipping and cracks relieves compressive residual stresses it is actually found that the average compressive stress is slightly higher when the laser is used, but leaving a damage free surface. For an optical material such as sapphire, an excellent surface finish is highly desirable, and a reasonable tradeoff for a small amount of extra residual stress, which may actually be advantageous as it can help to toughen the material. Additionally, the Micro-LAM method allows for faster and more cost effective machining of sapphire.

Acknowledgements:

References

1. Borovskii GV, Shavva MA, Zakharevich EM, Grubyi SV, Maslov AR. Ultraprecision machining of brittle optical materials. Russ Eng Res 2015;35;883-886

2. Chen LQ, Zhang X, Zhang TY, Lin HY, Lee S. Micro-Raman spectral analysis of the subsurface damage layer in machined silicon wafers. J Mater Res 2000;15;1441-1444

3. Moore DF, Syms RRA. Recent developments in micromachined silicon. Electron Commun Eng J 1999;11;261-270

4. Zhang B, Zheng XL, Tokura H, Yoshikawa M. Grinding induced damage in ceramics. J Mater Process Tech 2003;132;353-64

5. Chinn RE. Ceramography: Preparation and Analysis of Ceramic Microstructures. ASM International, 2002.

6. Patten J, Gao W, Yasuto K. Ductile regime nanomachining of single-crystal silicon carbide. J Manuf Sci and Eng 2005;127;522-32

7. Kovalchenko AM. Studies of the ductile mode of cutting brittle materials (a review). J Superhard Mater 2013;35;259-76

8. Patten J, Ghantasala M, Ravindra D, Poyraz H, Virkar S. The effects of laser heating of the material removal process in Si and SiC nanomachining. In: Proceedings of 2011 NSF Engineering Research and Innovation Conference, Atlanta, Georgia, USA. 2011.

9. Ravindra D, Virkar S, Patten J. Ductile mode micro laser assisted machining of silicon carbide in: Gerhardt R. editor: Properties and Applications of Silicon Carbide. Croatia: InTech, 2011. 505-34

10. Shayan A, Poyraz H, Ravindra D, Patten J. Pressure and temperature effects in micro-laser assisted machining (μ-LAM) of silicon carbide. In: 37th North American Manufacturing Research Conference 2009, Greenville, South Carolina, USA. 2011. Dearborn: Society of Manufacturing Engineers, 2009.

11. Tang H, Li H, Xu J. Growth and development of sapphire crystal for LED applications in: Ferreira SO. editor: Advanced Topics on Crystal Growth. Croatia: InTech, 2013.

12. Tatartchenko V. Sapphire crystal growth and applications in: Capper P. editor: Bulk Crystal Growth of Electronic, Optical and Optoelectronic Materials. Malden: John Wiley and Sons, Ltd., 2005.

13. Dobrovinskaya ER, Lytvynov LA, Pishchik V. Sapphire: Material, Manufacturing, Applications. New York: Springer Science and Business Media, 2009.

14. Mohammadi H, Poyraz H, Ravindra D, Patten J. An experimental study on single point diamond turning of an unpolished silicon wafer via micro-laser assisted machining. Adv Mater Res 2014;1017;175-80

15. Ravindra D, Ponthapalli S, Patten J. Micro-laser assisted single point diamond turning feasibility tests of single crystal silicon. In: Proceedings 28 Annual Meeting American Society for Precis Engineering, St. Paul, Minnesota, USA. 2013. Raleigh, NC, USA: ASPE Publications, 2013. 24-28

16. Ravindra D, Ghantasala M, Patten J. Ductile mode material removal and high-pressure phase transformation phase transformations in silicon during micro-laser assisted machining. Precis Eng 2012;36;364-76

17. Ravindra D, Patten J. Ductile regime single point diamond turning of CVD-SiC resulting in an improved and damage-free surface. In: 4th International Conference on Recent Advances in Materials, Minerals & Environment and 2nd Asian Symposium on Materials & Processing, Penang, Malaysia. 2009.

18. Ravindra D, Ponthapalli S, Patten J. Micro-laser assisted feasibility test on soda-lime-glass. ASME 2013 International Manufacturing Science and Engineering Conference collocated with the 41st North American Manufacturing Research Conference, Madison, Wisconsin, USA. 2013. New York, New York, USA: American Society of Mechanical Engineers, 2013.

19. Ravindra D, Patten J. Ductile regime single point diamond turning of quartz resulting in an improved and damage-free surface. Mach Sci andTechnol 2011;15;357-75

20. Ravindra D, Patten J. The effect of thermal softening on the ductile-to-brittle transition of sapphire. In: Proceedings of NAMRI/SME, Madison, Wisconsin, USA. 2013. Dearborn, Michigan, USA: Society of Manufacturing Engineers, 2013. 41 160-167

21. Colomban P. Analysis of strain and stress in ceramic, polymer and metal matrix composites by Raman spectroscopy. Adv Eng Mater 2002;4;535-42

22. "Chapter 2: Fundamental Limits in Confocal Microscopy" by James B. Pawley, in Handbook of Biological Confocal Microscopy, 3rd edition, editor James B. Pawley, p.20-42, 2006.

23. Gallas MR, Chu YC, Pieramrini GJ. Calibration of the Raman effect in α-Al_2O_3 ceramic for residual stress measurements. J Mater Res 1995;10;2817-22.

24. Johnson KL. Contact Mechanics. Cambridge: The Press Syndicate of the University of Cambridge, 2003. Dearborn, Michigan: Society of Manufacturing Engineers

25. Saint Gobain. Sapphire Products: Properties and Benefits, 2014.

26. Furuichi H, Matsuura K, Yamazaki K, Watanabe S. Amorphous state formation and structural change in alumina by repeated rubbing. Wear 1995;189;86-90.

27. Furuichi, H. Formation of new alumina by shearing at high pressure. In IOP Conference Series: Materials Science and Engineering, vol. 18, no. 7, p. 072006. IOP Publishing, 2011.

9. Broader Implications and Future Work

This study was an in depth examination of two materials, silicon and sapphire, and how they reacted to the Micro-LAM process. Valuable information on the residual stresses, additional phases, and changes in crystallinity that are generated by the Micro-LAM process was gained. However, this is only for two materials. Here, we seek to provide guidance based on our work as to selecting other materials that could potentially benefit from the Micro-LAM process.

While the laser assistance imparted by the Micro-LAM process has many benefits, perhaps the most well documented and understood is the reduction in hardness it allows. This reduction in hardness has been shown to be as much as 50% [17]. Fundamentally, based on equation 2.7, this reduction in hardness allows for ductile machining with greater depths of cut for the material in question, which in turn allows for faster and less damaging machining. It can be hard to machine at very low depths with control and efficiency; increasing the critical depth for ductile machining of the material helps to solve this problem.

In our study, this benefit was seen in sapphire. The high, medium, and no laser cuts were performed with the same machining conditions, just different laser powers and slightly different wavelengths. While the high and medium power cuts displayed what appears to be ductile behavior and a good surface finish, the cut without laser assistance showed brittle behavior and had an unacceptable surface finish. Laser assistance is not always necessary for ductile machining of sapphire, but here it was because the machining conditions requires an increased critical depth. Hardness is a key factor in determining how the material will be behave, but it is not the only material property

governing the critical depth as elastic modulus and fracture toughness also play a role as given in equation 2.7. Materials with high hardness, like sapphire, can be difficult to machine with traditional techniques as seen in this study when no laser or low laser power is used. The Micro-LAM method provides a potential solution since it enables ductile machining which is both faster and less damaging, and as such the Micro-LAM method is a good candidate for machining other materials of high hardness.

It is well known that silicon undergoes a complex series of phase transformations when loaded and unloaded under the pressures produces by machining. The secondary phases formed can be detrimental to the material's electrical, optical, and mechanical properties, and are a nuisance when machining silicon. In this study, it was found that these secondary phases can be annealed out during machining by the Micro-LAM method leaving a phase pure and low stress surface. This makes Micro-LAM an ideal candidate for machining of silicon and potentially other semiconductors that can undergo phase transformations. Germanium has two phase pathways available to it during loading and unloading, and can be left with secondary phases that are undesirable [50]. Similarly, this behavior can be seen in compound semiconductors, such as GeTe [51]. The different phases formed can make semiconductors difficult to machine, thus they are excellent candidates for machining with the Micro-LAM method due to its ability to anneal out secondary phases.

In his previous work Ravindra [52] examined numerous material classes, single crystal, amorphous, as well as polycrystalline, to see if material properties could be used to predict what would react well with the Micro-LAM process. He found that most correlations were weak, but there was one that was strong. It was found that the

brittleness index of a material correlates inversely with the critical depth for cutting of the material without laser assistance. The brittleness index is found by dividing hardness by fracture toughness, hence Ravindra's observations are consistent with equation 2.7. This clearly shows how laser assistance can improve the critical depth during machining by modifying the ratio of hardness and fracture toughness (note that the inverse of this ratio is squared in equation 2.7).

This kind of approach to predicting changes in the critical depth during machining is a good way of predicting if the Micro-LAM technique would work well with a new material. Only a limited number of materials have been tested with the method, but enough have been examined that similarities between candidate materials and a material that has been machined using the method can be found. From these similarities, preliminary predictions can be drawn about the techniques potential effectiveness on new materials.   This study highlighted two large areas of materials that the Micro-LAM technique would be useful for, those with high hardness, and those with undesired phase transformations that can occur during machining.

From there, it would be wise to perform laser assisted indentations similar to Ravindra [52] to see if the hardness of the material is being reduced by the laser. Selecting the proper laser can be done through a literature search of high pressure phase properties, or by experimenting with a diamond anvil cell. If the laser being absorbed leads to a reduction in hardness then the Micro-LAM technique is likely to be a good alternative method to regular ductile mode machining or traditional machining. From there, scratch tests, as seen in Chapter 5, can be used as a good way to look at how the material will react to various Micro-LAM parameters. These scratch tests allow a large

amount of parameters to be tested while using only a small amount of material. From there preferential machining conditions can be identified and the sample can be tested on an ultraprecision setup, as seen in Chapter 7.

The current study showed the effectiveness of Micro-LAM for machining silicon and sapphire with low stresses, high phase purity, and good crystallinity. However, the conclusions taken from this study can be applied to other materials to judge when the Micro-LAM process can be used to improve the results of surface machining. This will ultimately lead to better ceramic and semiconductor surfaces for technical and structural applications across the entire field of materials engineering.

While this work accomplished many of its goals, there is more work that can be done to understand it further.

An obvious step is to perform the same tests, but with more surface specificity. While the 514 and 633 nm lasers allow the user to look close to the sample surface, a shorter wavelength laser would allow even more surface specificity by penetrating less into the sample surface. While it is less conventional, Surface Enhanced Raman Spectroscopy, or SERS, could also be used to gain more surface specificity. As SERS uses localized surface plasmon resonance to amplify the signal of material near the nanoparticles, it is possible that it could decrease drastically the depth of scanning. This reduction in the depth the Raman is sensing would allow for a more complete picture of how machining affects a material, so it is worth pursuing.

This study looked only at two materials, silicon and sapphire, and, while there is literature on other materials that have undergone the Micro-LAM process, none of it

deals as much as this with residual stresses, phase purity, and relative crystallinity. Using this approach to look at more materials that had undergone the Micro-LAM process would be valuable. Besides, the results between materials could be compared to see how various material properties affect the machining process. The two materials looked at here do not allow for a large enough sample size, but a comparison of basic material properties such as hardness, strength, and Young's modulus with the results of machining would allow for a greater understanding of how the Micro-LAM process works, and could assist in the machining of new materials.

This study found the "sweet spots" of machining conditions that provide the best results. . Using the results from this study as a baseline, machining conditions similar to the best ones discovered here should be investigated to determine if these conditions actually are the best. Slightly changing one condition at a time near these "sweet spots" most likely would further refine each one, and better conditions would be discovered. The results of these new machining conditions would need to be tested rigorously for residual stress, additional phases generated, changes in relative crystallinity.

This tuning of the machining conditions would lead to perhaps the most important advancement, -correlating the stress, additional phases, and changes in crystallinity that result from the machining with the material performance. Unfortunately this is an area that has been neglected in traditional machining, and has not been covered at all with the Micro-LAM technique. While understanding how machining parameters affect material properties is very important, taking it to the next level and discovering how these parameters, and the properties they lead to, affect the performance of the material is

possibly more so. Materials are machined so they can be used, and a greater understanding of machining's effect on that performance is necessary.

Materials machined by the Micro-LAM process should be tested to see how they perform. Numerous characteristics could be tested, such as strength, toughness, and electrical and optical properties. From there, these properties should be correlated with the residual stress, additional phases, and changes in crystallinity present in the samples to discover how machining's effects impact material performance.

10. Conclusions

In this study the Micro-LAM machining process was examined for machining silicon and sapphire. The process was examined with micro-Raman spectroscopy to look at residual stress, relative phase purity, and relative crystallinity of the samples.

There were three main thrusts of the study of Micro-LAM: silicon machined with a load-controlled device, silicon machined with a high precision device, and sapphire. While the results were not always the same, there were some features that were consistent through all of the samples.

The first, and perhaps most important, is that the Micro-LAM process is an improvement over traditional SPDT. With the sapphire sample, the addition of laser assistance gave slightly larger stress, but gave a far superior sample surface. Without the laser assistance, the sample surface was chipped and cracked, and would be unacceptable for almost all of sapphire's applications. For the load-controlled silicon samples, parts machined without laser assistance almost universally gave large residual stresses, low phase purity, and low relative crystallinity. The laser assistance in the Micro-LAM process has several benefits. The first is thermal softening, allowing for a reduction in the apparent hardness and thus less stress on the piece being machined. Furthermore, the laser anneals the material as it passes over it, allowing for a reduction in residual stress as well as giving the energy needed for additional phases to change back into the original phase.

It is also clear that there is a "sweet spot" of machining parameters for Micro-LAM to be as effective as possible. In the scratched silicon samples, "burning" is visible

when the laser is too high, and there are large stresses associated with it. For the high precision silicon samples, when the laser was too high, almost no Si-I was present anymore, as well as low relative crystallinity and phase purity. Though the load-controlled silicon samples had the best results with high laser assistance, some high laser samples produced poor results. Conversely, often if the laser assistance was not high enough that was also a problem. This was seen in all the sample types, but especially sapphire where at low laser power there was almost no difference between the samples machined with and without laser assistance.

The final thread running through all the sample types is that Micro-LAM can produce excellent results when it is properly done. Many samples had residual stress values around 100 MPa, usually compressive, and featured high phase purity and relative crystallinity. Material properties like this, with the excellent surface finishes and time saving that Micro-LAM allows for, are extremely valuable.

Traditional machining is a chaotic and difficult to understand endeavor, and on a mechanistic level is still often poorly understood. Furthermore, there are often limited inputs that can be controlled. Perhaps the most valuable characteristic of Micro-LAM is that there are several inputs, including laser power, feed rate, and depth of cut, which can be controlled by the user to affect the outcome of the machining. Micro-LAM has many more inputs that can be tuned by the user than traditional machining has, and with the addition of laser assistance it also has more than traditional SPDT.

This study found that Micro-LAM is an excellent machining technique. It is a viable alternative to many traditional machining techniques for ceramics, semiconductors, and single crystals that often are extremely damaging processes. As the

understanding of the Micro-LAM process continues to improve, its value to industry will

continue to improve as well.

References

1. Callister, W., & Rethwisch, D. (2014) *Materials Science and Engineering: An Introduction,* Wiley.

2. Carter, C., & Norton, M. (2013) *Ceramic Materials,* Springer.

3. Bi Zhang, *et al.* (2003) "Grinding Induced Damage in Ceramics," *Journal of Materials Processing Technology,* 132, 353-364.

4. Chinn, R. E. (2002). *Ceramography: Preparation and Analysis of Ceramic Microstructures*. Wiley-American Ceramic Society.

5. Toenshoff, H., Lierse, T., & Inasaki, I. (1999). Chapter 3 – Grinding of Advanced Ceramics. Jahanmir, S. *Machining of Ceramics and Composites* (pp. 85-118). CRC Press.

6. Kovalchenko, A. M. (2013). Studies of the ductile mode of cutting brittle materials (A review). *Journal of Superhard Materials*, *35*(5), 259–276. http://doi.org/10.3103/S1063457613050018

7. *Lapping and Polishing Basics - South Bay Technology Inc*. Retrieved from http://itunesbooks.co/detaildocs/lapping-and-polishing-basics-south-bay-technology-inc-130509/

8. Spur, G. & Engel, H. (1999) Chapter 6 – Lapping and Polishing of Glass and Ceramics. Jahanmir, S. *Machining of Ceramics and Composites* (pp. 177-207). CRC Press.

9. F. Klocke, O. G. (1997). Polishing of advanced ceramics. *MACHINING SCIENCE AND TECHNOLOGY*, *1*(2), 263–273. http://doi.org/10.1080/10940349708945651

10. Samant, A. N., & Dahotre, N. B. (2009). Laser machining of structural ceramics—A review. *Journal of the European Ceramic Society*, *29*(6), 969 – 993. http://doi.org/http://dx.doi.org/10.1016/j.jeurceramsoc.2008.11.010

11. Tuersley, I. P., Jawaid, A., & Pashby, I. R. (1994). Review: Various methods of machining advanced ceramic materials. *Journal of Materials Processing Technology*, *42*(4), 377–390. http://doi.org/10.1016/0924-0136(94)90144-9

12. Kumar, J. (2013). ULTRASONIC MACHINING—A COMPREHENSIVE REVIEW. *Machining Science and Technology*, *17*(3). http://doi.org/10.1080/10910344.2013.806093

13. Bifano, T. G., Dow, T., & Scattergood, R. (1991). Ductile-regime grinding: a new technology for machining brittle materials. *Journal of Manufacturing Science and Engineering*, *113*, 184–189.

14. Patten, J., Gao, W., & Yasuto, K. (2005). Ductile regime nanomachining of single-crystal silicon carbide. *Journal of Manufacturing Science and Engineering*, *127*, 522–532.

15. Patten, J., Ghantasala, M., Ravindra, D., Poyraz, H., & Virkar, S. (2011) The Effects of Laser Heating on the Material Removal Process in Si and SiC Nanomachining. *Proceedings of 2011 NSF Engineering Research and Innovation Conference, Atlanta, Ga.*

16. Ravindra, D., Virkar, S., & Patten, J. (2011). Ductile Mode Micro Laser Assisted Machining of Silicon Carbide. In R. Gerhardt (Ed.), *Properties and Applications of Silicon Carbide*. InTech. Retrieved from http://www.intechopen.com/books/properties-and-applications-of-silicon-carbide/ductile-mode-micro-laser-assisted-machining-of-silicon-carbide

17. Shayan, A., Poyraz, H., Ravindra, D., & Patten, J. (2009). Pressure and Temperature Effects in Micro-Laser Assisted Machining (μ-LAM) of Silicon Carbide. *North American Manufacturing Research Conference (NAMRC)*.

18. Mohammadi, H., Poyraz, H., Ravindra, D., & Patten, J. (2014). An Experimental Study on Single Point Diamond Turning of an Unpolished Silicon wafer via Micro-Laser Assisted Machining. *Advanced Materials Research, 1017*, 175-180.

19. Ravindra, D., Ponthapalli, S., & Patten, J. (2013) Micro-Laser Assisted Single Point Diamond Turning Feasibility Tests of Single Crystal Silicon. *American Society for Precision Engineers (ASPE) 28th Annual Meeting*.

20. Ravindra, D., Ghantasala, M., & Patten, J. (2012) Ductile Mode Material Removal and High-Pressure Phase Transformation in Silicon During Micro-Laser Assisted Machining. *Precision Engineering, 36,* 364-367.

21. Ravindra, D., & Patten, J. (2009). Ductile regime single point diamond turning of CVD-SiC resulting in an improved and damage-free surface. *4th International Conference on Recent Advances in Materials, Minerals & Environment and 2nd Asian Symposium on Materials & Processing.*

22. Ravindra, D., Ponthapalli, S., & Patten, J. (2013) Micro-Laser Assisted Feasibility Test on Soda-Lime-Glass. *Proceedings of the ASME International Manufacturing Science and Engineering Conference.*

23. Ravindra, D., Patten, J. (2011) Ductile Regime Single Point Diamond Turning of Quartz Resulting in an Improved and Damage-Free Surface. *Machining Science and Technology*, *15*, 357-375.

24. Hosford, W. (2005). *Mechanical Behavior of Materials*. Cambridge University Press.

25. Watchman, J., Cannon, W., & Matthewson, M. (2009). *Mechanical Properties of Ceramics*. Wiley.

26. Jahanmir, S. (1999). Chapter 18 – Measurement of Machining-Induced Residual Stresses in Ceramics. *Machining of Ceramics and Composites* (pp. 85-118). CRC Press.

27. Drago, R. (1977). *Physical Methods in Chemistry*. Saunders.

28. Colomban, P. (2002) Analysis of Strain and Stress in Ceramic, Polymer and Metal Matrix Composites by Raman Spectrosopy. *Advanced Engineering Materials*, *4*, 535-542.

29. Ferraro, J. R. (2003). *Introductory Raman Spectroscopy*. Academic Press.

33. Sergo, V., Pezzoti, G., Katagiri, G., Muraki, N., & Nishida, T. (1996) Stress Dependence of the Raman Spectrum of β-Silicon Nitride. *Journal of the American Ceramic Society., 79,* 781-784.

30. Chi-Chang Lin, M.-T. K. (2010). Review: Raman Spectroscopy–A Novel Tool for Noninvasive Analysis of Ocular Surface Fluid. *Journal of Medical and Biological Engineering*, *30*, 343–354.

31. Harris, D., & Bertolucci, M. (1989). *Symmetry and Spectroscopy: An Introduction to Vibrational and Electronic Spectroscopy.* Dover Books.

32. Gouadec, G., & Colomban, P. (2007). Raman Spectroscopy of nanomaterials: How spectra relate to disorder, particle size and mechanical properties. *Progress in Crystal Growth and Characterization of Materials*, *53*(1), 1 – 56. http://doi.org/http://dx.doi.org/10.1016/j.pcrysgrow.2007.01.001

34. Shin, F., Pollak, F., & Raccah, P. (1974) Effects of Uniaxial Stress on Raman Frequencies of Ti_2O_3 and Al_2O_3, *Bulletin of the American Physics Society., 19,* 536

35. Watson, GH, Daniels, WB and Wang, C. (1981) Measurements of Raman Intensities and Pressure –Dependence of Phonon Frequencies in Sapphire. *Journal of Applied Physics*, *52,* 956

36. Wermelinger, T., Borgia, C., Solenthaler, C., Spolenak., R. (2007) 3-D Raman Spectroscopy Measurements of the Symmetry of Residual Stress Fields in Plastically Deformed Sapphire Crystals. *Acta Materialia, 55,* 4657-4665.

36. Schlucker, S. (2014) Surface-Enchanced Raman Spectroscopy: Concepts and Chemical Applications. *Angewandte Reviews, 53,* 4756-4795.

37. Stiles, P., Dieringer, J., Shah, N., & Duyne, R. (2008) Surface-Enchanced Raman Spectroscopy. *Annual Review of Analytical Chemistry., 1,* 601-626.

38. Boerio, F., Tsai, W. (1994) Chapter 2 – Raman Spectroscopy. Ishida, H. *Characterization of Composite Materials* (pp. 26-43). Manning Publications Co. Retrieved from https://books.google.com/books?id=Pw0hBQAAQBAJ&pg=PA29&lpg=PA29&dq=sers +surface+bulk+materials&source=bl&ots=ijKdryS43D&sig=rRGFuREVaUU_F9o1gUx hlwL1bVw&hl=en&sa=X&ei=2WSNVdiEG4v7-

AHl27jYBA&ved=0CEsQ6AEwCDgK#v=onepage&q=sers%20surface%20bulk%20mat
erials&f=false

37. Shimura, F. (1989). Chapter 1 - Introduction. In F. Shimura (Ed.), *Semiconductor Silicon Crystal Technology* (pp. 1 – 7). Academic Press. Retrieved from http://www.sciencedirect.com/science/article/pii/B9780126400458500057

38. Jasinevicius, R. G., Duduch, J. G., & Pizani, P. S. (2007). Structure Evaluation of Submicrometre Silicon Chips Removed by Diamond Turning. *Semiconductor Science and Technology*, *22*(5), 561. http://doi.org/10.1088/0268-1242/22/5/019

39. National Renewable Energy Laboratory, Best Research-Cell Efficiencies, Retrieved from http://www.nrel.gov/ncpv/images/efficiency_chart.jpg

40. Arif, M., Rahman, M., & San, W. Y. (2012). A state-of-the-art review of ductile cutting of silicon wafers for semiconductor and microelectronics industries. *The International Journal of Advanced Manufacturing Technology*, *63*(5-8), 481–504. http://doi.org/10.1007/s00170-012-3937-2

41. Weinstein, B. & Piermarini, G. (1975). Raman Scattering and Phonon Dispersion in Si and GaP at Very High Pressure. *Physical Review B, 12*, 1172-1186.

42. Jasinevicius, R., Duduch, J., Montanari, L., & Pizani, P. (2008). Phase Transformations and Residual Stress Probed by Raman Spectroscopy in Diamond-Turned Single Crystal Silicon. *Proceedings of the Institution of Mechanical Engineers, Part B: Journal of Engineering Manufacture, 222,* 1065-1073.

42. Shirai, Takashi, Watanabe, Hideo, Fuji, Masayoshi, & Takahashi, Minoru. (2010). Structural Properties and Surface Characteristics on Aluminum Oxide Powders. *Annual Report of the Ceramics Research Laboratory Nagoya Institute of Technology*, *9*, 23–31.

44. Sutorik, A. C., Neo, S. S., Treadwell, D. R., & Laine, R. M. (1998). Synthesis of Ultrafine β″-Alumina Powders via Flame Spray Pyrolysis of Polymeric Precursors. *Journal of the American Ceramic Society*, *81*(6), 1477–1486. http://doi.org/10.1111/j.1151-2916.1998.tb02506.x

45. Tang, H., Li, H., & Xu, J. (2013). Growth and Development of Sapphire Crystal for LED Applications. In S. Ferreira (Ed.), *Advanced Topics on Crystal Growth*. InTech. Retrieved from http://www.intechopen.com/books/advanced-topics-on-crystal-growth/growth-and-development-of-sapphire-crystal-for-led-applications

46. Tatartchenko, V. (2005) Chapter 10 – Sapphire Crystal Growth and Applications In Capper P (Ed.), *Bulk Crystal Growth of Electronic, Optical & Optoelectronic Materials* (pp. 299-338). John Wiley & Sons, Ltd.

47. Dobrovinskaya, E. R., Lytvynov, L. A., & Pishchik, V. (2009). *Sapphire: Material, Manufacturing, Applications*. Springer Science & Business Media.

48. Gallas, M., Chu, Y., & Piermarini, G. (1995). Calibration of the Raman Effect in α-Al_2O_3 Ceramic for Residual Stress Measurements. *Journal of Materials Research, 10,* 2817-2822.

49. Strain Measurements of a Si Cap Layer Deposited on a SiGe Substrate Determination of Ge Content. (n.d.). Horiba Scientific.

50. Deshmukh, S., Haberl, B., Ruffell, S., Munroe, P., Williams, J.S., & Bradby, J.E. (2014). Phase Transformation Pathways in Amorphous Germanium Under Indentation Pressure. *Journal of Applied Physics*, *115*, 153502.

51. Leger, J.M., & Redon, A.M. (1990). Phase Transformations and Volume of the IV-VI GeTe Semiconductor Under High Pressure. *Journal of Physics: Condensed Matter, 2*(26), 5655-5662.

52. Ravindra, D. Ductile Mode Material Removal of Ceramics and Semiconductors. ScholarWorks at WMU. Retrieved 7.18.17.